Connectivity, Throughput, and End-to-end Latency in Infrastructureless Wireless Networks with Beamforming-enabled Devices
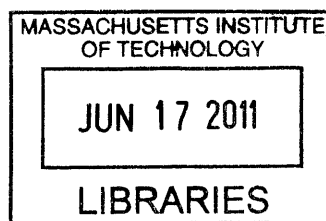
Matthew F. Carey

B.S. Electrical Engineering
Boston University (2009)

Submitted to the Department of Electrical Engineering and Computer Science
in partial fulfillment of the requirements for the degree of
Master of Science
in
Electrical Engineering and Computer Science
at the

MASSACHUSETTS INSTITUTE OF TECHNOLOGY

June 2011

Author ....

Computer Science
May 16, 2011

Certified by .

Vincent W. S. Chan
Juan and Irwin Jacobs Professor of Electrical Engineering and Computer Science
Thesis Supervisor

Certified by ....

John M. Chapin
Visiting Scientist in Claude E. Shannon Communication and Network Group, RLE
Thesis Supervisor

Accepted by ....

Leslie A. Kolodziejski
Chair, Department Committee on Graduate Students

Connectivity, Throughput, and End-to-end Latency in Infrastructureless Wireless Networks with Beamforming-enabled Devices

by

Matthew F. Carey

Submitted to the Department of Electrical Engineering and Computer Science on May 16, 2011 in partial fulfillment of the requirements for the degree of Master of Science in Electrical Engineering and Computer Science

Abstract

Infrastructureless wireless networks are an important class of wireless networks best fitted to operational situations with temporary, localized demand for communication ability. These networks are composed of wireless communication devices that autonomously form a network without the need for pre-deployed infrastructure such as wireless base-stations and access points. Significant research and development has been devoted to mobile ad hoc wireless networks (MANETs) in the past decade, a particular infrastructureless wireless network architecture. While MANETs are capable of autonomous network formation and multihop routing, the practical adoption of this technology has been limited since these networks are not designed to support more than about thirty users or to provide the quality of service (QoS) assurance required by many of the envisioned driving applications for infrastructureless wireless networks. In particular, communication during disaster relief efforts or tactical military operations requires guaranteed network service capabilities for mission-critical, time-sensitive data and applications. MANETs may be frequently disconnected due to device mobility and mismatches between routing and transport layer protocols, making them unsuitable for these scenarios.

Network connectivity is fundamentally important to a network designed to provide QoS guarantees to the end-user. Without network connectivity, at least one pair of devices in the network experiences zero sustainable data rate and infinite end-to-end message delay, a catastrophic condition during a search and rescue mission or in a battlefield. We consider the use of wireless devices equipped with beamforming-enabled antennas to expand deployment regimes in which there is a high probability of instantaneous connectivity and desirable network scalability.

3

Exploiting the increased communication reach of directional antennas and electronic beam steering techniques in fixed rate systems, we characterize the probability of instantaneous connectivity for a finite number of nodes operating in a bounded region and identify required conditions to achieve an acceptably high probability of connectivity. Our analysis shows significant improvements to highly-connected regimes of operation with added antenna directivity.

Following the characterization of instantaneous network connectivity, we analyze the achievable network throughput and scalability of both fixed and variable rate beamforming-enabled power-limited networks operating in a bounded region. Our study of the scaling behavior of the network is concerned with three QoS metrics of central importance for a system designed to provide service assurance to the end-user: achievable throughput, end-to-end delay (which we quantify as the number of end-to-end hops), and network energy consumption. We find that the infrastructureless wireless network can achieve scalable performance that is independent of end-user device density with high probability, as well as identify the existence of a system characteristic hopping distance for routing schemes that attain this scaling-optimal behavior. Our results also reveal achievable QoS performance gains from the inclusion of antenna directivity. Following these insights, we develop a scalable, heuristic geographic routing algorithm using device localization information and the characteristic hopping distance guideline that achieves sub-optimal but high network throughput in simulation.

Thesis Supervisor: Vincent W. S. Chan
Title: Joan and Irwin Jacobs Professor of Electrical Engineering and Computer Science

Thesis Supervisor: John M. Chapin
Title: Visiting Scientist in Claude E. Shannon Communication and Network Group, RLE

Acknowledgments

Despite the name on the cover, this thesis is not the product of a single individual. It is only through the inspiration, guidance, and support of many that this work came to be, and I am honored to acknowledge them here.

First and foremost, I thank my research advisor, Professor Vincent Chan, for everything he has done for me during my time at MIT. From the first instant I arrived on campus, he was ready and willing to offer invaluable mentorship to help guide me through the slightly overwhelming experience of being a first year graduate student. And it was his unfaltering dedication, his intellectual curiosity, and his engaging teaching ability that brought me to the Claude E. Shannon Communication and Network Group. Throughout the duration of my thesis work, he continued to inspire and support me at every moment, providing me with this academic opportunity that I had only once dreamed of.

I would like to thank Dr. John Chapin for his involvement in the development of this thesis. His experience, feedback, and contributions to this research helped to develop the results more fully. I am also grateful for his dedication to the student members of our group,

particularly with regard to his attention to detail and clarity in preparation and presentation of research material.

My gratitude extends to many professors in the Electrical Engineering and Computer Science department at MIT for their guidance, support, and teaching. I would particularly like to acknowledge Professor Muriel Médard, who adopted me as a research nephew. My interaction with her enriched my MIT journey and often provided me with new ways to consider my own research and academic interests. Additionally, I am forever grateful to Professor Robert Gallager. Not only did he write the textbooks that introduced me to all of the fundamentals of digital communication and data networks, but he was an important source of academic guidance and inspiration even before I began my graduate studies. I would also like to recognize Professor Alan Oppenheim for his dedication to mentoring first year graduate students and making sure that we had a successful and comfortable transition into the MIT lifestyle.

I am thankful for the faculty at Boston University who first got me interested in academic research. In particular, Professor Mark Horenstein endowed me with the amazing opportunity to work in his lab as a lowly college sophomore. It was there that I first experienced the excitement of pursuing the unknown and the importance of combining analytic analysis with sound scientific methods. I am grateful for the opportunity he gave me to contribute to his research, even with the little knowledge that I had at the time. And I would also like to recognize Professor David Starobinski, who introduced me to the exciting field of data networks and offered me the opportunity to engage in an enriching semester of research under his mentorship and guidance.

My time at MIT so far would not have been quite as amazing without my friends and fellow researchers that have made every day memorable. My officemates Rui Li and Shane Fink

have been a constant source of support, riveting discourse, and laughter. And all of the other members of the Claude E. Shannon Communication and Network Group, including Andrew Puryear, Lei Zhang, Katherine Lin, David Cole, Mia Yinuo, and Henna Huang, have similarly helped developed a culture of friendship that made work and study feel that much less like work and study. I am indebted to past members of the group as well for their academic encouragement, particularly Lillian Dai's work in infrastructureless wireless networks which was a huge inspiration. I would like to thank Donna Beaudry for her assistance with logistics and for her own "research." I am grateful to my friends across the hall in the Network Coding and Reliable Communications Group, including Arman Rezaee, Flávio Calmon, Jason Cloud, Weifei Zeng, and Soheil Feizi. Time spent with them is always fun and rewarding, regardless of whether it is to take a moment to discuss the intricacies of our academic work or to catch my breath and relax. Additionally, I am forever thankful for all of my other friends outside of the network and communication family for making these two years at MIT a blast, especially Bridget Navarro, Armon Sharei, Collin Mechler, Ryan Thurston, Pantea Khodami, and Elliot Sedegah, among everyone else.

Finally, I would like to thank the most important people in my life: my family. My parents, Francis and Kathleen, instilled in me the importance of education and a curiosity for learning at a young age, ultimately making my academic journey possible. Without their dedication to my educational development, this thesis would never have come to fruition. I also want to thank them for their unconditional love. They have always been there for me, and I am lucky to have had such encouragement at each step in my life adventure. And I am also grateful to my brother Robert; I could not ask for a better sibling or friend. It is to my family that I dedicate this thesis.

Contents

6 Conclusion   161

Appendices

A Derivation of (2.8) in Chapter 2   167

B Derivation of (3.16) in Chapter 3   169

C Derivation of Results in Chapter 4   173

Bibliography   181

List of Figures

14

15

List of Notation

D	Transmitting antenna aperture size
λ	• Transmitting signal wavelength (Chapter 2)
	• Uniform traffic model data rate (Chapter 4)
P_r	Received power
P_t	Transmitted power
k	Attenuation exponent of the path loss model
d	Distance between transmitter and receiver
d_o	Reference distance for path loss model
γ	Frequency and antenna gain constant in path loss model
W	System bandwidth
n	Number of end-user devices in network
N_E	Number of discrete antenna elements in uniform circular antenna array (UCAA)
R	• Radius of array or aperture antenna (Chapter 2)
	• Fixed transmission rate of fixed rate system (Chapter 4 and 5)
$U(d, \theta, \phi)$	Radiated field
P_{rad}	Total time-averaged radiated power constraint
$G(\theta, \phi)$	Directive gain
N_{sat}	UCAA element saturation point
D_{array}	Directivity of the UCAA
$D_{aperture}$	Directivity of ring aperture antenna

D_{tx}	Transmit antenna directivity
D_{rx}	Receive antenna directivity
r	Transmit range of omnidirectional transmitter in fixed rate system
r_{bf}	Transmit range of directional transmitter in a fixed rate system
L	Length of operational line in 1-D network, or dimension of operational area in 2-D network
X_i	Unordered location of end-user node i
$X_{(i)}$	Ordered location of end-user node i
Y_i	Spacing between ordered node $X_{(i)}$ and $X_{(i+1)}$
Δ	Normalized omnidirectional transmission range in fixed rate system
$P_C^{omni}(n, \Delta)$	Probability of connectivity for 1-D omnidirectional network in fixed rate system
$P_C^{bf}(n, \Delta, D_{tx})$	Probability of connectivity for 1-D directional network in fixed rate system
N	Random 2-D network
N_x	Projection of random 2-D network onto the x-axis
N_y	Projection of random 2-D network onto the y-axis
$P_{2D}^{omni}(n, \Delta)$	Probability of connectivity for 2-D omnidirectional network in fixed rate system
$P_{2D}^{bf}(n, \Delta, D_{tx})$	Probability of connectivity for 2-D directional network in fixed rate system
m	Number of cells (bins) in balls and bins approximation
$P_C^{bb}(n, m)$	Probability of connectivity for 2-D network under balls and bins approximation
I_i	Indicator random variable that cell i is empty in balls and bins approximation
n_i	Number of nodes (balls) needed in the ith stage of deployment
n^*	Number of end-user nodes needed for at least one in each cell (bin) in balls and bins approximation
$\hat{\lambda}$	Uniform capacity of omnidirectional network
$\hat{\lambda}^{bf}$	Uniform capacity of directional network
$\tilde{\lambda}$	Uniform throughput of omnidirectional network
$\tilde{\lambda}^{bf}$	Uniform throughput of directional network
P_{avg}	Total time-averaged power constraint for both transmission and processing
R_{ij}	Data rate between node i and node j
C_{ij}	Shannon Capacity of link (i, j)
d_{ij}	Distance between node i and node j
P_t^{ij}	Time-averaged transmitted power from node i to node j

N_0	Noise spectral density
P_r^{ij}	Time-averaged received power at node j from node i
R_i^t	Aggregate averaged transmitted data rate at node i
R_i^r	Aggregate averaged received data at node i
P_i	Time-averaged total power consumed at node i in omnidirectional network
α_r	Per bit energy cost for receiving data
α_0	Per bit energy cost for processing and storing received data
α_1	Per bit energy cost for storing and processing transmitted data
α_t	Per bit energy cost for transmitting data
η	Inverse of transmitting amplifier power conversion efficiency
P_{path}	Time-averaged source to destination path power consumption in omnidirectional network
d_i	Distance of the ith hop in a source to destination path
α	Total per bit energy cost for processing data
β	Total per bit transmission energy cost
P_i^{bf}	Time-averaged total power consumed at node i in directional network
P_{path}^{bf}	Time-averaged source to destination path power consumption in directional network
ρ_{max}	Maximum omnidirectional network hopping distance in fixed rate system
ρ	Transmission hopping distance
L_i	Distance between the ith source-destination pair in the network
$\bar{L}$	Average distance between all source-destination pairs under uniform traffic
ρ_{max}^{bf}	Maximum directional network hopping distance in fixed rate system
Λ_{lm}^{ij}	Rate of traffic from node i to node j carried by link (l, m)
d_{char}	Characteristic hopping distance of omnidirectional network
n_i^*	Optimal number of hops in the route of the ith source-destination pair
L_{max}	Maximum distance between all source-destination pairs under uniform traffic
d_{char}^{bf}	Characteristic hopping distance of directional network
v	Dimension of square cell in cell routing scheme
A	Area of square cell in cell routing scheme
$\boldsymbol{A}$	Network adjacency matrix
a_{ij}	Individual element of network adjacency matrix
$\underline{L}$	Network localization vector
l_i	Individual element of network localization vector

C	Network "cost" or "resource" matrix
c_{ij}	Individual element of network cost matrix
P	Permanently labeled set of the Dijkstra-based Widest Path Algorithm
D_i^t	Estimate of the widest path width from node 1 to node i on the tth iteration of the Dijkstra-based Widest Path Algorithm
ϕ_o	Initial angle of consideration for Algorithm 2
$\tilde{\phi}$	Angular increment for Algorithm 2
d_o	Initial radial range of consideration for Algorithm 2
$\tilde{d}$	Radial range increment for Algorithm 2
K	Set of next hop candidates for Algorithm 2

Chapter 1

Introduction

In recent years, wireless infrastructure has become widely prevalent and available to the end-user. This includes cellular base stations, private and public wireless access points, and even satellite gateways to access geosynchronous satellite communication systems. Wireless access to voice and data communication is becoming an embedded part of modern life; we expect to have instantaneous access to this technology wherever we are. However, this type of wireless access requires infrastructure and reliance upon a wired backbone network. Fig. 1-1 provides a basic schematic overview of the wireless communication world from an infrastructure-based point of view. All of the wireless end-user devices are connected through high-capability wireless infrastructure points, which are in turn connected to one another through a wired network grid.
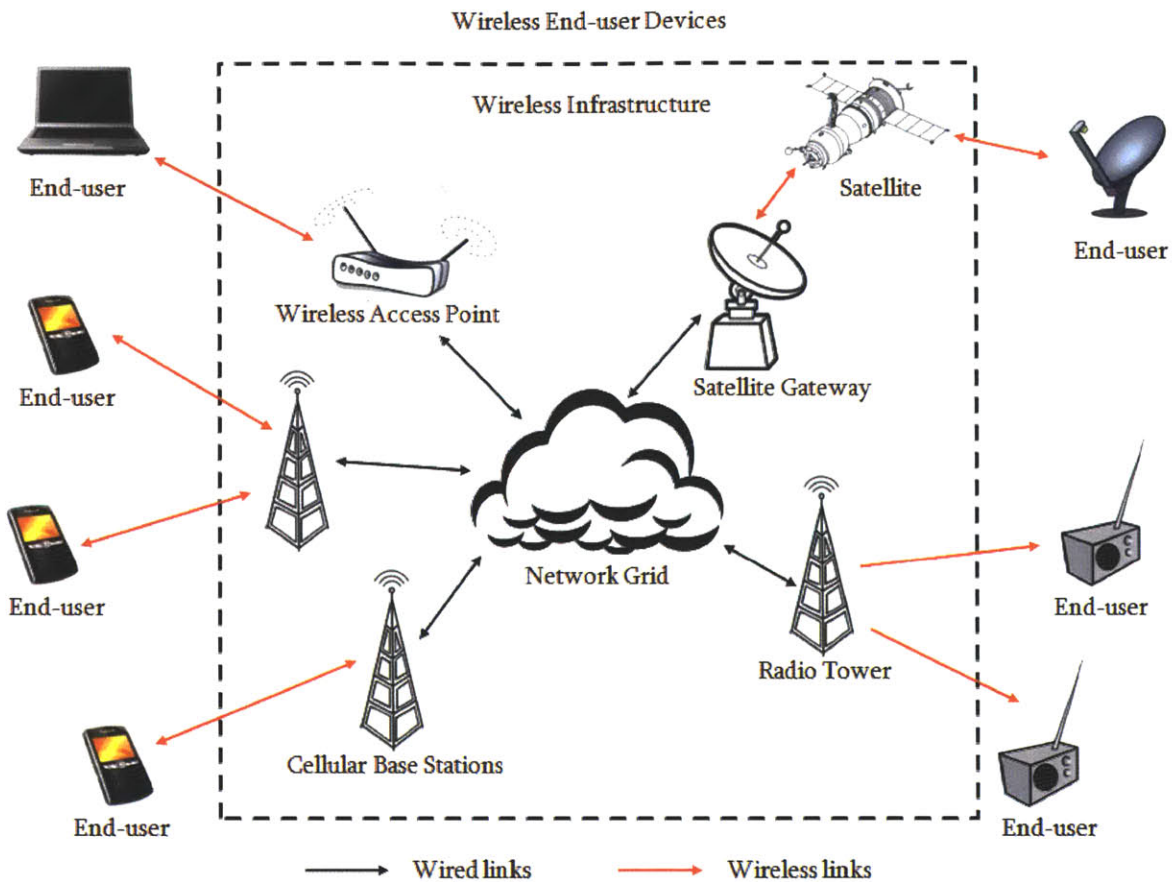
Figure 1-1: An infrastructure-based wireless network.

Future heterogeneous networks may need to incorporate infrastructureless wireless network technology alongside the traditional infrastructure-based wireless network access. A large body of work in wireless telecommunication has identified infrastructureless wireless networks as an alternative to wireless infrastructure-based networks where there is temporary and localized demand to communication capabilities and highly-contended or no access to infrastructure points of wireless communication access. Infrastructureless wireless networks are those which consist of end-user devices that can autonomously discover other devices in proximity and establish direct network connections with them, becoming data relays for source-destination pairs that cannot establish efficient one-hop connections. Fig.
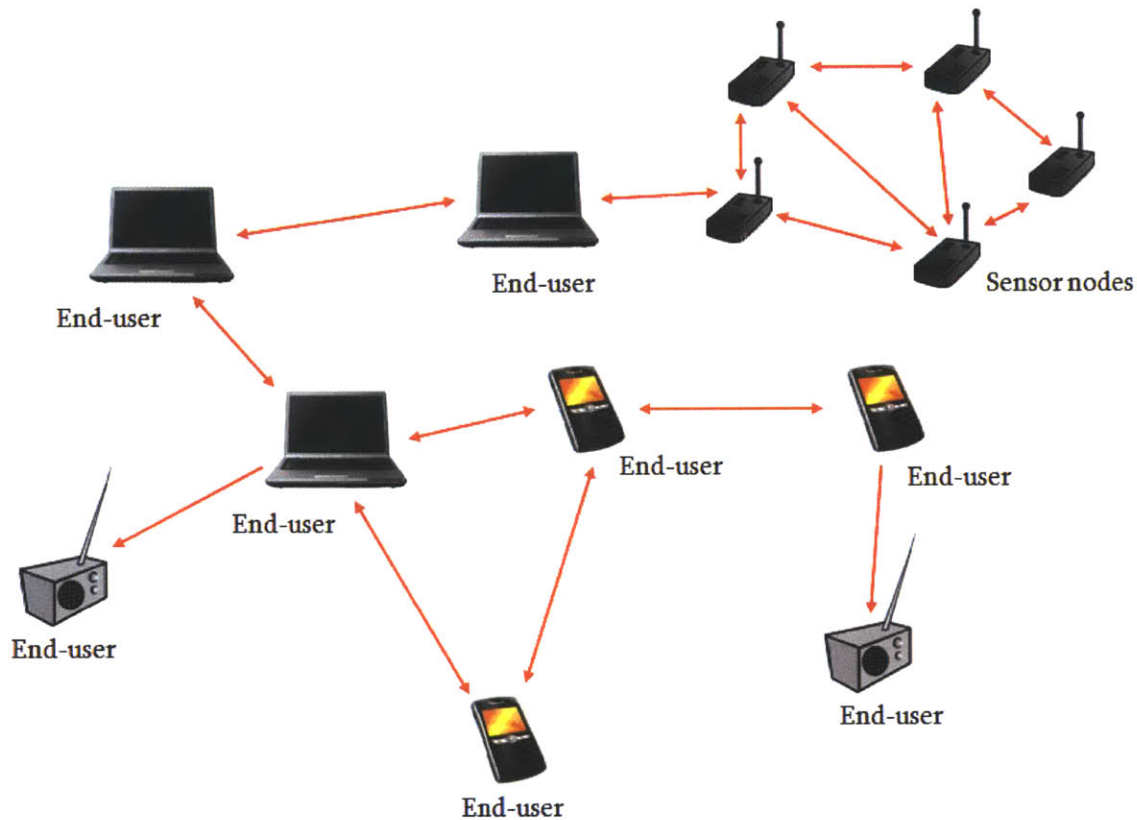
Figure 1-2: An infrastructureless wireless network.

1-2 shows a schematic example of an infrastructureless wireless network formed purely of wireless connections between autonomous, untethered wireless devices.

Since an infrastructureless wireless network does not rely on the availability of pre-deployed infrastructure, it can be rapidly deployed and autonomously configured in challenging environments where temporary communication capabilities are required. We now describe a few driving applications that create challenges for traditional infrastructure-based wireless networks and identify the need for this infrastructureless wireless network technology.

- **Wartime communications**—Future combat theaters may contain a large number of wireless communication devices, including personal handheld devices, communication devices affixed to ground and aerial vehicles, sensor nodes, and even

23

communication modules included in autonomous robotic units. In a foreign combat zone, a military force may not have access to local points of wireless communication infrastructure. Furthermore, pre-operation deployment of fixed infrastructure is often infeasible and undesirable as these points would both constrain operational flexibility and present tactical targets for destruction.

- **Disaster relief**—Natural causes may cripple local wireless communication infrastructure, making relief effort communication impossible through traditional wireless access points. In a scenario like this, emergency response teams need a way to coordinate the relief and rescue effort in a quick and efficient manner. It is normally mission-infeasible to first concentrate on re-establishing communication infrastructure, thus an autonomous infrastructureless wireless network is an alternative means for telecommunication ability for this localized burst of wireless device presence. A purely satellite-based network is not a viable alternative because of the high cost associated with this infrastructure.

- **Remote communication**—Some distant or underdeveloped regions may not have established wireless infrastructure. In this case, an infrastructureless wireless network can allow for increased communication reach into these areas without the need for the build-up of costly access points and wired connections, even if this is only used as a temporary means of network access to these locations.

We can additionally imagine that infrastructureless wireless networks could aid in relieving high user-demand on the limited infrastructure-based network resources by diversifying available communication options to the end-user device. For example, the gravity and urgency of a disaster relief scenario could lead to high network loading and severe contention at wireless access points, such that some users may be denied the communication capacity required to participate in the relief effort to those in dire need. The additional

availability of infrastructureless wireless communication could allow these blocked users to remain connected to those leading rescue and relief teams.

The benefits of an infrastructureless wireless network do not come without a price; successful deployment of these networks is impeded by many unsolved technical problems. There is increased computational and power demand on each end-user device, since end-user nodes in these networks must serve as relay points for communication in addition to acting as data sources and sinks. Further complexity arises from the volatile nature of the wireless environment, where an end-user may be powered down at any given time, any communication link along a path is subject to a multitude of wireless RF effects like fading, shadowing, and nearby device interference, and user mobility gives rise to rapidly changing network topologies. Catastrophically, a device may even move beyond the communication range of all other end-user devices and become temporarily or permanently partitioned from the network.

Many of the driving applications for infrastructureless wireless networks, including tactical military communication and disaster relief, require stringent quality of service (QoS) guarantees, particularly in data throughput, end-to-end message delay, and network power consumption. While throughput requirements may be low to moderate, needing only to support text-based messages, guaranteed instantaneous access to communication resources to support the transmission and relay of these messages may be required. Applications like these may demand higher levels of end-to-end message latency guarantees. Since stale information becomes useless in time-critical scenarios such as wartime and disaster relief communication, a message may have a lifetime of only a few seconds and thus must reach its recipient or recipients in the time scale of seconds or less. Network power consumption must be simultaneously considered alongside throughput and end-to-end delay performance since many untethered wireless devices that are part of an infrastructureless wireless

network rely on battery power. The need to be instantaneously connected to send or receive time-critical data messages means that devices must conserve power as possible to maximize device lifetime. These challenges, while difficult to meet, become impossible to consider without first addressing the issue of determining and maintaining infrastructureless wireless network connectivity. The ability to satisfy QoS requirements, particularly with respect to end-to-end sustainable data rate and message delay, is dependent first and foremost on network connectedness. Sustainable throughput and end-to-end delay guarantees to the end-user cannot be provided in a partitioned network. And if infrastructureless wireless networks are to become a widely-adopted communication modality in future commercial heterogeneous networks outside of these driving application examples, the ability to address network connectivity and, subsequently, end-to-end throughput and data latency guarantees will become increasingly important to satisfy the QoS demands of familiar civilian network applications, including real-time streaming video and financial trading.

1.1 Current and Proposed Approaches

The needs and challenges of the infrastructureless wireless network problem has led to research in ad-hoc mobile wireless networks (MANETs) that offer best-effort network connectivity (see [1,2]). Commonly, ad-hoc wireless networks refer to networks in which every device is capable of message forwarding and where messages may potentially take multiple wireless hops from the source node to the destination node. This framework often includes wireless sensor networks [3,4], which have enjoyed relative success. Work on MANETs has been active for nearly three decades. Despite large strides in many of the fundamental problems in the wireless ad-hoc network architecture, including physical layer issues, random access considerations, and network-layer routing, there has been limited

26

practical adoption of MANET architectures [5]. These networks are generally not designed to provide for QoS assurance. Devices in a MANET may be often disconnected due to the combination of low device density, end-user mobility, and the lack of an architecture that proactively seeks to maintain network connectivity and meet application and network demands.

The most prominent research effort to address the problem of infrastructureless wireless connectivity for mobile end-users has been Disruption Tolerant Networking. The Internet Research Task Force (IRTF) formed the Delay-tolerant Networking Research Group (DTNRG) in 2002 to propose an architecture and protocol design for network scenarios where instantaneous end-to-end network connectivity cannot be assumed [6,7]. This work further spawned the DARPA-funded Disruption Tolerant Networking (DTN) program in 2005 [8]. Motivated by interplanetary networking, this architecture is grounded in a store-and-forward networking approach, where each relay node stores incoming messages until communication opportunities present themselves and allow the message to be forwarded to the next hop along a path that will eventually reach the destination. While this approach is sensible in the interplanetary domain of orbiting celestial bodies and geosynchronous satellites, the DTN architecture does not consider providing assurance levels to QoS measures like end-to-end delay. Messages may be delayed within the network for long durations waiting for an appropriate communication opportunity in this architecture. Thus, DTN is only suitable for applications that are delay-insensitive, in stark contrast to the driving applications for infrastructureless wireless networks that we have discussed.

Whereas the DTN architecture makes no attempt to proactively maintain connectivity between mobile users in the network, [9] argues that service assurance in infrastructureless wireless networking environments can best be achieved by an architecture that proactively predicts potential network disconnections and responds by allocating resources to maintain

network connectivity. The author proposes two features of a proactive architecture that support throughput and delay QoS requirements: (1) network disconnection prediction using localization, trajectory prediction, and large-scale channel estimation and (2) topology control through the deployment of mobile relay nodes that provide support at areas of predicted network disconnection. The results presented by this work suggest that the ability to predict and proactively combat network partitioning is a keystone to providing QoS guarantees in the infrastructureless wireless network scenario. Adhering to this insight, the work of this thesis focuses first on possible improvements for infrastructureless wireless network connectivity, and the identified high-connectivity regimes are those that are of primary interest in subsequent analytical study.

In addition to the techniques introduced in [9], other approaches to address connectivity and QoS assurance issues in infrastructureless wireless networks have been proposed [10]. These include:

- **Beamforming**—This is a "smart antenna" technology that uses electronic signal processing techniques at the multi-element transmitting antennas to focus radiation energy towards the receiver through constructive interference, while providing receivers the opportunity to place nulls in the direction of interferers. Receiver array processing techniques also enable receive beamforming. These antenna array processing techniques can be used either to reduce required power allocation for a given transmission rate, to increase the achievable bit rate between a communication pair, or to increase transmitter reach, while leveraging directionality to reduce interference noise levels from other transmitters in the infrastructureless wireless network.

- **MIMO**—Diversity receivers and transmitters attempt to excite multiple independent wireless modes between the transmitting wireless device and the receiving wireless device when available. This technique takes advantage of wireless multipath effects

to achieve throughput gains without additional power or bandwidth allocation. This "smart antenna" technique requires the existence of RF reflectors and multiple stable paths, and thus may not be a feasible approach when end-user nodes are highly mobile or in an uncluttered RF environment where the only stable path between transmitter and receiver is line-of-sight (LoS).

- **New Transport Layer Protocol**—Transmission Control Protocol (TCP) is the primary transport layer protocol in today's Internet. Its attractive features include end-to-end reliability, congestion control, transmission rate control, and a notion of fair network resource allocation to different users. However, this protocol was designed for a stationary network topology composed primarily of wired links. It does not distinguish between congestion-based losses and losses resulting from wireless RF phenomena, and its functions break down under frequent losses that lead to underutilization of available network resources. A new protocol that addresses these inefficiencies in the heterogeneous network domain while preserving the goals of end-to-end reliability, congestion control, rate matching, and fair resource allocation would help to maintain high-throughput and low-delay end-to-end connections in the infrastructureless wireless network setting.

1.2 Scope of Thesis Work

Recognizing the need for improved connectivity in infrastructureless wireless networks in order to meet application QoS demands, this thesis focuses on a combination of electronic beamforming (the first of the proposed techniques mentioned at the end of Section 1.1) and the use of localization and channel state estimation, as in [9]. Directional transmission and reception using electronic antenna array processing techniques provides several significant

benefits in the infrastructureless wireless network domain that can be used to address the issues encountered in traditional MANET research, including:

- **Reach**—By focusing the antenna power radiation pattern in a localized direction of interest, the communication range of a power-constrained fixed transmission rate end-user can be extended beyond that of a fixed rate transmission device using an omnidirectional radiator.

- **Data rate/power tradeoff**—At the same transmit power level, a communication pair can exchange information at a higher bit rate than if they were using omnidirectional antennas. Alternatively, a communication pair can exchange information at a particular bit rate while using less power for data transmission than if they were using omnidirectional radiators.

- **Pass-through traffic reduction**—Given the increased transmitter reach in a fixed transmission rate system, beamforming-enabled nodes are able to forward messages along a route that eliminates unnecessarily short intermediate hops required of a network using only omnidirectional antennas with identical transmission power constraints. This, in turn, decreases the pass-through traffic load on intermediate end-user devices that would have to act as data relays in the omnidirectional network case.

- **Interference suppression**—Focusing energy in the direction of the intended receiver reduces the interference levels at ancillary receivers in the network outside the main beam (and any significant side lobes), thus reducing interference noise and overhearing when compared to the omnidirectional network in which transmitted power is radiated equally in all directions regardless of the intended receiver location.

- **Interference nulling**—A receiving end-user can strategically place nulls to cancel out energy from nearby interfering end-users or other radiating devices.

- **Spectrum reuse**—Focused radiation patterns allow neighboring network nodes to transmit to separate receivers on the same frequency channel without creating unwanted interference at the receivers.

This work focuses on a power-limited network model, which is in contrast to related work in the area that considers an interference-limited network model (as made famous by [11]). The interference-limited model is well-studied in the context of infrastructureless wireless networks, including some results using beamforming-enabled end-user nodes [12]. Bandwidth scaling is a physical layer system option that has been shown to improve the scalability of network performance with respect to sustainable throughput, end-to-end delay, and network power consumption. Given large enough system bandwidth, network performance is limited by the end-user power consumption rather than the interference and overhearing levels at the receiver. Bandwidth scaling is used as an analytical technique here since it allows our results to focus on the effects of increasing the probability of network connectivity with beamforming-enabled end-user nodes.

This work considers an infrastructureless network of power-limited wireless devices equipped with localization capability, Global Positioning System (GPS) hardware for example, and multi-element antenna arrays or apertures capable of transmit and receive beamforming. While long-accepted as an important feature in satellite communication [13], multi-element antenna arrays and transmit and receive beamforming have recently been shown to provide gains in achievable capacity in the infrastructureless wireless setting [14]. Furthermore, node localization information has been shown to provide throughput and end-to-end latency gains in infrastructureless wireless networks when combined with a strategy that can exploit this information to promote network connectivity [9]. In our context, localization information is required for a transmitting node to focus its transmission beam in the direction of the intended receiver, and antenna array processing can be viewed as a

strategy to exploit user location information to promote network connectivity by overcoming RF effects and the disconnection of nodes that lie beyond the reach of an omnidirectional network. The combination of these techniques creates an improved network topology that can address core service traffic demands through improved connectivity and, subsequently, achievable throughput, end-to-end delay, and power consumption.

1.3 Thesis Organization

The following is a brief description of the organization of this thesis.

Chapter 2 introduces the assumptions, models, and technologies that are used throughout the work. Specifically, it describes the RF and channel model used in the network analysis, an overview of beamforming and the associated transmission model, and a condensed overview of localization technology that could be used to provide geolocation information to the network end-users.

Chapter 3 considers the improvement in infrastructureless wireless network connectivity from beamforming in randomly deployed networks of a finite number of stationary end-user nodes. The analysis is done in both one and two dimensions. This study identifies regimes of high probability of connectivity, which is of interest in subsequent chapters that study the scaling behavior of QoS metrics.

Chapter 4 examines the scaling behavior of throughput, end-to-end delay (in terms of number of end-to-end hops), and energy consumption in power-limited infrastructureless

wireless networks with beamforming-enabled end-user devices and large-enough system bandwidth. After characterizing capacity bounds of these networks for any arbitrary topology of a finite number of end-users, we show that the throughput-optimal scaling behavior can be achieved alongside the delay-optimal and per bit energy-optimal scaling behavior, all of which are independent of increasing end-user device density.

Chapter 5 develops routing algorithm solutions for both the omnidirectional and directional infrastructureless wireless network that optimize over individual QoS metrics of interest. Insight from Chapter 4 is then employed to develop a heuristic routing algorithm that achieves the scaling-optimal behavior for all QoS metrics of interest simultaneously.

Chapter 6 provides a summary of the thesis results and discussion of possible future research topics.

Chapter 2

Models, Assumptions, and Technologies

We consider wireless infrastructureless networks with beamforming-enabled end-user nodes and their capability to provide some level of QoS guarantees that will enable this type of network to be used for scenarios and applications with stringent service requirements. Whereas similar work has focused on the addition of autonomous helper relay nodes to promote connectivity for delay-sensitive services [9], we are interested in addressing instantaneous network connectivity and QoS performance using array or aperture antennas and onboard signal processing technology, along with geolocation information in order to extract the full benefit of beamforming-capable antenna systems. Otherwise, the wireless infrastructureless network that this work considers is the same as traditional MANETs: the network is a set of wireless end-user devices that autonomously form a network in a given operating environment and then proceed to generate, sink, and forward data as necessary.

We note that this work does not consider end-user mobility in the presented analysis. Although the mobility of untethered wireless devices is an important feature of an infrastructureless wireless network, we can see this stationary network deployment analysis as a snapshot of a dynamic network on an appropriate time scale with respect to the degree of node mobility. Considering the probability of connectivity and network QoS performance behavior of these stationary snapshots is necessary before including an end-user mobility model as part of the analysis.

This chapter has several goals. First, we explain exactly what kind of service we wish to provide to end-users through this type of infrastructureless wireless network. Second, we discuss various models that are used throughout the remaining chapters to facilitate analytical study of the proposed system. This discussion of models focuses on the RF environment and channel model that we use throughout, along with the antenna and transmission model that is employed when discussing beamforming-enabled end-user devices. To this end, we begin by discussing beamforming in general, which motivates the transmission model. Our work requires an additional network power consumption model. However, the development of this model is deferred to Chapter 4, where it is required for the analysis presented. Finally, the last part of this chapter touches upon localization technology, another tool that we assume to be at the disposal of the end-user devices in our network.

2.1 Core Services

In proposing an infrastructureless wireless network design capable of supporting throughput- and time-critical data applications, we need to distinguish the class of service that we are considering. In general, there are two main classes of service: best-effort and guaranteed QoS (or "core"). Best-effort services are for those messages without stringent requirements on throughput and end-to-end latency. Core services provide for mission critical messages that come with a pre-specified set of QoS requirements that need to be satisfied, such as required throughput and end-to-end latency. Core services messages are given priority over those in the best-effort class. Considering the applications discussed in Chapter 1, these core service messages may include critical military commands to be disseminated to a unit of troops or time-sensitive alert messages to be distributed to relief workers aiding response teams after a natural disaster.

Since core services are at the forefront of consideration in this work, the next chapter is dedicated to analyzing how the use of beamforming-enabled devices can improve instantaneous network connectivity for fixed rate transmission systems. A connected network is a prerequisite for providing QoS performance guarantees to end-users. In the absence of connectivity, the network throughput is zero between at least one end-user pair and the end-to-end message delay can be considered to be infinite between at least one end-user pair. A disconnected, or partitioned, network is a catastrophic condition when viewed in the context of the driving applications we have discussed.

As discussed in [9], instantaneous network connectivity is often ill-defined in the wireless setting. For variable rate transmission wireless systems, all pairwise end-users are theoretically connected and able to communicate in an obstacle-free RF environment, even

though the data rate they can support becomes arbitrarily small as the physical distance between the pair of nodes increases. Given an increasingly long interval of time, two users can exchange a finite length message even as their separation distance grows unbounded. We note that this is a theoretical scenario. In reality, there are device hardware limitations on the power threshold required for reception. Even so, an increasingly long interval of time is not a luxury that we can assume to have in a network intended to provide core services. For fixed rate transmission systems, users must communicate at a set rate when they exchange data. This imposes a limit on the range of a transmitter assuming that we have some transmission power constraint at the sender (a realistic constraint for a wireless system of untethered end-user nodes). It is in this type of fixed rate transmission system that we primarily discuss the metric of instantaneous network connectivity, since connectivity is a first requirement for providing core services. Throughout this work, we distinguish between fixed rate and variable rate transmission systems when necessary.

2.2 The RF and Channel Model

Before coming to beamforming and the transmission model, we begin with a discussion of the RF environment and channel model used in this work. These are necessary to understand the directional antenna transmission model that is discussed in the subsequent section.

2.2.1 Empirical Channel Model

For analytical simplicity, we assume that our networks operate in a simple one- or two-dimensional RF environment free of specific obstructions, absorbers, and scatterers. In a real world scenario, all of these would need to be considered based on the specific deployment environment, as they contribute to important time-varying wireless effects: shadowing and fading.

Instead, we focus on a simple and commonly-used empirical model for system analysis, the path-loss model. In free space, it is known that signal power at the receiver is inversely proportional to the square of the distance between transmitter and receiver. However, should there be imperfections in the RF environment, this relationship may not hold. The path-loss model combines the effects of typical propagation losses along with absorption and diffraction losses that may arise from an imperfect RF environment. We assume that our receivers are in the antenna far-field (a distance of more than $\frac{2D^2}{\lambda}$ from the transmitter, where D [m] is the transmitting antenna aperture size and λ [m] is the signal wavelength). Then the path-loss model describes the power loss factor between the transmitter and receiver in dB:

$$\frac{P_r}{P_t} [\text{dB}] = 10 \log_{10} \gamma - 10k \log_{10} \left(\frac{d}{d_0}\right) \tag{2.1}$$

where P_r [J/sec] is the received power, P_t [J/sec] is the transmitted power, and their ratio is the power loss factor. In (2.1), k is the path-loss exponent (sometimes called the attenuation exponent), usually in the range of $2 \leq k \leq 6$, where $k = 2$ is free space propagation loss only, and $k = 6$ can be reached in some indoor environments. Furthermore, d [m] is the distance between transmitter and receiver, d_0 [m] is the reference distance (usually set to $d_0 = 1$, as we use it throughout this thesis) and γ is a constant accounting for system losses that is a function of both frequency and antenna gain [15].

39

The parameters of this model can be estimated either from theoretical analysis or empirical measurements. Throughout this work, we assume the existence of a homogeneous RF operating environment and that each end-user node is capable of making an estimate of the path-loss exponent in the particular operating environment. We also assume a homogeneous end-user device set throughout, and thus we allow γ to be a constant for all nodes in the network. Finally, the value of d between any communicating pair is known to the network end-user devices since localization information is available to each node (see Section 2.4 on localization technology).

This model fails to account for important wireless RF phenomena that would realistically impact the system. Key parameters of a more sophisticated statistical channel model, such as shadowing and fading, are absent. These effects are typically modeled as random variables of particular statistics that are added to the path-loss model shown in (2.1). There is a large body of literature dedicated to studying different statistical channel models (see [15-28]). However, the parameters of these models are heavily dependent on the operating environment and communication frequencies used. While allowing for a more detailed description of the wireless channel, a more sophisticated channel model is not required for the analysis in this work. The use of the basic path-loss model here aims for simplicity and first-order intuition.

Alternatively, it is possible to use site-specific models for the wireless channel estimates. These models utilize detailed knowledge about RF obstacles in a given operating environment that are gathered a priori from available resources (such as maps and blueprints) or learned during system operation (such as with sensors designed to detect and map environmental obstacles). The interested reader is referred to Section 2.2.1 of [9] for a

concise overview of these models and methods. However, these more specific channel models are not pursued further in this work.

2.2.2 A Power-limited Network

A bulk of the literature analyzing wireless infrastructureless networks focuses on narrowband systems (such as [11]). These systems are deemed interference-limited, since it is the signal interference from nearby transmitters that dominate the noise levels at the receivers. Wireless infrastructureless networks using directional antennas have been studied using this framework [12]. The work of Dai in [9] shows that significant improvements to network scalability through bandwidth scaling, where interference levels become negligible with the availability of large enough system bandwidth and appropriate channelization. In this regime, called the power-limited regime, the network performance is limited by the power available to each node.

Following this analytical lead, we consider wireless infrastructureless networks operating in the power-limited regime by assuming the availability of sufficiently-large system bandwidth. Analyzing network performance in the power-limited regime shows the best that we can achieve with the network architecture, since the inclusion of interference effects at the receivers will reduce achievable performance capabilities despite the ability of antenna arrays to null interfering signals. Analysis of the power-limited network gives an "upper bound" on system performance, although network performance can closely approach this upper bound with effective beamforming.

In the power-limited regime, we assume the availability of at least $n(n-1)$ available frequency channels for a network with n end-user devices, such that each possible communication pair shares its own pair of unique communication channels. This channelization suppresses the effect of unwanted interference and overhearing at the receivers. For analysis, we model this as the limit of large bandwidth ($W \to \infty$, where W is the system bandwidth). We assume that appropriate channel coding is used such that the capacity between any given pair of nodes is upper bounded by the Shannon Capacity for an additive white Gaussian noise (AWGN) channel.

2.3 Beamforming and the Transmission Model

The primary objective of this work is to compare the performance of an infrastructureless wireless network with end-user nodes equipped with beamforming-enabled antennas to one with end-user nodes using only omnidirectional transmit and receive antennas. To this end, we discuss a transmission model for the beamforming-enabled node that allows us to develop a comparative analysis between the two cases. This section first discusses beamforming technology generally, both from the transmission and reception ends. Then it develops the abstract model that we employ throughout the remainder of the work to distinguish between the two different network scenarios.

2.3.1 The Antenna Model

In this section, we distinguish between two main types of antenna models: the omnidirectional model and the directional model. The performance of an infrastructureless wireless network with nodes using omnidirectional transmit and receive antennas is well-studied and is considered as a baseline for comparison throughout this work. The directional beamforming antenna model is further subdivided into two categories: discrete element and continuous aperture. This follows the analytic presentation for antenna beamforming performance in infrastructureless wireless networks in [14].

We begin with the omnidirectional antenna model. This work analyzes infrastructureless wireless networks in both one- and two-dimensional scenarios. Regardless of the dimensionality of the operating area, we assume that end-user nodes use isotropic point-source radiators to produce a spherical radiation pattern. The isotropic point-source radiator is a theoretical antenna construction with absolute uniformity over its radiation pattern. Brouwer's hairy ball theorem of algebraic topology shows that a continuous vector field of uniform magnitude cannot be everywhere tangent to a sphere, thus proving that the ideal isotropic radiator is not a realizable entity [29]. However, this ideal radiator is often assumed in literature on omnidirectional antennas and is used to define directive gain, thus it is an acceptable model for the antennas used in the baseline omnidirectional network.

For the directional antenna model, we begin by considering an array of identical antenna elements that can concentrate power in an arbitrary direction in a two-dimension operational plane. The simplest antenna array geometry that can achieve this rotational symmetry in the plane is a uniform circular antenna array (UCAA). Each UCAA is made of N_E discrete and identical antenna elements, indexed $i \in \{1,2, \ldots, N_E\}$, equally-spaced around

a circle with radius R [m] (see Fig. 2.1). Each element is modeled as an infinitesimally small isotropic radiator as used for the omnidirectional antenna. The radiation pattern created by this array is then a linear superposition of the fields radiated by each point-source, which is called the array factor. The array factor captures the interference pattern among all the radiators, which also incorporates the antenna geometry and spacing of the antenna elements. The goal of beamforming is then to adjust the signal amplitudes and delays at each radiator such that the interference radiation pattern is maximized in the desired direction of signal transmission rather than over the entire sphere as for the single isotropic point-source radiator. We assume that there is no mutual coupling between the point-source radiators in the array for simplicity, however it should be recognized that mutual coupling effects could distort radiation patterns once the elements are packed in such a way that element spacing is less than $\frac{\lambda}{2}$.

Given our assumption of no mutual coupling between antenna elements and a fixed array radius R, the antenna construction can be theoretically packed with an arbitrarily large number of infinitesimally-small point-source elements. As $N_E \to \infty$, we effectively get a model for a continuous ring aperture antenna (see Fig. 2.1). So we consider a continuous ring aperture antenna as a limiting case of the UCAA for the directional antenna model that can achieve full rotational symmetry in the network operating plane. It turns out that regardless of the exact directional antenna construction (UCAA or ring aperture), we use the same transmission model. This is discussed in detail in Section 2.3.3.
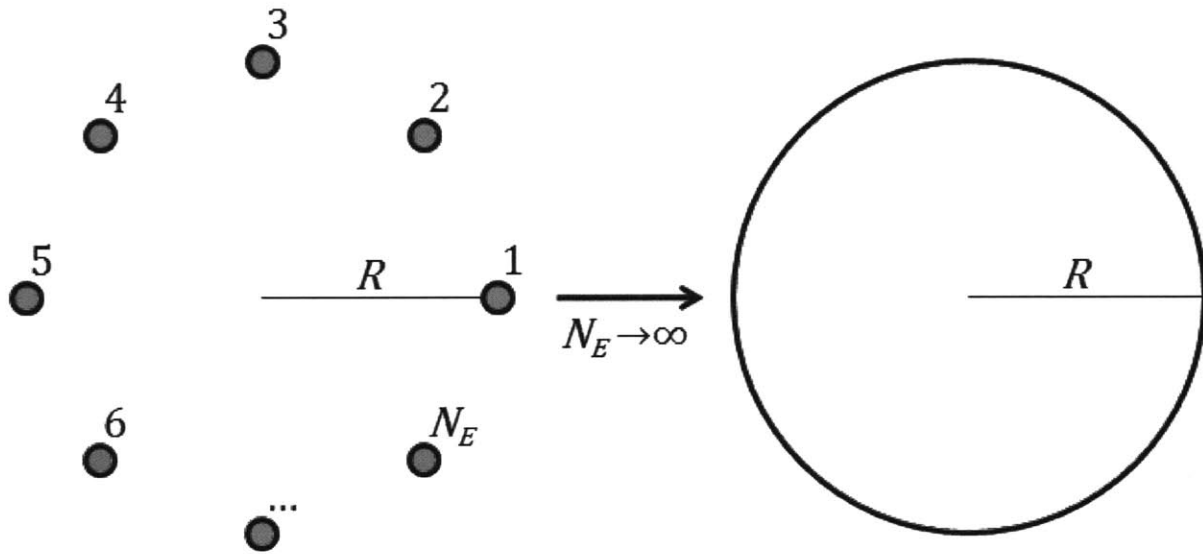
Figure 2-1: The uniform circular antenna array (UCAA) geometry with N_E discrete isotropic radiator antenna elements, and the continuous ring aperture antenna as a limiting case of the UCAA.

2.3.2 Aperture and Array Beamforming Overview

A beamforming antenna array (or aperture) is multiple antenna element system that is capable of forming a radiation pattern with high gain in a desired direction while minimizing the antenna gain in undesired directions. Fig. 2-2 shows a typical beamforming radiation pattern for a UCAA in the operating plane of interest. This is in stark contrast to an omnidirectional antenna system, which radiates power equally in all directions, regardless of the direction of interest for communication.

Normalized UCAA Beampattern
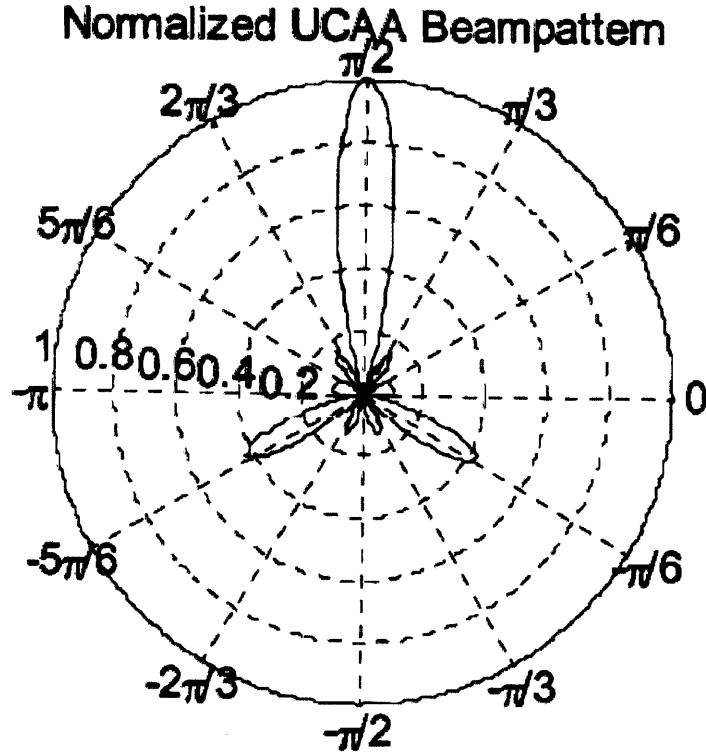
Figure 2-2: Beam pattern in the network operating plane for a UCAA with $N_E = 9$ [14]. The direction of maximum gain is normalized to unity.

The beamforming radiation pattern (or beam pattern) is generated by controlling the phase and amplitude of the field at the different elements of the antenna array (or by adjusting the phase and amplitude over the antenna continuum when considering a continuous aperture antenna design). Not only does the signal amplitude and phase at each element affect the radiation pattern, but the antenna geometry does as well. As mentioned in the previous section, we focus on a UCAA or ring aperture antenna since they are able to produce a beam pattern with complete rotational symmetry in the network operating plane purely by adjusting the signal at each element of the antenna array or over the antenna continuum (in other words, without any mechanical antenna steering).

To mathematically describe beamforming, we consider a UCAA or ring aperture antenna of radius R centered at the origin of the x-y plane transmitting to other end-user nodes with identical UCAAs or ring aperture antennas also lying on the x-y plane. Using spherical coordinates for notational simplicity, we let $U(d, \theta, \phi)$ be the radiated field from the transmitter measured at the location (d, θ, ϕ). The total time-averaged radiated power by the transmitter, P_{rad} [J/sec], is given by:

$$P_{rad} = d^2 \int_0^{2\pi} \int_0^{2\pi} |U(d, \theta, \phi)|^2 \sin\theta \, d\phi \, d\theta. \qquad (2.2)$$

Directive gain, $G(\theta, \phi)$, is defined as the ratio of the power along a specified radial (θ, ϕ) to the total power radiated over 4π steradians (this can be seen as normalizing the radiated power in the specified radial by the power radiated in the radial if the transmitter were an isotropic radiator using the same transmit power):

$$G(\theta, \phi) = \frac{|U(d, \theta, \phi)|^2}{P_{rad}/4\pi d^2} = \frac{4\pi |U(d, \theta, \phi)|^2}{\int_0^{2\pi} \int_0^{2\pi} |U(d, \theta, \phi)|^2 \sin\theta \, d\phi \, d\theta} \qquad (2.3)$$

where the second equality follows from (2.2). The antenna directivity is defined as the maximum directive gain, denoted D. Thus, D is defined as:

$$D \triangleq \max_{(\theta, \phi)} G(\theta, \phi). \qquad (2.4)$$

Reference [14] proceeds to derive the radiated field from a UCAA and continuous ring aperture using conventional beamforming weights (uniform amplitude determined by the maximum average radiated power constraint with phase shift that varies along the curvature of the antenna array or aperture). The directivity of a ring aperture antenna is well-studied and can be found in many textbooks on antenna theory and array processing (see [13,30]). However, this direction of maximum directivity is along the z-axis for a ring aperture centered at the origin of the x-y plane. In our problem, we are interested in the maximum

47

directive gain with the constraint that $\theta = \frac{\pi}{2}$ (the field radiated in the x-y plane to other users in the same plane). In [14], it is shown that while a simple closed-form expression for the directivity of the UCAA or ring aperture antenna cannot be found given this constraint, numerical results allow for an easy approximation to the directivity for each type of antenna. For a UCAA, it is shown that the directivity is approximately equal to N_E up to a point where the element density becomes large enough and the antenna construction approximates the continuous ring aperture antenna. This point of element saturation is denoted N_{sat}. Explicitly, the directivity of the UCAA, denoted D_{array}, is approximated as:

$$D_{array} \cong \begin{cases} N_E, & N_E \leq N_{sat} \\ N_{sat}, & \text{otherwise} \end{cases} \tag{2.5}$$

where N_{sat} is approximated as:

$$N_{sat} \cong \left\lceil \frac{4\pi R}{\lambda} \right\rceil = \left\lceil \frac{2\pi R}{\lambda/2} \right\rceil. \tag{2.6}$$

The author of [14] makes the interesting observation that the second equality of (2.6) corresponds to an element spacing of $\frac{\lambda}{2}$ along the circumference of the antenna array, which is the number of discrete elements required to sample the continuous ring aperture at the appropriate spatial Nyquist rate. Since the UCAA approximates the continuous ring aperture once the number of elements has exceeded N_{sat}, [14] also shows numerically that the directivity of the ring aperture antenna constrained to the x-y plane, denoted $D_{aperture}$, can be approximated as:

$$D_{aperture} \cong \frac{4\pi R}{\lambda}. \tag{2.7}$$

In our transmission model, the antenna directivity is a key parameter, but the distinction between a UCAA and a ring aperture antenna is lost in the model. Thus, we actually allow the underlying antenna geometry and construction to be arbitrary as long as it allows for

electronically-steerable rotational symmetry in the network operating plane like the UCAA and ring aperture antenna described here. Correspondingly, we denote the directivity of this transmitting directional antenna, constrained to the operating plane (equivalently, for $\theta = \frac{\pi}{2}$), as D_{tx} from this point on in our work.

As shown in [14], the receive beamforming problem is symmetric to transmit beamforming. Using a similar conventional beamforming phase shift pattern on the receiving UCAA or ring aperture antenna, we can realize a receive directional gain just as in the transmit case. Unlike a traditional steered receive antenna that must know a priori which direction the transmitted field is arriving from, processing techniques at the receiver allow receive beamforming to be implemented by solving for the largest eigenvalue in receive antenna element correlation matrix without this a priori knowledge [31]. This reduces required network overhead to set up communication between a transmitter-receiver pair. The transmitting node knows where the receiving node is located and steers its transmitting beam in the direction of the receiver. The receiving node does not need to be aware that the transmitting node transmitting. It can use post-processing to discover the direction of arrival of the transmitter's signal and leverage receive beamforming gain. We note that receive beamformers are not limited by a time-averaged radiated power constraint like the transmitting device. Receive beamformers have the additional ability to place nulls in the direction of undesired interferers to reduce perceived noise and interference levels. As mentioned in Section 2.2.2, our work is concerned primarily with the power-limited network regime and not the interference-limited regime. Thus, we do not leverage the use of receiver null formation in our analysis. In fact, throughout this work, we normalize the receive directivity in the network plane of operation (as in [32]). This means that the receive gain is unity in the direction of interest and less than unity in all other directions. This normalization is intended to make the analysis more tractable and highlight the dependency of the results on the transmit directivity parameter. However, one should bear in mind that

a receive directivity gain can easily be included in the presented analytical framework by adding another gain term, D_{rx}, that represents the signal power gain at the receiving antenna array or aperture.

2.3.3 The Transmission Model

We now proceed to combine transmit beamforming with our previously discussed channel model to develop a more abstract transmission model that can be used in our network analysis to compare a network using omnidirectional transmission antennas with a network using directional transmission antennas.

We begin by considering an end-user device equipped with an omnidirectional transmission antenna. As discussed in Section 2.3.2, this antenna radiates power uniformly in all directions, but we are only concerned with a one- or two-dimensional operating scenario. Thus we can imagine a node that radiates power uniformly in a circular pattern in the plane on which the device lies, which we continue to refer to as the x-y plane. We place a maximum time-averaged radiated power constraint on the end-user node. For a variable rate transmission system, such a node can theoretically communicate with any other node at any arbitrary distance, although the data rate it can sustain decreases with increasing physical separation. In the fixed rate transmission scenario with the assumption of a homogeneous RF operating environment, we can conclude that a transmitting end-user device has a limited range in which its signal can be successfully received and decoded at the specified fixed rate. This reduces our omnidirectional transmission model to the popular disk model that is frequently considered in network performance analyses [11,33]. We denote the range

of the end-user node with an omnidirectional transmission antenna in the fixed rate transmission system as r [m], and this is represented visually in Fig. 2-3.

Using the omnidirectional transmission model as the baseline, we develop the directional transmission model for an end-user node equipped with a directional antenna array or aperture with transmit directivity D_{tx}. We reiterate that the receive gain is normalized to unity in the signal direction of arrival. Also, we retain the same maximum time-averaged radiated power constraint on the transmitting node as in the omnidirectional case. In a variable rate transmission system, each node is again theoretically connected to any other node, although the rate that can be sustained between the pair decreases as the physical separation between them increases. However, the transmitter directivity allows for a higher sustainable data rate between the pair than in the omnidirectional case at the same node pair separation distance (and same time-averaged radiated power constraint). In the fixed rate transmission system, using the simple path-loss channel model discussed in Section 2.2.1 and assuming a homogeneous RF operating environment such that the path-loss exponent k is the same everywhere, we can derive the following relationship for the transmission range of the beamforming-enabled end-user device, denoted r_{bf} [m]:

$$r_{bf} = rD_{tx}^{1/k} \qquad (2.8)$$

where r is the omnidirectional transmission range in the fixed rate transmission system as previously discussed. The full derivation of (2.8) is presented in Appendix A. Since we only consider unicast communication in this thesis, we can continue to use the disk model for analysis of the directional infrastructureless wireless network if we allow the beamforming-enabled end-user node to steer its transmitting main beam in an arbitrary direction in the operational plane. This disk model for the directional transmitter does not work if we consider multicast or broadcast transmission scenarios. By focusing on the range of signal transmission, this transmission model does not account for the main beam width (as seen in the beam pattern of Fig. 2-2). The described transmission model and the difference between

51

the omnidirectional and directional case is illustrated in Fig. 2-3. The normalized directional

transmission range, $\frac{r_{bf}}{r}$, is shown as a function of D_{tx} in Fig. 2-4.

2.3.4 Beamforming Pitfalls

While the objective of this work is to reveal the potential gains of beamforming in an infrastructureless wireless network in terms of connectivity, throughput, and end-to-end delay, this technology does come with some points of caution that the network architect must consider for specific network designs and deployments. First, the use of both transmit and receive beamforming requires computationally intensive signal processing and matrix operations. This requires that end-user devices meet some minimal requirement on computational ability. The use of these techniques additionally consumes more processing power at each network hop. Second, the efficient use of electronic beam steering requires the additional overhead of equipping each end-user node with some localization technology, which we discuss more in the next section. It also requires nodes to exchange location data as part of the network management data overhead. Finally, the use of transmission beamforming may actually degrade system performance in some cases where the RF environment is not the ideal unobstructed environment free of absorbers, reflectors, and scatterers that we assume in this analysis. In these scenarios, we cannot assume the existence of an unobstructed line of sight (LoS) path. For example, we can consider a situation where the LoS between a node pair is blocked by an opaque RF obstruction, yet there is an indirect path using an RF reflector between the two. Using localization information to point the main beam directly at the receiver in this case would result in the failure of signal penetration. However, if the transmitter had been radiating the signal uniformly in all directions as with an omnidirectional transmission antenna, the indirect path using the
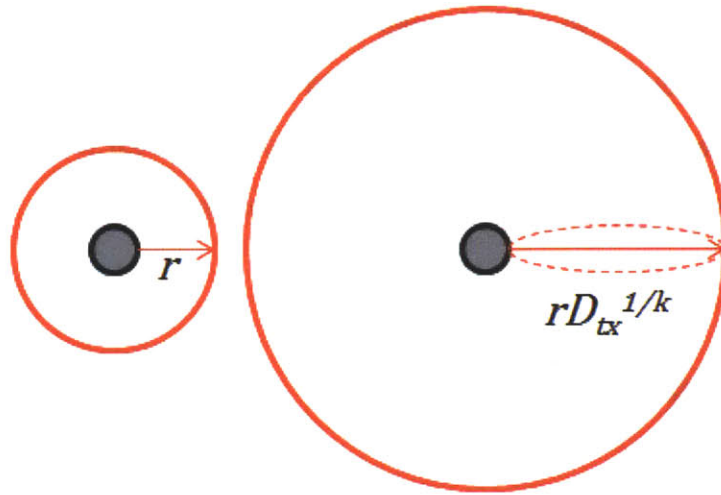
Figure 2-3: Comparison of the omnidirectional transmission range model (left) and the associated directional transmission range model (right) for fixed rate transmission systems. While the beam pattern of the directional antenna does not radiate power uniformly in all directions at any given time, the main beam can be steered electronically to achieve this depicted range in any desired direction in the plane of operation. We note that this transmission range model suppresses the width of the main beam as well as any radiation pattern side lobes, although the main beam is shown by the dotted line in the model.
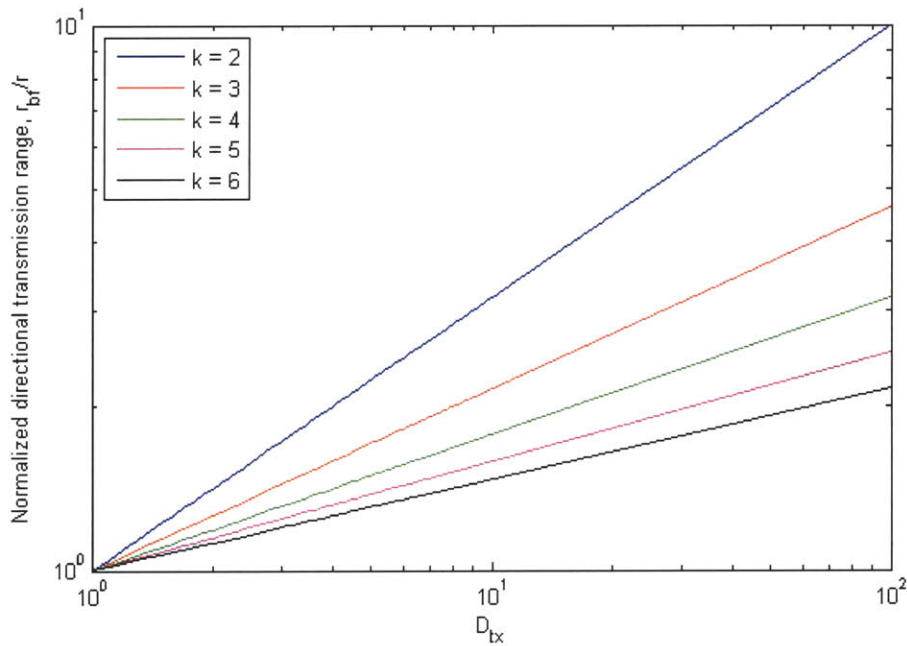
Figure 2-4: Directional transmission range normalized by the omnidirectional transmission range, $\frac{r_{bf}}{r}$, as a function of the transmitting antenna directivity, D_{tx}, for fixed rate transmission systems and for different values of the attenuation exponent, k.

53

reflector could be leveraged to achieve some data rate between the two end-user nodes. Thus, in heavily obstructed operating environments, the direction of signal transmission would need to be determined by feedback or reciprocity to find and excite the optimum transmission mode rather than relying on localization information.

2.4 Node Localization

Knowledge of the location of network nodes helps leverage beamforming to improve network connectivity and employ location-based routing schemes (as we discuss in Chapter 5). To this end, we assume the availability of node localization information (with a sufficiently small error range) in our infrastructureless wireless networks. This section provides a brief overview of some of the localization technology that is available to the network architect, although the analytic results presented in this work are technology-independent as long as the localization information is accurate enough for transmitter beam steering.

2.4.1 GPS Systems

The Global Positioning System (GPS) is a system of satellites in medium Earth orbit designed in a way such that there are at least four satellites visible by any point on Earth at any given time (assuming no physical obstructions are present). A GPS ground receiver captures the periodic beacon information with time and location information from each of these visible satellites in order to synchronize its clock and compute its location through trilateration.

Augmented GPS systems, such as Differential Global Positioning System (DGPS), have been designed to increase the accuracy of GPS by using wireless ground terminals at known locations in addition to the satellite constellation. Although the system is widely used and allows for a relatively high degree of accuracy, a major problem with relying on GPS is the lack of service when the LoS between the GPS satellites and ground receivers has been obstructed (such as for indoor environments) [34].

2.4.2 Beamforming-based Localization Techniques

In some non-commercial networks, particularly military networks, there is a desire to determine location without relying upon easily-jammed systems like GPS. In these networks, we can use the receive beamforming techniques discussed in Section 2.3.2 to gather location information about network end-user devices. Specifically, if end-user devices are equipped with omnidirectional transmitters, then nodes can beacon at some known power level on their specified frequency channel. Beamforming-enabled receivers can then solve the received power correlation matrix formed by considering the signal arriving at each antenna element to find the eigenvalues and eigen-rates corresponding to user locations. This solution provides the receiver with the direction of arrival of the signal and the received signal power level. If we assume network operation in a homogeneous RF environment, then the received power level can be used to determine the distance between the transmitter and the receiver. Combining the signal direction of arrival with the calculated distance, the receiving node can determine the location of the transmitter with respect to its position. If all nodes participate in this process and then exchange information with each other, they can synchronize information and map out the relative locations of all end-user devices in the network [31].

2.4.3 Inertial Navigation Systems

Another option that does not require the use of GPS is an Inertial Navigation System (INS), which uses a combination of inertial sensors (accelerometers and gyroscopes) to measure acceleration and rotation about each of its axes with respect to some common reference frame. The output of these sensors is combined to calculate the location of the INS-enabled device with respect to some known starting location. The rapidly-increasing availability of microelectromechanical systems (MEMS) sensor modules has made this a popular choice for position tracking in missile, submarine, and satellite systems. However, INSs are subject to mechanical imperfections, vibrations, temperature fluctuations, and drift, which accumulate over time and must be corrected. For this reason, these systems are often used in concert with other localization techniques (such as GPS) to help correct for these errors and allow for recalibration [34].

2.4.4 Map-assisted Localization

If a map of the operating region is available prior to network deployment, it can be used simultaneously with other localization methods to improve the accuracy of location information. Many techniques have been developed in the field of robotics (such as algorithms for simultaneous localization and mapping [35]) that could be adapted for wireless device localization to make highly-precise position information available to end-user nodes and network algorithms.

Chapter 3

Impact of Directional Antennas on the Probability of Connectivity in Random 1D and 2D Networks

We begin our investigation on the impact of beamforming-enabled devices in wireless infrastructureless networks by analyzing their benefits for instantaneous network connectivity. The probability of connectivity metric is an important place to start, since a connected network is a vital prerequisite for the analysis of throughput and end-to-end delay performance. A partitioned network implies zero throughput and infinite end-to-end latency between at least one source-destination pair.

This work builds upon the probability of connectivity analysis using omnidirectional transmit and receive antennas presented in Chapter 3 of [9]. Using models amenable for

analytic studies, we seek to identify directional network regimes with a high probability of connectivity. This section focuses on fixed rate transmission systems, since given a maximum time-averaged transmitter power constraint at each node, this fixed communication rate constraint implies a limited communication range for each node. In a variable transmission rate system, we recognize that every node in the network is trivially connected to every other node in the network, even though the communication rate between the two nodes may become arbitrarily small as their separation distance increases. Therefore, a variable rate system can always be considered to be fully-connected, whereas the fixed rate transmission system may be disconnected. And while this analysis only considers stationary node placement as discussed in Chapter 2, the random distribution of nodes is a stepping-stone towards including the effect of node mobility.

We first study connectivity of one-dimensional random networks (on a line). The results using directional antennas are compared to the base case of nodes using only omnidirectional transmission and reception. Subsequently, we extend our analysis to two dimensions (in a square planar area) and employ well-studied approximation methods to identify regimes of interest with high probability of instantaneous connectivity. The results in this chapter identify trends and guidelines for the design and deployment of fixed rate transmission infrastructureless wireless networks intended to provide end-user QoS assurance.

For the purpose of result visualization in this chapter, we adopt the convention of [37] and define high probability of connectivity as a probability greater than $1 - \frac{1}{n}$, where n is the number of end-user nodes. We make the threshold of high probability of connectivity a function of n both because we expect to satisfy a fixed threshold of connectivity trivially as the end-user density grows large in a bounded operating region, and because the behavior of this bound agrees with the definition of "with high probability" (the probably of a sequence of events approaching unity as n goes to infinity). Although this definition of high

probability of connectivity is appropriate when n is large enough (in particular, when $n \geq 20$), we must be careful of how the results are interpreted with respect to this definition for smaller values of n since we are interested in network operating regimes with very high instantaneous probability of connectivity. While this is a shortcoming of the definition, we note that our analytical results in this chapter still hold for any arbitrary value of n. This definition of high probability of connectivity is only used in a few visualizations and design tradeoff expressions, where the reader should be appropriately careful with interpretation when n takes on smaller values.

3.1 Random Line Network Analysis

We consider a simple, idealized random network scenario with end-user nodes distributed along a fixed-length line region. This analysis identifies insights that drive the analysis for the planar random network case. It also reveals the effect of antenna directivity on the probability of network connectivity for a given density of end-user nodes. While the random line network case is a crude approximation to many realistic scenarios, one can imagine circumstances where this represents a reasonable estimate of the operational region, such as vehicular-based end-user nodes distributed along a particular stretch of highway or a sensor network deployed in a tunnel underpass.

The following is a description of the idealized model that we consider for the subsequent analysis. End-user nodes are independently and identically distributed along a line of length L [m] according to a uniform distribution. Adopting the fixed rate system transmission model for both omnidirectional antennas and directional antennas discussed in Section 2.3.3, each node with an omnidirectional antenna is assumed to have a maximum transmission

range of r [m] and each node with a directional antenna array is assumed to have a maximum transmission range that is an appropriately scaled version of the omnidirectional antenna range, $D_{tx}^{1/k}r$, where D_{tx} is the antenna directivity and k is the attenuation exponent of the path-loss model. The value for r is determined by the maximum allowable transmission power, the exponent of the path-loss model, and the required communication rate under the fixed rate transmission scenario. An expression for the maximum transmission range of the fixed rate omnidirectional system is developed after the introduction of the power model in Chapter 4. However, in this chapter, r is taken as a constant dictated by the constraints of the end-user node construction and the RF environment. The omnidirectional or directional network is then deemed disconnected if there is at least one adjacent node pair separated by more than r or $D_{tx}^{1/k}r$, respectively. Note that receive beamforming is suppressed (normalized to a receive directivity of unity, equivalently) in this analysis, although it could easily be included by adding an appropriate receive directivity term to the range in the directional network analysis.

This idealized "disk model" is a gross simplification of reality, as it does not account for possible RF obstacles and scatterers or the potential use of a non-homogeneous set of end-user nodes. Despite this, the disk model is often used in network connectivity studies [11,33] since it allows for analytical tractability and first-order insight.

Now we define the notation that is used in our mathematical analysis. Let there be n end-user nodes randomly distributed along a line bounded by $[0, L]$. Each node's location is selected independently of all other nodes. The location of a node is distributed according to a uniform distribution over the line. We denote the location of node i as X_i. Thus, the locations of the user nodes $\{X_1, X_2, \ldots, X_n\}$ are independent and identically distributed (IID) random variables. For analytical simplicity, the origin of the line is defined to be the deterministic location of an additional user node, indexed node 0. Now we let

$\{X_{(1)}, X_{(2)}, \ldots, X_{(n)}\}$ represent random variables that denote the ordered locations of the user nodes, such that $X_{(0)} \leq X_{(1)} \leq X_{(2)} \leq \cdots \leq X_{(n)} \leq L$. We define random variables that represent the distances between neighboring nodes, $\{Y_i\}_{i \in B}$, where the index set $B = \{0, 1, \ldots, n - 1\}$. By this construction, $Y_i = X_{(i+1)} - X_{(i)}$. We note that while each Y_i is identically distributed, they are not independent (consider that one very large distance between a neighbor pair implies shorter spacings between other adjacent pairs on the bounded line). Finally, using a well-known result from basic order statistics [36], each Y_i has the following cumulative distribution function (CDF):

$$\Pr\{Y_i \leq y\} = 1 - \left(1 - \frac{y}{L}\right)^n. \tag{3.1}$$

An example realization of a random line network with a node anchored at the origin of the line is shown in Fig. 3-1.

3.1.1 Probability of Connectivity Using Omnidirectional Nodes

We are interested in network regimes with a high probability of connectivity. In these regimes of interest, we continue our study of the analytical and algorithmic details of QoS provision for throughput, end-to-end delay, and network energy consumption.

In order for all network users to be able to communicate, the random deployment of end-user nodes in the line network must be fully connected. With an additional end-user anchored at the origin of the line for a total of $n + 1$ network nodes, the probability of connectivity, denoted $P_C^{omni}(n, r, L)$, is derived in [38] and shown alternatively using the well-studied problem of circumference cover with random arcs in [9]:
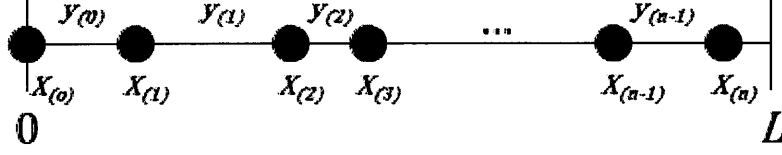
Figure 3-1: Example realization of random line network with anchored node 0. For analysis, these networks have a total of $n + 1$ end-user nodes.

$$P_C^{omni}(n, r, L) = \sum_{i=0}^{n} (-1)^i \binom{n}{i} \left(1 - \frac{ir}{L}\right)^n u(L - ir) \qquad (3.2)$$

where $u(\cdot)$ is the unit step function.

We observe that this expression can be rewritten such that $P_C^{omni}(n, r, L)$ depends on the pair of arguments (r, L) only through the ratio $\frac{r}{L}$. Thus, for notational simplicity, we define the normalized omnidirectional transmission range as $\Delta \triangleq \frac{r}{L}$, and rewrite (3.2) as:

$$P_C^{omni}(n, \Delta) = \sum_{i=0}^{n} (-1)^i \binom{n}{i} (1 - i\Delta)^n u(1 - i\Delta). \qquad (3.3)$$

The expression in (3.3) is precise, but it does not yield much insight into how $P_C^{omni}(n, \Delta)$ varies with its arguments. We bound this equation from both sides as proposed in [9] to elucidate the matter.

- Lower bounds:

$$P_C^{omni}(n, \Delta) \geq 1 - n(1 - \Delta)^n \qquad (3.4)$$

$$> 1 - ne^{-n\Delta} \qquad (3.5)$$

where equality is met in the first bound for $n = 1$. These results hold for $0 \leq \Delta \leq 1$, realizing that the network is trivially connected if $\Delta > 1$. For (3.4), the bound is

derived by simple application of Boole's Inequality, and (3.5) follows from the fact that $1 - x < e^{-x}$ for $x > 0$. It is also quickly verified for the second bound that the value approaches 1 as $n \to \infty$. We note that these lower bound expressions can yield negative values for certain combinations of input parameters. For these regions we instead employ the trivial lower bound, $P_C^{omni}(n, \Delta) \geq 0$.

- Upper bound:

$$P_C^{omni}(n, \Delta) \leq (1 - (1 - \Delta)^n)^n \tag{3.6}$$

where equality is met for $n = 1$. Again, this result holds for $0 \leq \Delta \leq 1$. This bound is derived by noting that conditioned on the event that $Y_j < r$, the probability that $Y_i > r$ for some $i > j$ increases. Taking the binomial expansion of the upper bound and observing that $(1 - \Delta)^n \xrightarrow[n \to \infty]{} e^{-n\Delta}$, it is verified that the bound approaches 1 as $n \to \infty$.

The probability of connectivity and the associated bounds (except the weaker lower bound) are shown in Fig. 3-2 and Fig. 3-3 for several normalized omnidirectional transmission ranges, along with the $1 - \frac{1}{n}$ threshold for high connectivity. Fig. 3-3 plots of the probability of connectivity in log scale to capture the behavior of the low probability of connectivity portion of the results, although this is not the interesting regime of network operation. We note that the exact expression and the upper and lower bounds are tight, and essentially interchangeable, for larger values of n, as seen in Fig. 3-2 and Fig. 3-3. These results show that by increasing the normalized omnidirectional transmission range from 0.1 to 0.3, we can decrease the number of end-user nodes needed for high-connectivity from almost 100 to 10, an order of magnitude difference. Another interesting aspect of these results is the initial decrease in the probability of connectivity as the value of n grows from 1 (recall that there are actually $n + 1$ total end-user nodes in this random line network scenario). This reflects the fact that as nodes are initially added to the network, there are more opportunities for

63
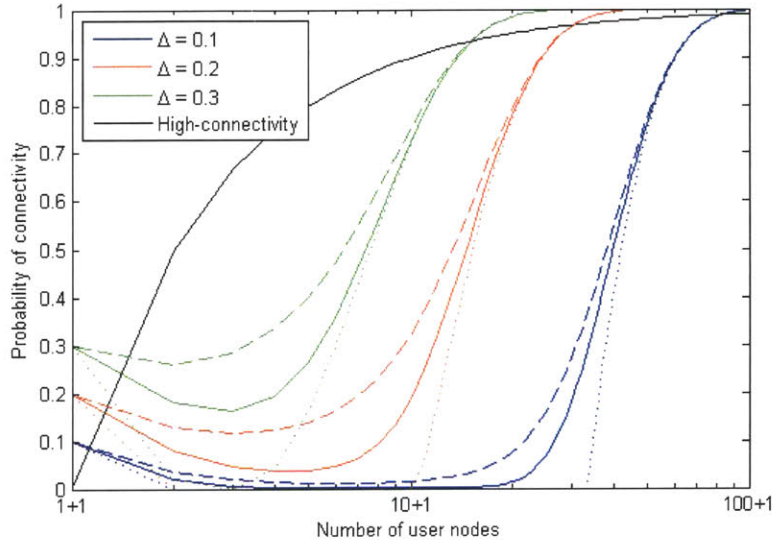
Figure 3-2: Probability of connectivity and upper and lower bounds for random line networks using omnidirectional antennas for different values of Δ, the normalized omnidirectional transmission range. Solid lines are $P_C^{omni}(n, \Delta)$, dashed lines (---) are upper bounds, and dotted lines (...) are the tighter lower bounds. The solid black line is the $1 - \frac{1}{n}$ threshold for high-connectivity. The "+1" in the labeling of the x-axis is a reminder of the additional anchored node at the origin of the line. This labeling is used throughout the chapter to serve as a reminder of this $(n + 1)^{th}$ end-user node.

Figure 3-3: Probability of connectivity and upper and lower bounds for random line networks using omnidirectional antennas for different values of Δ, the normalized omnidirectional transmission range, on a log-log plot. This is the log-log scale version of Fig. 3-2.

disconnections to arise. Thus we see a decrease in the probability of connectivity. Once enough nodes have been added, however, it becomes increasingly likely that gaps where disconnections occur are filled by the additional end-user nodes, and this is when we see the sharp increase in the probability of network connectivity. We can manipulate the weak lower bound (3.5) to show that for a fixed value of n, we require $\Delta > \frac{1}{n}\ln(n^2)$ for the $n + 1$ node network to fall within the high probability of connectivity regime. As mentioned in the beginning of this chapter, one should be wary of this expression when n is small (in particular, when $n < 20$) due to the behavior of the defined high probability of connectivity threshold. This caution should be used whenever the high probability of connectivity threshold is invoked, although we do not reiterate this statement of caution in each section of this chapter.

3.1.2 Probability of Connectivity Using Directional Nodes

We consider the same scenario of a random distribution of n end-user nodes over a bounded line region with an additional user node anchored at the origin of the line. However, we now employ end-user nodes equipped with directional antennas instead of omnidirectional antennas. For the purpose of this section, we suppress receive beamforming gain by normalizing the receive directivity to unity and focus on deriving analytic expressions with respect to the transmit directivity gain, D_{tx}.

As before, in order for all end-users to have the opportunity to communicate, the random deployment of the nodes must form a fully connected network. In other words, no neighboring nodes can be separated by a distance more than $D_{tx}^{1/k}r$. With an additional end-user anchored at the origin of the line for $n + 1$ nodes in total, the probability of

connectivity, denoted $P_C^{bf}(n, r, L, D_{tx})$, can easily be shown by following the analysis in [38] to be:

$$P_C^{bf}(n, r, L, D_{tx}) = \sum_{i=0}^{n} (-1)^i \binom{n}{i} \left(1 - \frac{irD_{tx}^{1/k}}{L}\right)^n u(L - irD_{tx}^{1/k}). \qquad (3.7)$$

We note that while the result is dependent on the attenuation exponent of the path-loss model, k, the attenuation exponent is not included as an argument to the function because it is an inherent characteristic of the operating environment and not explicitly under the control of the network architect.

Following the analytical approach for the omnidirectional case, we simplify this expression by rewriting it in terms of the normalized omnidirectional transmission range:

$$P_C^{bf}(n, \Delta, D_{tx}) = \sum_{i=0}^{n} (-1)^i \binom{n}{i} \left(1 - i\Delta D_{tx}^{1/k}\right)^n u(1 - i\Delta D_{tx}^{1/k}). \qquad (3.8)$$

We also derive bounds similar to the omnidirectional case to reveal how this result depends on its input parameters.

- Lower bounds:

$$P_C^{bf}(n, \Delta, D_{tx}) \geq 1 - n\left(1 - \Delta D_{tx}^{1/k}\right)^n \qquad (3.9)$$

$$> 1 - ne^{-n\Delta D_{tx}^{1/k}} \qquad (3.10)$$

where equality is met for $n = 1$. Again, we note that these lower bound expressions can yield negative values for some sets of input parameters. So for these regions, we employ the trivial lower bound, $P_C^{bf}(n, \Delta, D_{tx}) \geq 0$. Also, if $\Delta D_{tx}^{1/k} \geq 1$, then our network realization is trivially connected. Under these conditions, the lower bound does not provide useful information as $P_C^{bf}(n, \Delta, D_{tx}) = 1$.

- Upper bound:

$$P_C^{bf}(n, \Delta, D_{tx}) \leq \left(1 - \left(1 - \Delta D_{tx}^{1/k}\right)^n\right)^n \qquad (3.11)$$

where equality is met for $n = 1$. This result again holds for $0 \leq \Delta D_{tx}^{1/k} \leq 1$. If $\Delta D_{tx}^{1/k} \geq 1$, then our network realization is connected, $P_C^{bf}(n, \Delta, D_{tx}) = 1$, and we can use the trivial upper bound.

The probability of connectivity and the associated bounds (except for the weaker lower bound) are shown in Fig. 3-4 and Fig. 3-5 for several values of the directivity, along with the $1 - \frac{1}{n}$ threshold for high connectivity. In this figure, we see results that appear similar to the omnidirectional case. If we were to replace $\Delta' = \Delta D_{tx}^{1/k}$ in (3.8) to (3.11), we would in fact have the same expressions as in the omnidirectional case with a scaled version of the normalized transmission range. Despite the similarity in analytic expressions, we continue to use $\Delta D_{tx}^{1/k}$ in the directional network expressions to explicitly highlight the effect of the directivity gain term. Comparing Fig. 3-4 and Fig. 3-5 to the $\Delta = 0.1$ omnidirectional case, we see a significant improvement even with $D_{tx} = 2$, which reduces the number of end-user nodes required for high-connectivity from approximately 100 to 50. Increasing the transmitter directivity to 20 reduces the required number of end-user nodes to only 6 for a high probability of connectivity. We can manipulate the weaker lower bound (3.10) to show that for a fixed value of n, we require $\Delta D_{tx}^{1/k} > \frac{1}{n}\ln(n^2)$ for the $n + 1$ node network to fall within the high probability of connectivity regime, where $\Delta D_{tx}^{1/k}$ can be viewed as the normalized directional transmission range. Moving the directivity to the right side of this expression, we see that the required value of Δ is improved by a factor of $\left(\frac{1}{D_{tx}}\right)^{1/k}$ compared to the omnidirectional case, which corresponds to savings in the required transmission power required to attain the same level of high probability of connectivity.
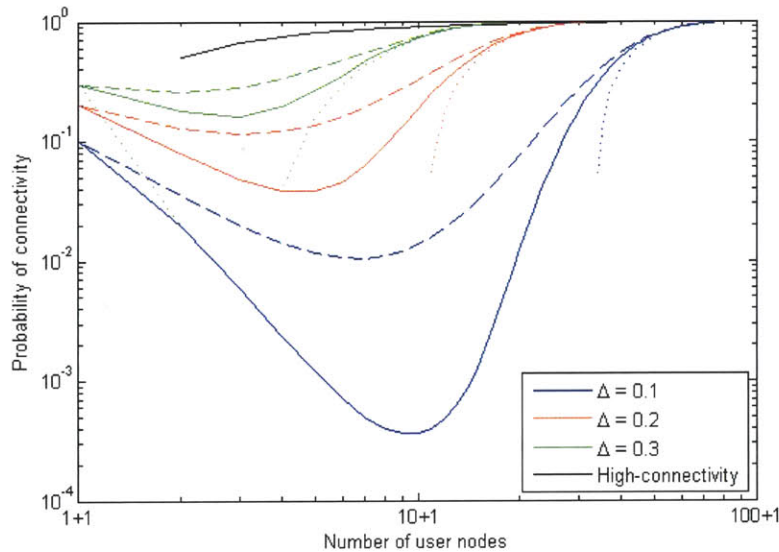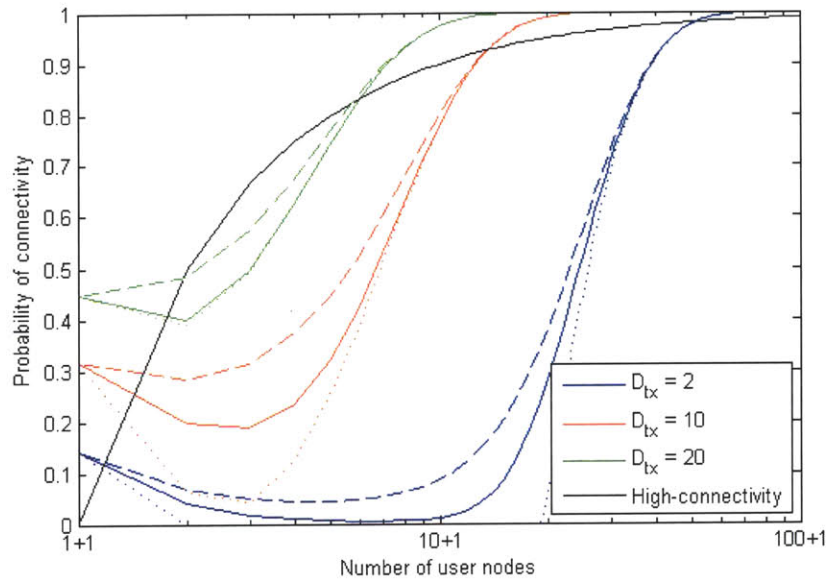
Figure 3-4: Probability of connectivity and upper and lower bounds for random line networks using directional antennas. Solid lines are $P_C^{bf}(n, \Delta, D_{tx})$, dashed lines (---) are upper bounds, and dotted lines (...) are the tighter lower bounds. The solid black line is the $1 - \frac{1}{n}$ threshold for high-connectivity. For this figure, $\Delta = 0.1$ and the free space attenuation exponent is used, $k = 2$.
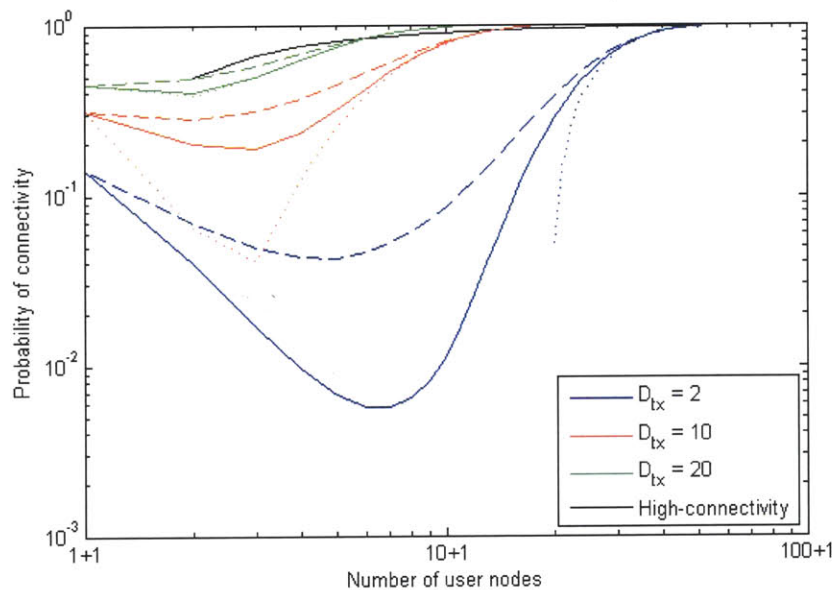
Figure 3-5: Probability of connectivity and upper and lower bounds for random line networks using directional antennas on a log-log plot. This is the log-log scale version of Fig. 3-4.

For a fixed directivity gain, the probability of connectivity and associated bounds (except for the weaker lower bound) are shown in Fig. 3-6 and Fig. 3-7 for different values of the attenuation exponent k. This illustrates how the operating environment (assumed to be homogeneous) affects the directivity gain as the path-loss exponent increases. In these figures, the leftmost set of curves are the same as in Fig. 3-4 and Fig. 3-5. The two other sets of curves in each figure demonstrate how dramatically the gains disappear due to undesirable RF phenomena including environmental absorption and diffraction. We note that the value for r would also decrease with increasing value of k, however for this analysis we assume that the value of r (and equivalently Δ) can be held fixed by increasing available transmit power as k increases.

3.1.3 Probability of Connectivity Comparison Between Directional and Omnidirectional Networks

Given the results from Sections 3.1.1 and 3.1.2, we compare the directional network connectivity performance with the baseline omnidirectional network case. Fig. 3-8 and Fig. 3-9 show the omnidirectional and directional results simultaneously (as well as the $1 - \frac{1}{n}$ high connectivity threshold) for a common normalized omnidirectional transmission range Δ and different values of the transmit directivity. These plots show that, when $k = 2$, we can see almost an order of magnitude decrease in the number of user-nodes required for the same probability of connectivity using an antenna with directivity $D_{tx} = 20$. A higher probability of network connectivity with decreased end-user device density significantly increases our network regime of interest for subsequent study in throughput and end-to-end delay QoS measures, thus these results make a strong case for using beamforming-enabled nodes in the design and deployment of a wireless infrastructureless network.
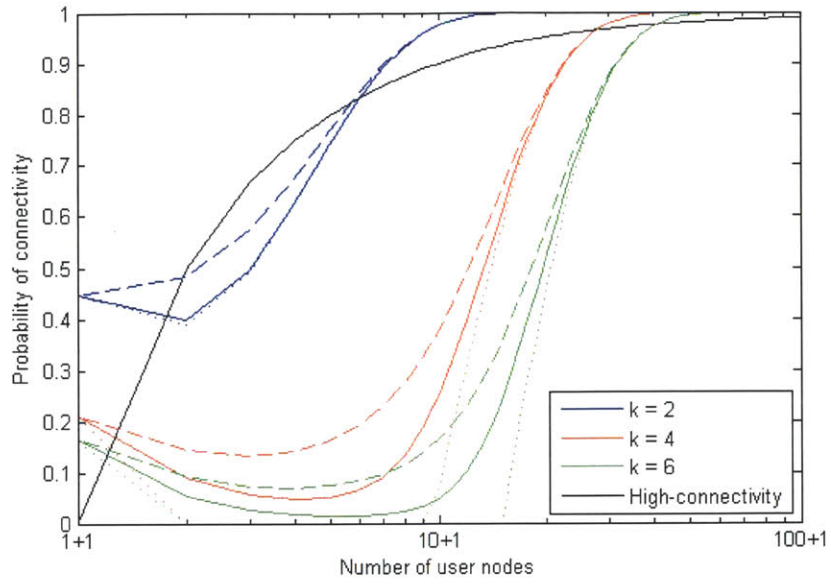
Figure 3-6: Probability of connectivity and upper and lower bounds for random line networks using directional antennas for different values of the attenuation exponent. Solid lines are $P_C^{bf}(n, \Delta, D_{tx})$, dashed lines (---) are upper bounds, and dotted lines (...) are the tighter lower bounds. The solid black line is the $1 - \frac{1}{n}$ threshold for high-connectivity. For this figure, $\Delta = 0.1$ (even as k increases) and the antenna directivity is set to $D_{tx} = 20$.
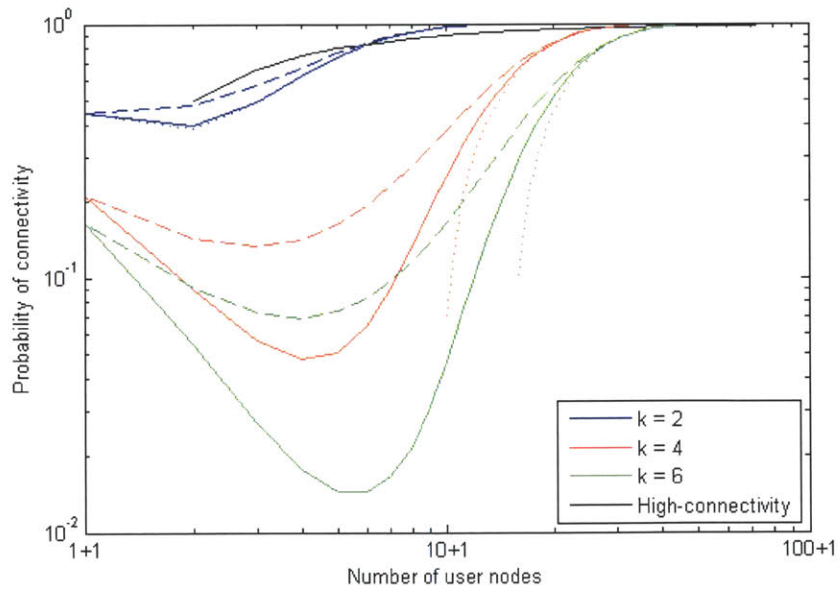
Figure 3-7: Probability of connectivity and upper and lower bounds for random line networks using directional antennas for different values of the attenuation exponent on a log-log plot. This is the log-log scale version of Fig. 3-6.
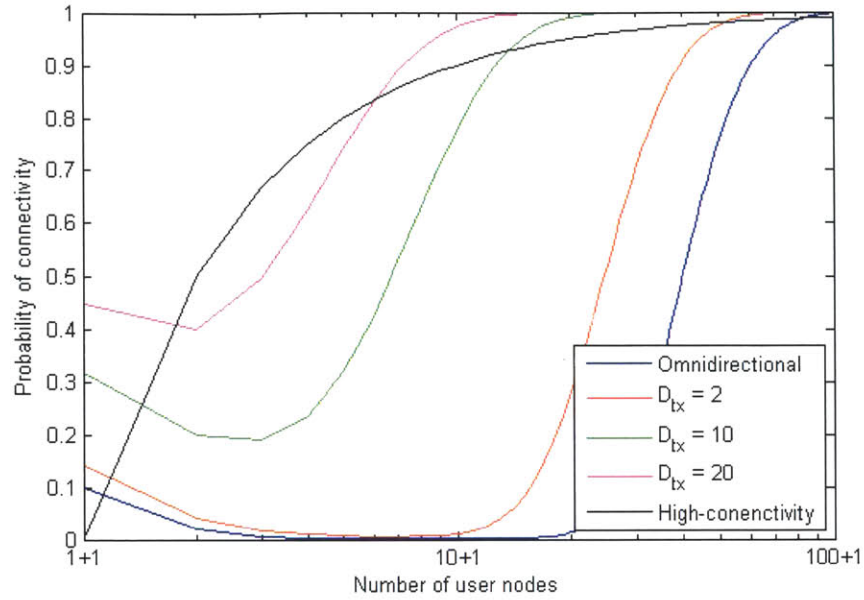
Figure 3-8: Probability of connectivity comparison between nodes equipped with omnidirectional transmit antennas and beamforming-capable antennas. The solid black line is the $1 - \frac{1}{n}$ threshold for high-connectivity. For this figure, $\Delta = 0.1$ and $k = 2$.
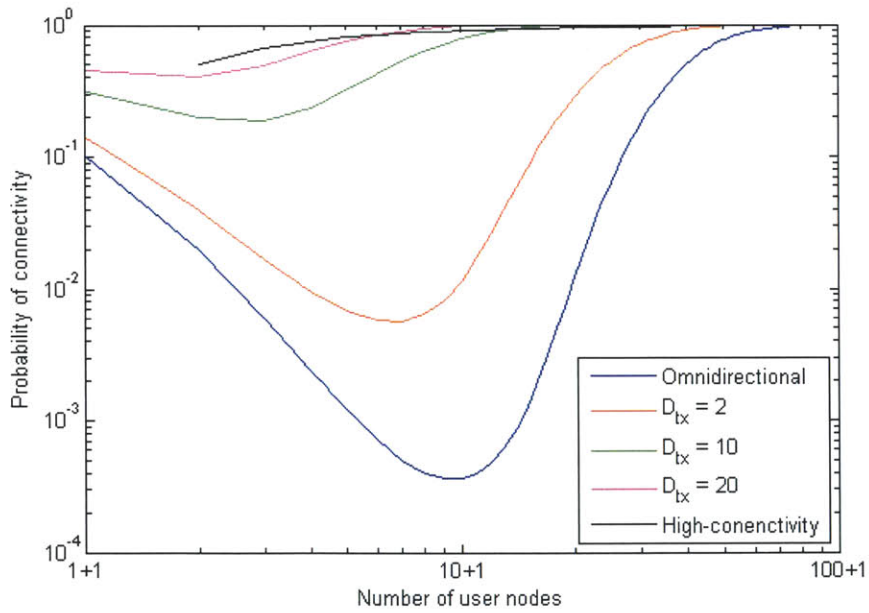
Figure 3-9: Probability of connectivity comparison between nodes equipped with omnidirectional transmit antennas and beamforming-capable antennas on a log-log plot. This is the log-log scale version of Fig. 3-8.
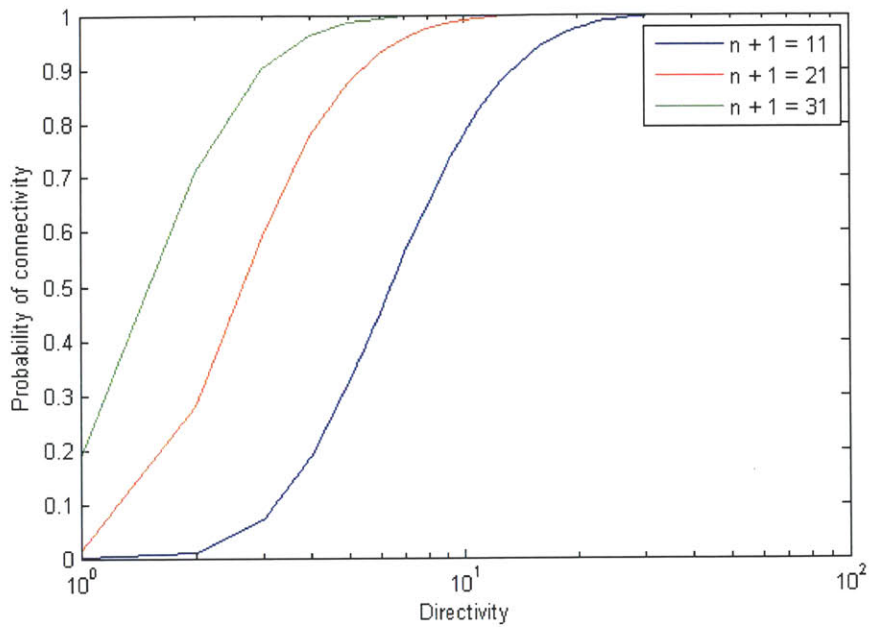
Figure 3-10: Probability of connectivity versus transmitter directivity for selected values of n. These lines correspond to exact values, $P_C^{bf}(n, \Delta, D_{tx})$. For this figure, $\Delta = 0.1$ and $k = 2$.
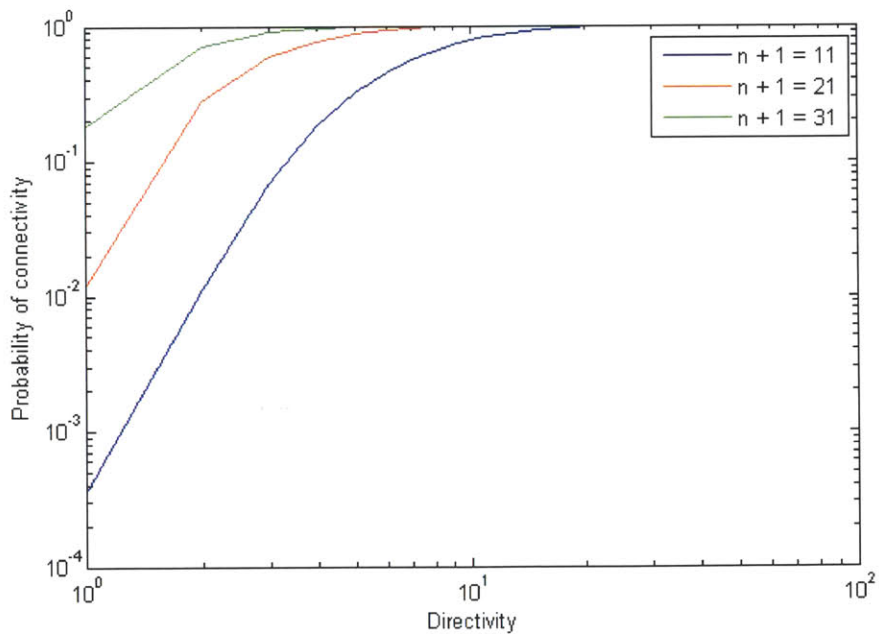
Figure 3-11: Probability of connectivity versus transmitter directivity for selected values of n on a log-log plot. This is the log-log scale version of Fig. 3-10.

Since transmitter directivity is a crucial design parameter for the network architect, we consider how the probability of connectivity changes explicitly with the directivity gain for fixed end-user node density. Fig. 3-10 and 3-11 show the relationship between probability of connectivity and transmitter directivity for fixed values of n, noting that the far left of each plot represents the probability of connectivity for a specific end-user node density using omnidirectional transmission antennas (equivalently, $D_{tx} = 1$).

The addition of transmitter directivity allows the end-user device density to decrease while maintaining a high probability of instantaneous connectivity. With the definition of high probability of connectivity, we can use the lower bound on the probability of connectivity in (3.10) to find the required number of end-users to achieve a high probability of connectivity for a given transmitter directivity. Explicitly, we require that $\frac{n}{\ln n^2} \geq \frac{1}{\Delta D_{tx}^{1/k}}$ in order for the probability of connectivity to fall within the defined high probability of connectivity regime. This tradeoff between transmitter directivity and the required end-user node density for a high probability of instantaneous connectivity is shown in Fig. 3-12. The far left side of this plot represents the number of end-users required to achieve a high probability of connectivity in an omnidirectional network (equivalently, $D_{tx} = 1$). We observe that an order of magnitude increase in directionality corresponds to approximately an order of magnitude decrease in the number of nodes required when $k = 2$. The shape of the curve is a result of the high probability of connectivity threshold that varies with n. If we were to consider a fixed threshold of high probability of connectivity, the curve would not drop off suddenly on the far right side.
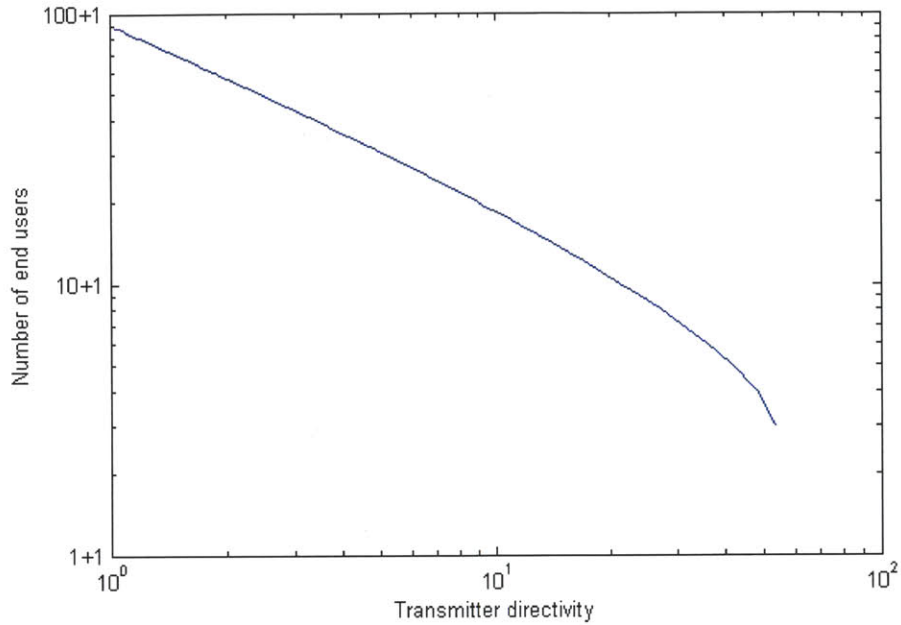
Figure 3-12: Number of end-user nodes required to achieve a probability of connectivity greater than $1 - \frac{1}{n}$ in a random line network as a function of transmitter directivity. For this figure, $\Delta = 0.1$ and $k = 2$.

3.2 Random Two-dimensional Network Analysis

While we made an effort to fit the random line network to actual operating scenarios, it is much more common to encounter networks operating in a planar region. As such, the line network scenario is a special case used to provide insight and analytical expressions that help us to analyze the more general and realistic case in this section.

We consider a similar network deployment scheme as before, allowing n users to be identically and independently distributed in a bounded planar region with area $L \times L$ [m²] according to a uniform distribution over the area. In order to apply the analytical results from Sections 3.1.1 and 3.1.2, we need to anchor an additional end-user node, indexed node

0, at the origin of the planar region (lower left corner). We continue to use the transmission model for both omnidirectional antennas and directional antennas discussed in Section 2.3.3. As such, each node is assumed to have a circular transmission range of radius r in the omnidirectional case and $D_{tx}^{1/k}r$ in the directional case.

Under the theory of random geometric graphs, the asymptotic properties of a network scenario like this are well studied. A thorough overview of the results from this field are presented in [39]. Applying this theory to infrastructureless wireless networks, Gupta and Kumar have shown similar asymptotic properties for connectivity in a two-dimension disc operating region [40]. Although random geometric graph theory allows for analytical connectivity results as the number of network nodes goes to infinity, we are interested in identifying regimes of high probability of instantaneous connectivity for finite values of n. The general problem of identifying the probability of connectivity for a bounded planar region with finite-valued n is difficult to solve, but we can bound the exact probability with approximations from each side. The first two subsequent sections develop these approximations, and the third compares these results and provides visualizations of the bounds to enable us to identify network operating regimes of interest for discussing QoS performance.

3.2.1 An Upper Bound Approximation

We consider the randomly deployed network of $n + 1$ end-user nodes as proposed, with node 0 anchored at the origin of the plane and the other n nodes placed independently according to a uniform distribution over the $L \times L$ planar operating area. The operating area is considered to lie in the x-y plane. For the purpose of this section, we denote this random

network as N. Next, we consider the projection of N onto the x-axis of the plane, which is bounded by $[0, L]$. We denote the random one-dimensional line network that results from this projection as N_x. Simultaneously, we consider the projection of N onto the y-axis of the plane, which is also bounded by $[0, L]$. In a similar manner, we denote the random one-dimensional line network that results from this projection as N_y. By the projection of the two-dimensional random network deployment onto the separate axes, we have created two independent one-dimensional random line networks, just as we have analyzed in Section 3.1. Fig. 3-13 shows an example realization of N and the associated one-dimensional projection realizations, N_x and N_y.

Next, we recognize that the probability that N forms a connected network, regardless of the type of antenna technology considered, is less than or equal to the probability that both N_x and N_y each form a connected network. It is this realization that allows us to use the probability of connectivity of the two line network projections to create an upper bound for the probability that N is connected. The random network N is disconnected if either N_x or N_y is disconnected, since the projection process of node locations in two-dimensions to node locations on a line can only reduce the separation between a neighboring pair of nodes. Thus, we deem the one-dimensional projection approximation to be connected if both N_x and N_y form connected line networks. The one-dimensional projection approximation imposes a less stringent requirement on connectivity than our requirement on N to be connected, making the probability that the projection approximation is connected an upper bound to the actual probability of connectivity. We can prove that this projection approximation is an upper bound by the example of Fig. 3-14. We see in this example that both projections, N_x and N_y, form connected line networks with the given r. However, the one end-user node in N is actually partitioned from the rest of the nodes in the network.
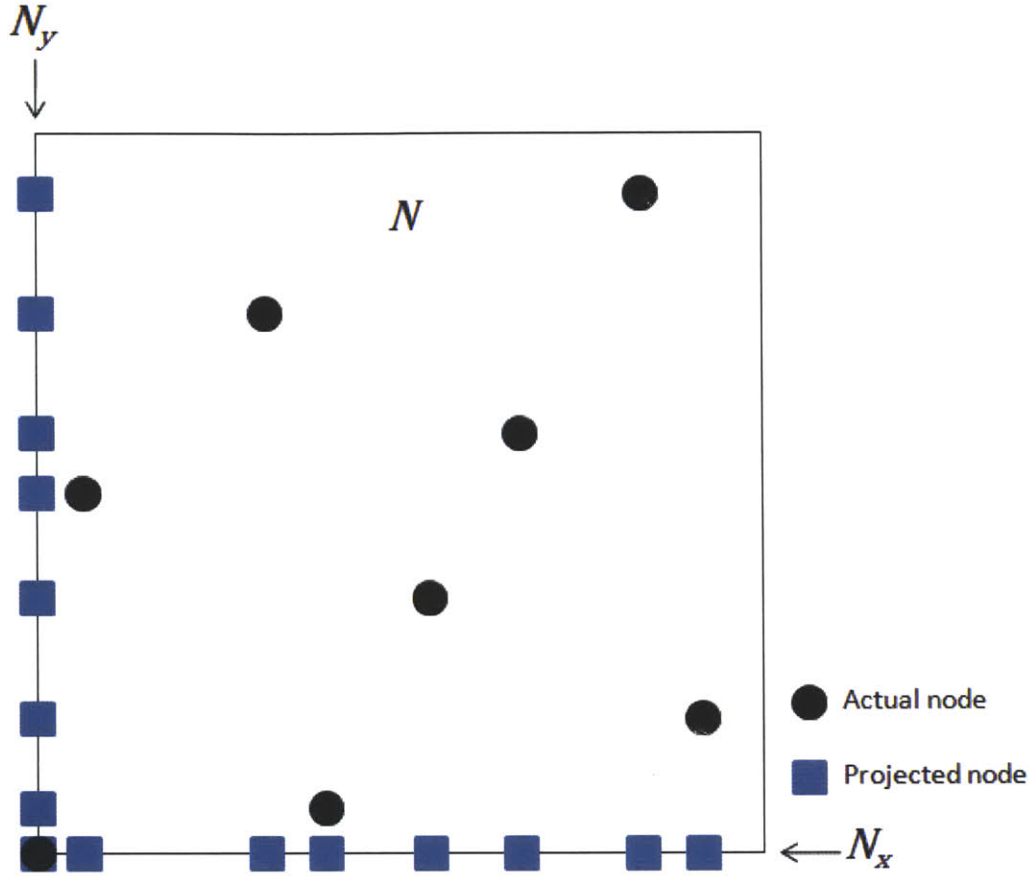
Figure 3-13: Example realization of N and its one-dimensional projections, N_x and N_y.

By these arguments, we can now write the upper bound expressions for both the omnidirectional network and directional network cases. If the end-user nodes are equipped with omnidirectional antennas for transmission, we denote the probability that the random planar network is connected by $P_{2D}^{omni}(n, \Delta)$, and we have:

$$P_{2D}^{omni}(n, \Delta) \leq \left(P_C^{omni}(n, \Delta)\right)^2 \tag{3.12}$$

$$\leq (1 - (1 - \Delta)^n)^{2n} \tag{3.13}$$

where (3.12) follows from the independence of the two random line network projections and (3.13) follows from the bound to the exact expression of $P_C^{omni}(n, \Delta)$ shown in (3.6).
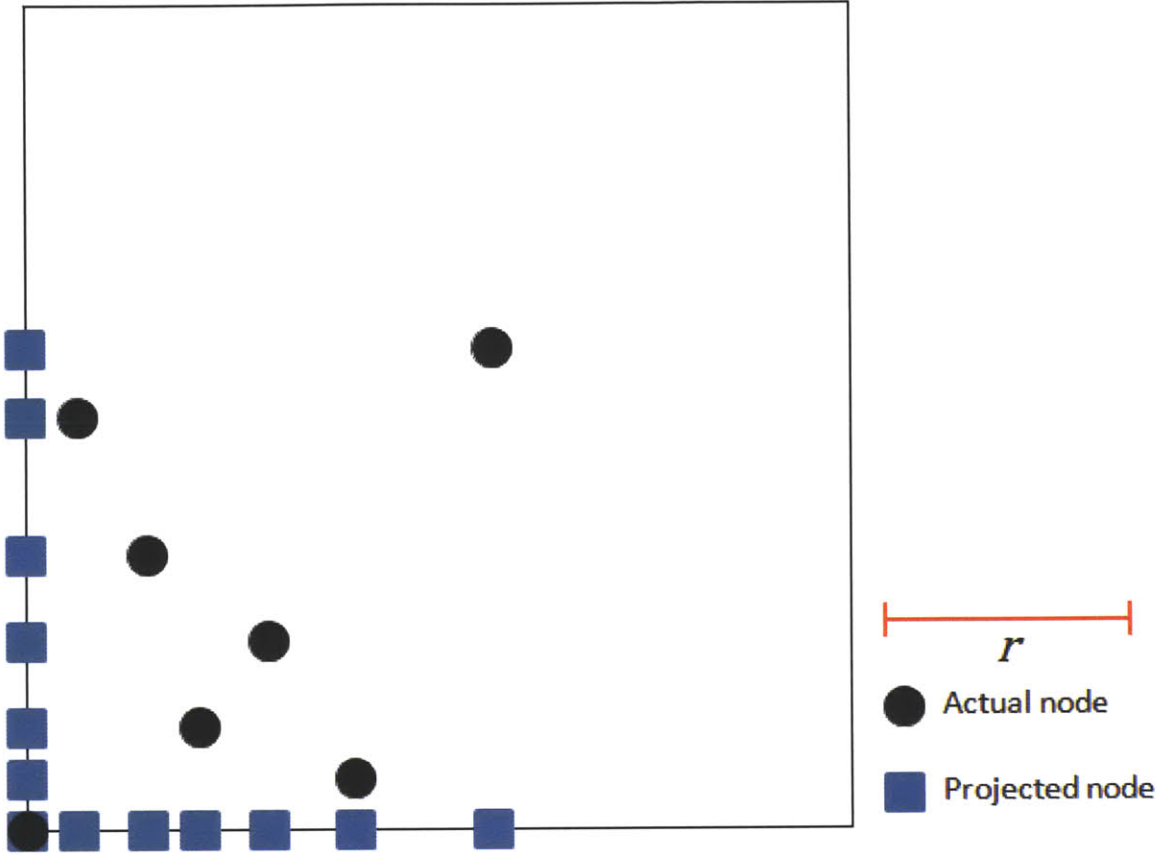
Figure 3-14: Example where both N_x and N_y one-dimensional projections are connected, but the actual realization of N has a partitioned node.

Similarly, if the end-user nodes are equipped with directional antennas for transmission, we denote the probability that the random planar network is connected by $P_{2D}^{bf}(n, \Delta, D_{tx})$, and we have:

$$P_{2D}^{bf}(n, \Delta, D_{tx}) \leq \left(P_C^{bf}(n, \Delta, D_{tx}) \right)^2 \tag{3.14}$$

$$\leq \left(1 - \left(1 - \Delta D_{tx}^{1/k} \right)^n \right)^{2n} \tag{3.15}$$

where (3.14) follows from the independence of the two random line network projections and (3.15) again follows from (3.11), the bound to the exact expression of $P_C^{bf}(n, \Delta, D_{tx})$.

3.2.2 A Lower Bound Approximation

To derive a lower bound to the probability that the two-dimensional network is connected, we take up the well-studied "balls and bins" model, following the example of [9]. This model describes the act of randomly dropping balls into a set of bins and considers properties such as the distribution of how many balls land in a bin and the expected number of bins that are empty [41].

We first tessellate our planar area into m equal-sized cells. Next, we map the end-user nodes to balls, the cells to bins, and the act of randomly distributing the n end-user nodes in the plane to the act of randomly dropping the balls into the bins. Additionally, we recognize that an end-user node can land anywhere within a cell, while the balls and bins model only considers the binary question of whether or not a ball lands in a given bin. Thus, we need to size the cells appropriately so that we can gain insight from this model. If we set the cell edge length to be $\frac{r}{\sqrt{5}}$ (in the omnidirectional network case) or $\frac{D_{tx}^{1/k}r}{\sqrt{5}}$ (in the directional network case), then we ensure that a node anywhere within a cell is within communication range of a node anywhere within the cell directly above, below, to the right, or to the left of it. This is illustrated in Fig. 3-15. This cell sizing corresponds to having $m = \left\lceil \frac{\sqrt{5}}{\Delta} \right\rceil^2$ (in the omnidirectional network case) or $m = \left\lceil \frac{\sqrt{5}}{\Delta D_{tx}^{1/k}} \right\rceil^2$ (in the directional network case). With this structure, we deem the network using the balls and bins approximation to be connected if there is at least one ball in each bin (or equivalently, at least one end-user node in each cell), a common question to ask in the balls and bins framework.

Before we derive the probability of connectivity under the balls and bins model, we note that this approximation imposes a more stringent requirement for connectivity on the random

two-dimension network than the requirement for N to be connected, thus making the probability that the balls and bins approximation is connected a lower bound to the actual probability of connectivity. We can prove that this approximation is a lower bound by the example illustrated in Fig. 3-16. In this example, the underlying network of end-user nodes is connected. However, the balls and bins approximation would be deemed disconnected, since there is an empty cell.

We now consider how to analyze this two-dimensional connectivity approximation. As mentioned before, we require at least one end-user node to fall in each cell to deem the approximation connected. Given that we deterministically have a node within the bottom leftmost cell by definition, we need the n nodes to cover the other $m - 1$ cells for connectivity. We can find this exact probability by realizing that the described cell tessellation of the operational plane means that an end-user node is equally likely to land in any cell, and then we can apply the inclusion-exclusion principle for determining the size of the union of events in the probability space [42]. We denote the probability of connectivity for this balls and bins approximation parameterized by n and m as $P_C^{bb}(n, m)$. The derivation is shown in Appendix B, and the exact result is:

$$P_C^{bb}(n, m) = \sum_{i=0}^{m-1} (-1)^i \binom{m - 1}{i} \left(1 - \frac{i}{m}\right)^n. \tag{3.16}$$

This result applies as long as $n \geq m - 1$. It can be readily verified that $P_C^{bb}(n, m) \rightarrow 1$ as $n \rightarrow \infty$ for a fixed value of m. The expression (3.16) holds when considering either end-user nodes with omnidirectional or directional antennas since this difference is captured by the value of m in the equation. We now have the following lower bounds on the actual probability of connectivity:
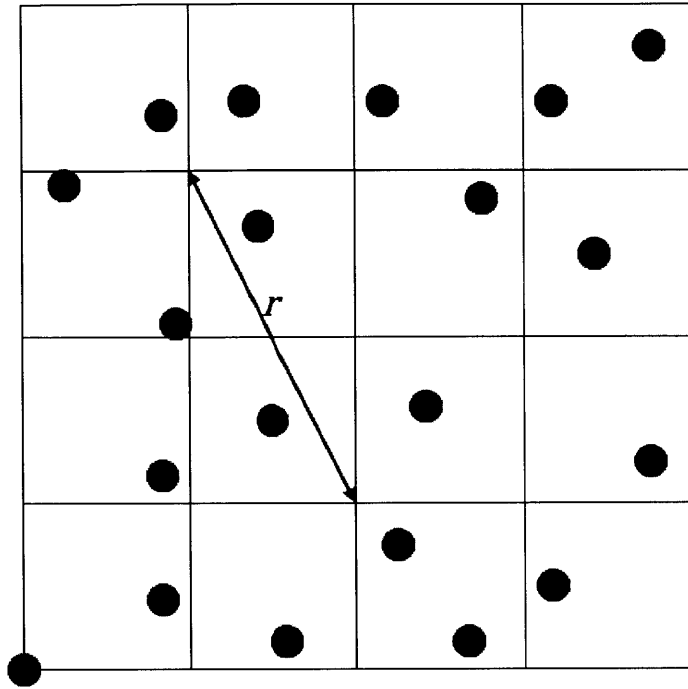
Figure 3-15: The "balls and bins" model with appropriate tessellation (cell sizing) of the operating region.
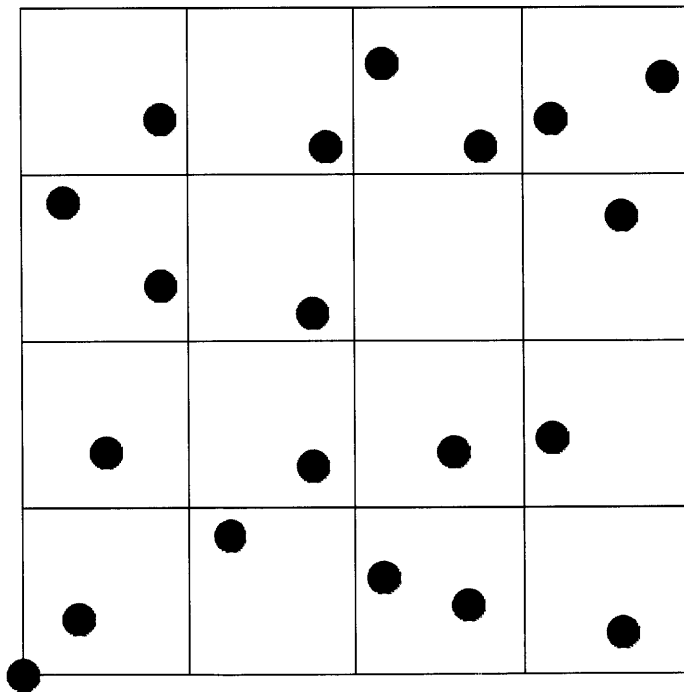
Figure 3-16: Example of disconnected balls and bins approximation, whereas the underlying network realization is actually connected.

$$P_{2D}^{omni}(n, \Delta) \geq P_C^{bb}\left(n, \left\lceil \frac{\sqrt{5}}{\Delta} \right\rceil^2\right), \tag{3.17}$$

$$P_{2D}^{bf}(n, \Delta, D_{tx}) \geq P_C^{bb}\left(n, \left\lceil \frac{\sqrt{5}}{\Delta D_{tx}^{1/k}} \right\rceil^2\right). \tag{3.18}$$

The form of the exact expression does not give a very intuitive understanding of $P_C^{bb}(n, m)$. So we derive a lower bound to this expression by indexing the cells from 1 to m and defining an indicator random variable I_i such that:

$$I_i = \begin{cases} 1 & \text{if cell } i \text{ has no user node} \\ 0 & \text{otherwise.} \end{cases} \tag{3.19}$$

As before, we recognize that each user-node is equally like to fall into any cell and the bottom leftmost cell is always deterministically full. Then, we apply the union bound to the union of the events that these indicator random variables equal 1 to get:

$$P_C^{bb}(n, m) \geq 1 - (m-1)\left(1 - \frac{1}{m}\right)^n \tag{3.20}$$

$$> 1 - (m-1)e^{-n/m}. \tag{3.21}$$

The looser bound (3.21) follows from the fact that $1 - x < e^{-x}$ for $x > 0$, and it can be easily seen that this bound goes to 1 as $n \to \infty$ for a fixed value of m.

A well-known result for the balls and bins analysis is that $P_C^{bb}(n, m) > 1 - \frac{1}{2n \ln n} > 1 - \frac{1}{n}$ when $m \leq \frac{n}{2 \ln n}$. A derivation of this result can be found in [43]. In other words, as the number of end-user nodes in the network increases, the number of cells can also increase while maintaining network connectivity. An increase in the number of cells for a fixed

operating area corresponds to a decrease in the required end-user device transmission radius, which translates into transmission power savings. Explicitly, this condition says we need

$$\Delta \geq \frac{1}{D_{tx}^{1/k}} \sqrt{\frac{10 \ln n}{n}} \tag{3.22}$$

to guarantee that we are in the regime of high probability of connectivity using the balls and bins formulation (note that $D_{tx} = 1$ for nodes equipped with omnidirectional transmission antennas). The normalized omnidirectional transmission range Δ can decrease as n increases. And while the normalized omnidirectional transmission range decreases at the same rate with increasing n for both omnidirectional and directional networks, the directivity gain scales down Δ by a factor of $D_{tx}^{1/k}$ for beamforming-enabled nodes. Recall that a decrease in the required normalized omnidirectional transmission range for high probability of connectivity corresponds to a decrease in required transmission power for high probability of connectivity.

We briefly consider another common question in this balls and bins framework: for a fixed m, what is the number of end-user nodes we need such that there is at least one node in each of the m cells? We denote this quantity as n^*. Commonly, textbooks consider the expected value of this quantity (see [44]). If we divide node deployment into sequential stages such that a stage ends when a node first lands in a previously empty cell and we let n_i represent the number of balls needed for the ith stage, then it follows that n_i is a geometric random variable with a probability of success equal to $\frac{m-i}{m}$. Thus, we have:

$$\mathrm{E}[n_i] = \frac{m}{m-i} \tag{3.23}$$

for $i \in \{1, 2, \ldots, m-1\}$. Since $n^* = \sum_{i=1}^{m-1} n_i$, we have the following for the expected value of n^*:

$$E[n^*] = \sum_{i=1}^{m-1} E[n_i] \qquad (3.24)$$

$$= m \sum_{i=1}^{m-1} \frac{1}{i} \qquad (3.25)$$

$$= mH_{m-1} \qquad (3.26)$$

where H_m is the mth harmonic number.

3.2.3 Probability of Connectivity in Random Planar Networks

Using the bounds derived in Sections 3.2.1 and 3.2.2, we now provide visualization of these results and compare results when using omnidirectional antennas versus directional antennas for transmission.

First we examine the bounds on the probability of connectivity for a random planar network with end-user nodes equipped with omnidirectional transmission antennas. Fig. 3-17 shows the upper and lower bounds using the two approximations to the probability of connectivity we have described for three different values of the normalized omnidirectional transmission range, Δ, which corresponds to three different values for the number of cells in the tessellated operating plane, m. As we observe from these results, the upper and lower bounds are not tight. When considering the methods of approximation to the planar network probability of connectivity, we expect that the lower bound is closer to the actual probability of connectivity, since it more realistically models the two-dimensional end-user node deployment, whereas the upper bound is a very liberal approximation to the two-dimensional deployment of nodes. We also observe that, as expected, an increase in the

normalized omnidirectional transmission range corresponds to a dramatic decrease in the number of end-user nodes we need to achieve a connected planar network with high probability.

Next we examine the bounds on the probability of connectivity for a random planar network with end-user nodes equipped with directional transmission antennas. Fig. 3-18 shows the upper and lower bounds using the two approximations to the probability of connectivity for three different values of the antenna array directivity, D_{tx}. As in the omnidirectional case, we observe that the upper and lower bounds are not tight and sometimes provide us with little information about the true probability of connectivity value (the plot sometimes indicates that, trivially, the value lies between 0 and 1). Still we have reason to believe that the true values lies closer to the lower bound due to the nature of the two approximation formulations. Focusing our attention on the lower bound results, we see that an increase of transmit directivity gain from $D_{tx} = 2$ to $D_{tx} = 20$ reduces the number of nodes required for a high probability of connectivity from approximately 500 to less than 20 when $k = 2$. This is a very significant increase to the high probability of instantaneous connectivity regime.

Finally, we look at the omnidirectional and directional results together, with a focus on the lower bound approximation to random planar network connectivity. Fig. 3-19 and Fig. 3-20 simultaneously show lower bound results from Fig. 3-17 and Fig. 3-18 along with the defined threshold for high-connectivity when $\Delta = 0.25$ (we use a larger value of Δ than we did in the random line network analysis only for illustrative purpose—the same distinction between the omnidirectional and directional network cases is seen when $\Delta = 0.1$). The highlighted results here show that using directivity gain $D_{tx} = 20$, we can reduce the number of end-user nodes needed in the network to ensure a high probability of connectivity from approximately 1000 to 20, almost two orders of magnitude difference, when $k = 2$. This makes an extremely strong case for the use of end-user devices equipped with beamforming-
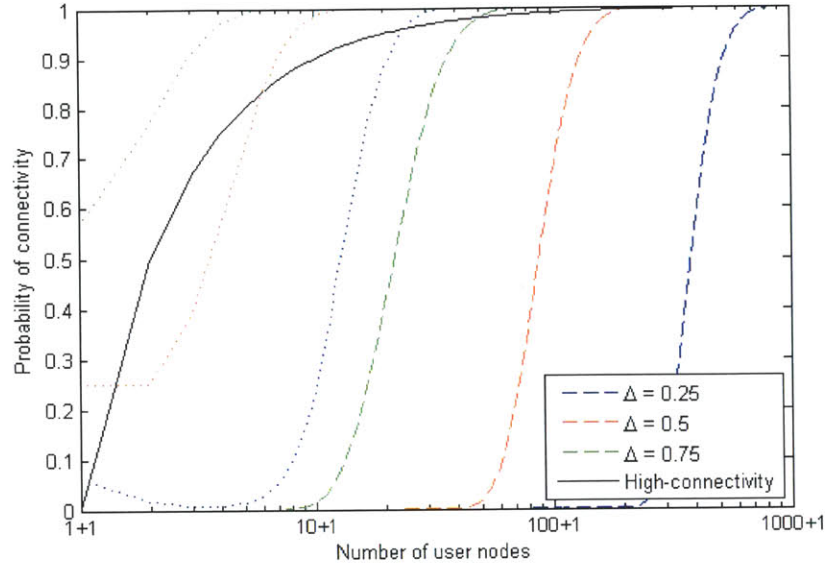
Figure 3-17: Upper and lower bounds on $P_{2D}^{omni}(n, \Delta)$ for random planar networks using omnidirectional antennas. Dashed lines (---) are lower bounds using the balls and bins approximation, and dotted lines (...) are upper bounds using the one-dimensional projection approximation. The solid black line is the $1 - \frac{1}{n}$ threshold for high-connectivity.
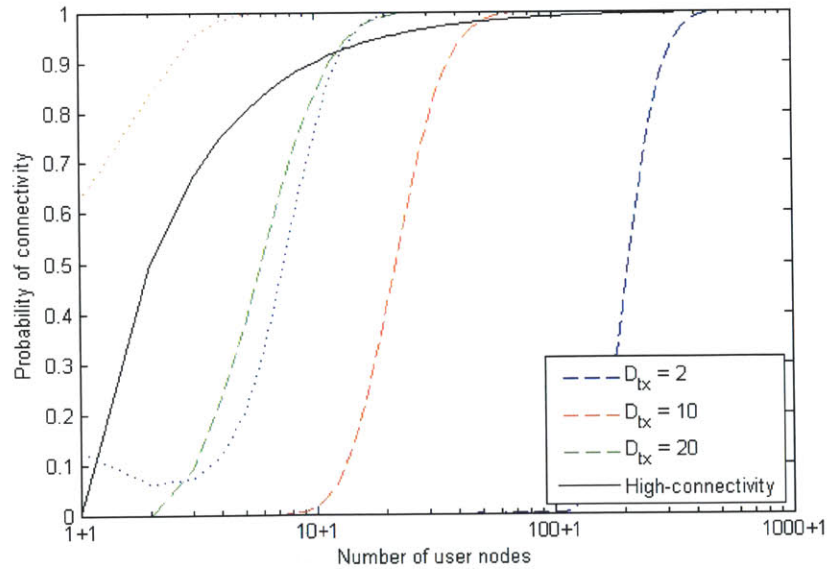
Figure 3-18: Upper and lower bounds on $P_{2D}^{bf}(n, \Delta, D_{tx})$ for random planar networks using beamforming-enabled antennas. Dashed lines (---) correspond to lower bound using balls and bins approximation, and dotted lines (...) correspond to upper bound using one-dimensional projection approximation. The solid black line is the $1 - \frac{1}{n}$ threshold for high-connectivity. For this figure, $\Delta = 0.25$ and the free space path-loss exponent is used, $k = 2$.

86
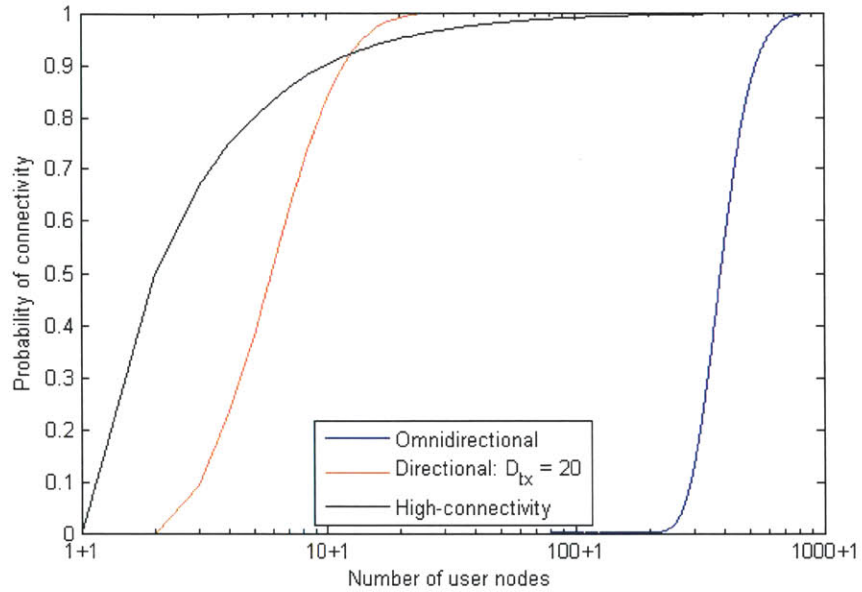
Figure 3-19: Lower bounds on $P_{2D}^{omni}(n, \Delta)$ and $P_{2D}^{bf}(n, \Delta, D_{tx})$ shown simultaneously for $\Delta = 0.25$ and $k = 2$, contrasting the performance of random planar networks with nodes using omnidirectional antennas and beamforming-enabled antennas. The solid black line is the $1 - \frac{1}{n}$ threshold for high-connectivity.
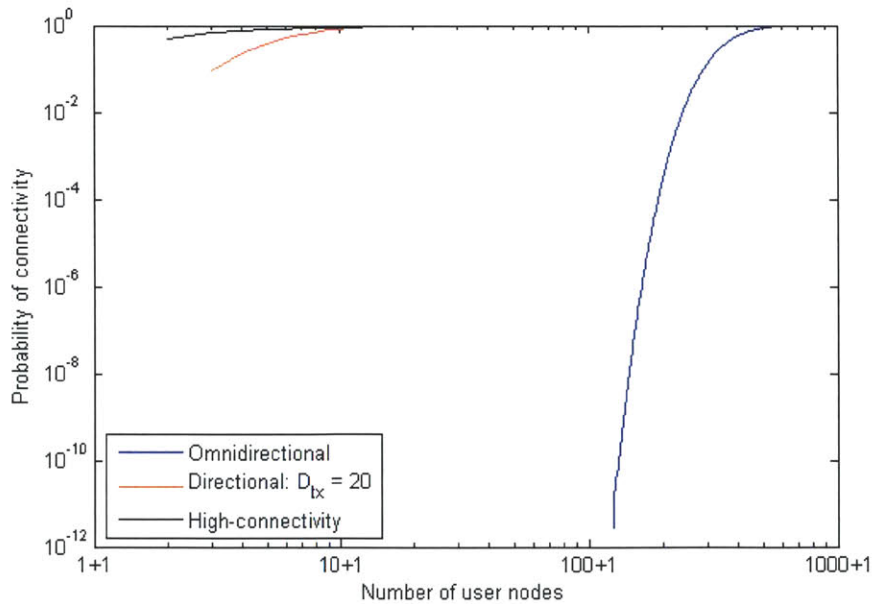
Figure 3-20: Lower bounds on $P_{2D}^{omni}(n, \Delta)$ and $P_{2D}^{bf}(n, \Delta, D_{tx})$ shown simultaneously for $\Delta = 0.25$ and $k = 2$, contrasting the performance of random planar networks with nodes using omnidirectional antennas and beamforming-enabled antennas on a log-log plot. This is the log-log scale version of Fig. 3-19.

enabled antennas in wireless infrastructureless networks, thus providing a reason to study their performance in more detail in the following chapters.

As in the random line network case, the addition of transmitter directivity allows the end-user device density to decrease while maintaining a high probability of instantaneous connectivity. With the definition of high probability of connectivity, we can use the lower bound result on the probability of connectivity to find the required number of end-users to achieve a high probability of connectivity for a given transmitter directivity. Since $P_C^{bb}(n,m) > 1 - \frac{1}{2n \ln n} > 1 - \frac{1}{n}$ when $m \leq \frac{n}{2 \ln n}$ in the balls and bins lower bound approximation, we need to satisfy $\frac{n}{\ln n} \geq \frac{10}{\Delta^2 D_{tx}^{2/k}}$ to ensure that a network deployment falls within the high probability of connectivity regime. This tradeoff between transmitter directivity and the required end-user node density for a high probability of instantaneous connectivity is shown in Fig. 3-21 for different values of the attenuation exponent k. The far left side of this plot represents the number of end-users required to achieve a high probability of connectivity in an omnidirectional network (equivalently, $D_{tx} = 1$). We observe that an order of magnitude increase in directionality corresponds to approximately an order of magnitude decrease in the number of nodes required when $k = 2$, just as in the random line network case.

3.3 Summary

This chapter considered random networks operating in fixed one- and two-dimensional regions and the probability of connectivity using end-user nodes equipped with either omnidirectional antennas or directional antennas. In particular, the exact probability of connectivity was shown for random line networks, while two different approximations were

presented to bound the actual probability of connectivity in the random planar network case. Connectivity with high probability was defined and used to identify required transmission range as a function of the node density of the network. Key design parameters that were identified included the number of user nodes in the network n, the normalized omnidirectional transmission range Δ, the directivity of the directional antenna used for beamforming-enabled nodes D_{tx}, and the attenuation exponent of the path-loss channel model k (this is not under the control of the network designer, but important to consider). It was also pointed out that while receive beamforming gain was suppressed in the analysis, this is another important design parameter that can be readily added to the analysis to realize even more gain in the directional network case over the omnidirectional network baseline.

These analytical results were used to compare the connectivity performance of random line and planar networks using end-user nodes with omnidirectional antennas to those with directional antennas for transmission. In the line network analysis, it was shown that the use of modest directivity gain could decrease the number of user nodes required for a high probability of connectivity by an order of magnitude. In the planar network analysis, we observed that this same modest amount of directivity could allow the network designer to reduce the required density of end-users by two orders of magnitude while still attaining a high probability of network connectivity. Furthermore, in the line network analysis, it was shown analytically that for a given number of end-user nodes in the network, the required normalized omnidirectional transmission range (equivalently the transmission power) could be improved by a factor of $\left(\frac{1}{D_{tx}}\right)^{1/k}$ while still maintaining a high probability of connectivity. These results indicate that the use of beamforming-enabled end-user nodes can significantly increase the network operating regimes of interest for providing QoS assurance to the end-user (specifically, the regimes with high probability of instantaneous network connectivity).
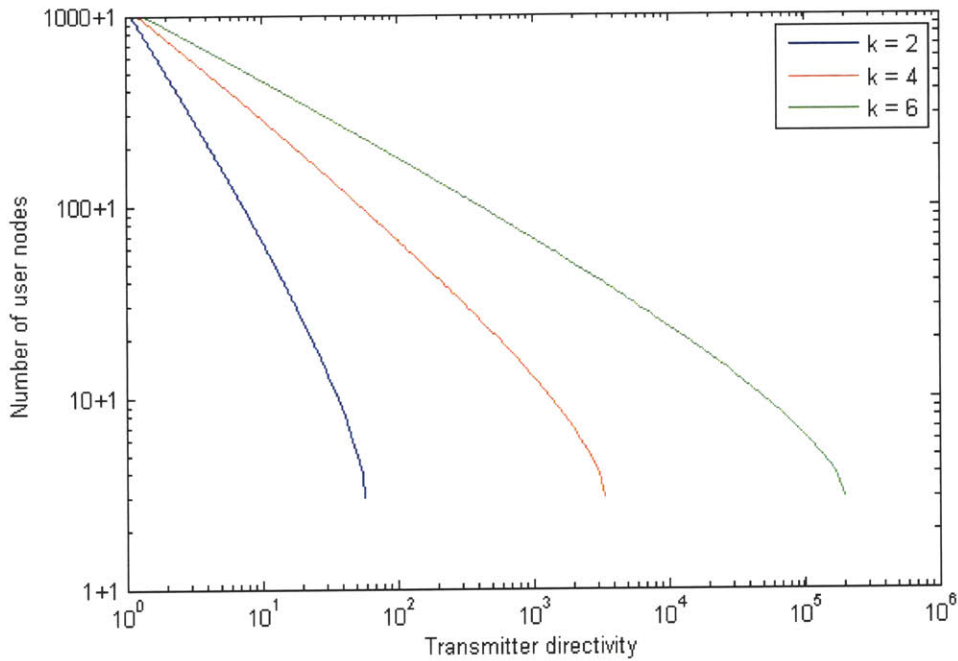
Figure 3-21: Number of end-user nodes required to achieve a probability of connectivity greater than $1 - \frac{1}{n}$ in a random planar network as a function of transmitter directivity for several values of the operation environment attenuation exponent k. For this figure, $\Delta = 0.25$.

As alluded to before, the analysis of this chapter uses very simple models. It does not consider possible device heterogeneity, RF environment heterogeneity, RF environment obstacles, or even more realistic node deployment distributions (for example, one would expect some level of end-user clustering in many infrastructureless wireless networks). These results, then, are only intended to guide network designers by identifying important parameters and tradeoffs and to motivate our continued study of the benefits of using beamforming-enabled devices in wireless infrastructureless networks.

Chapter 4

Throughput, Delay, and Energy Scaling for the Power-limited Network

In the previous chapter, we characterized network regimes with a high probability of connectivity. Identifying deployment scenarios with a high probability of connectivity is the first step in discussing a network's ability to satisfy end-user QoS requirements. We now consider other important performance metrics that are central to end-user QoS: throughput, end-to-end delay, and energy consumption. In particular, since we are considering infrastructureless wireless networks that may be composed of hundreds of end-users in a bounded operating environment, we focus on the scalability of these metrics. After identifying the network scaling behavior, we can use the resulting analytical insight to

develop efficient network algorithms to achieve the most desirable scaling behavior. This is the subject of the following chapter.

Throughput is a clear first-consideration for delivering core service to the end-users, since it is this metric that initially determines if data can be exchanged between devices in the network. However, the existence of a sustainable level of throughput alone does not guarantee that a system of battery-limited wireless nodes can support core services. Thus, we consider the relationship between the sustainable throughput and the per-bit energy and delay scaling (in terms of number of end-to-end hops) as well, which helps us to establish the capability of the network to provide assured QoS.

After the work of Gupta and Kumar [11], there has been a large body of work concerned with identifying the scaling behavior and tradeoffs of infrastructureless wireless networks. The majority of this work has considered interference-limited networks, in which the interference from nearby transmitters is the dominant source of noise at the receivers and the limiting factor in network scalability. This area is well-studied, and the framework has been extended to networks with beamforming-enabled end-user nodes [12]. In terms of scalability, however, better behavior has been shown by exploring the physical layer option of bandwidth expansion (or in the network regime where bandwidth is not the limiting factor). With enough system bandwidth available, interference noise at the receivers can be suppressed through appropriate channelization. In this network regime, the power constraints at each node become the limiting factor in network scalability and performance.

We use the unlimited bandwidth assumption in our performance analysis, since this analytical approach allows us to obtain an upper bound on the best performance that we can achieve with a beamforming-enabled infrastructureless wireless network. While the

inclusion of interference may decrease network performance, the achievable network performance can closely approach the upper bound with effective beamforming.

This chapter proceeds in the following manner. We first identify important assumptions, definitions, and additional energy consumption models that we invoke throughout the analysis presented in this chapter. We then consider the sustainable throughput of an arbitrary (non-random) infrastructureless wireless network operating in a bounded region for both fixed-rate and variable-rate transmission systems. We include derivations and discussions of the omnidirectional infrastructureless wireless network alongside the directional network for completeness and comparison. Finally, we use insight from the analysis of arbitrary networks to identify the scaling behavior of random infrastructureless wireless networks, both omnidirectional and directional, operating in the same bounded region. We show that this analysis provides insight on routing solutions that attain the best network scaling behavior in terms of all QoS performance metrics considered. This insight guides the routing algorithm development of Chapter 5.

4.1 Assumptions, Definitions, and Models

4.1.1 Assumptions

Throughout this chapter, we invoke several key assumptions that make the analysis tractable. This section summarizes those assumptions, although we repeat them in the appropriate sections throughout this chapter in order to highlight the effect these assumptions have on the interpretation of the results.

First, we consider an infrastructureless wireless network with n nodes. Each node in the network can generate new traffic intended for any other node in the network, and each node can also help forward pass-through traffic for other source-destination (SD) node pairs. We find throughout the analysis in this chapter that many results show that the best behavior of the network in question does not depend on n explicitly. Since we are primarily interested in scaling behavior, we employ order notation to express some results. Hidden in this notation is the assumption that n is "large enough." We attempt to clarify what this large enough n assumption means in context as we proceed. Nonetheless, results in this chapter are still valid for small values of n.

Next, we assume end-user device homogeneity. The analytical framework presented could be extended to heterogeneous nodes at the cost of analytical simplicity. By assuming homogeneous nodes, we are able to find first-order results that reveal the fundamental limiting behavior of the networks. Maintaining simplicity can guide further network design, including the algorithmic routing approaches in the following chapter.

Another important assumption is that of a geographically-bounded, two-dimensional operating region that grows slower than the number of nodes so that the node density increases as the number of end-users in the operating region increases. If the density of nodes does not increase with increasing number of end-users, very little can be said about the scaling behavior of the network. In the analysis of random networks in Section 4.3, we use a fixed-size bounded operating region for tractable analysis.

We assume enough available system bandwidth, W [Hz], so that through appropriate channelization, each possible communication pair in the network can use its own set of unique communication channels (equivalently, for a network with n end-user nodes, there are at least $n(n-1)$ available frequency channels). It is this assumption that allows the

receivers to resolve the desired signal from noise and interfering signals and focuses our analysis on the performance of a power-limited network. With this assumption, the system bandwidth can be modeled as approaching infinity.

Finally, we assume in our model that node power availability is the limiting factor for our network. Specifically, we assume that both distance-dependent transmission energy and signal processing energy are non-negligible (which diverges from many analytical studies in the power-limited network regime [49,50]).

4.1.2 Definitions

Before proceeding with the specific model we use for analysis in this chapter, we establish a few key definitions. Using the uniform traffic model to be discussed in Section 4.1.3, SD pairs all exchange data at an average rate of λ [bit/sec]. We define uniform capacity, $\hat{\lambda}$ [bit/sec], as the maximum achievable data rate under uniform traffic subject to a per-node power constraint, where achievable means that this data rate can be sustained by all SD pairs in the uniform traffic pattern. Uniform capacity is the maximum achievable data rate over all possible routing strategies. Mathematically, we let P represent the set of all possible routing strategies, and then we have:

$$\hat{\lambda} = \max_{P} \{\text{Achievable } \lambda\}. \tag{4.1}$$

For an arbitrary network, $\hat{\lambda}$ is a deterministic quantity. But, for random networks, $\hat{\lambda}$ is a stochastic quantity. Alternatively, we define uniform throughput, $\tilde{\lambda}$, as the maximum achievable data rate with high probability under uniform traffic given a specific routing scheme. We add the phrase "with high probability" to this definition because we only consider this metric in our analysis of random networks. This definition is used when we

95

analyze the uniform throughput of a routing scheme that achieves the best uniform capacity scaling behavior, while comparing this to the uniform throughput using the WtNN routing scheme (as presented in [51]).

As in the definition of uniform throughput above, we make use the phrase "with high probability" (whp) throughout the stochastic analysis in this chapter which deals with random network deployments and uniform traffic patterns. The phrase "with high probability" is defined as a sequence of events with probability approaching one as n goes to infinity. The definition of "with high probability" in Chapter 3 (an event with probability greater than $1 - \frac{1}{n}$) satisfies this more general definition.

4.1.3 Traffic and Power Models

We adopt the network model of [49] with two key differences:

1. Along with distance-dependent transmission energy consumption, we also model signal processing energy consumption as in [9].

2. Depending on our transceiver design, the transmission rate we consider can be either fixed or variable. We consider both of these cases, recognizing that the fixed rate system implies a maximum transmission range, whereas the variable rate system allows for a connection between every possible node pair in the network albeit sometimes at low rate. Regardless of the case, we assume that nodes employ power control such that they can adjust the radiated power depending on the distance between the transmitter and the receiver.

We consider a uniform traffic model, as in [11], where each node arbitrarily chooses a destination and then sends data to that destination node at an average rate of λ [bits/sec]. Our analysis closely follows the framework of Chapter 4 in [9], although that work considers a different traffic pattern. Consequently, some of our omnidirectional network results vary from those presented in [9], but they do agree with [51] in which the uniform traffic model is used.

Since our work is focused on a power-limited network regime, we develop and discuss the energy consumption models that we use in this analysis. For most infrastructureless wireless networks, nodes are required to be untethered and, thus, the devices are limited by available battery power. For the purpose of this analysis, we assume that the maximum time-averaged power available to an end-user node, both for transmission and processing, is limited to P_{avg} [J/sec]. Decreasing the value of P_{avg} increases node lifetime, but we show that this is at the expense of degraded network performance.

We begin with discussion of energy consumption models for omnidirectional nodes, and then we show how the models change for a directional network. In the node communication electronics, the average power expended is related to the average data rate of the transmitted and received signals. Using the simple path-loss model, the Shannon Capacity Theorem tells us that the data rate that node i can transmit to node j, denoted R_{ij} [bit/sec], is upper-bounded by the link capacity, C_{ij} [bit/sec], under the limit of large bandwidth:

$$R_{ij} \le C_{ij} \xrightarrow[W \to \infty]{} \frac{\gamma_{ij} P_t^{ij}}{N_0 d_{ij}^k} \tag{4.2}$$

where γ_{ij} is the RF gain (including antenna gains and RF processing losses), P_t^{ij} [J/sec] is the time-average transmitted power from node i to j, d_{ij} [m] is the distance between nodes i and j, k is the attenuation exponent of the path-loss model, and N_0 is the noise spectral density.

The time-averaged received power at node j from node i, denoted P_r^{ij} [J/sec], can be seen in (4.2) as:

$$P_r^{ij} = \frac{\gamma_{ij} P_t^{ij}}{d_{ij}^k}. \tag{4.3}$$

In the limit of large bandwidth, the capacity of the link increases linearly with the received power.

We define the aggregate average transmitted data rate for new and pass-through traffic at node i, denoted R_i^t [bit/sec], and the aggregate average received data rate for new and pass-through traffic at node i, denoted R_i^r [bit/sec], as follows:

$$R_i^t = \sum_{j:\, j \neq i} R_{ij}, \tag{4.4}$$

$$R_i^r = \sum_{j:\, j \neq i} R_{ji}. \tag{4.5}$$

The time-average total power consumed at node i, denoted P_i [J/sec], can be modeled as shown in [9]:

$$P_i = \alpha_r R_i^r + \alpha_0 R_i^r + \alpha_1 R_i^t + \alpha_t R_i^t + \eta \sum_{j:\, j \neq i} P_t^{ij} \tag{4.6}$$

where α_r, α_0, α_1, and α_t are the per bit energy costs for receiving data, processing and storing received data, storing and processing transmitted data, and transmitting data (which excludes the transmission power amplifier), all measured in [J/bit]. The amplifier power is modeled by the last term, where η represents the inverse of the amplifier power conversion efficiency. Due to device homogeneity, we let $\gamma_{ij} = \gamma$, $\forall i, j$. Then, using (4.2), we can rewrite (4.6) as:

Systems	Data Rate (Mbps)	Tx Power (mW)	Signal processing power (mW)	α nJ/bit	β nJ/bit·m^{-k}	d_{max}
Wireless sensor [46]	2.5	12.5	50	20	0.002	100
UWB [47,48]	16.7	0.8	42	2.5	0.008	18

Table 4.1: Transmit and processing energy consumption information for two low-power wireless systems [9].

$$P_i = \sum_{j:\, j \neq i} (\alpha_r + \alpha_0) R_{ji} + \sum_{j:\, j \neq i} \left(\alpha_1 + \alpha_t + \frac{\eta N_0}{\gamma} d_{ij}^k \right) R_{ij}. \qquad (4.7)$$

Now, we consider the total end-to-end path power consumed by a single transmission of rate λ [bit/sec], which we denote P_{path} [J/sec]. We allow this transmission to be routed through a total of h hops, where d_i [m] represents the distance of the ith hop. If we let $\alpha = \alpha_r + \alpha_0 + \alpha_1 + \alpha_t$ and $\beta = \frac{\eta N_0}{\gamma}$, we use (4.7) to get:

$$P_{path} = \lambda \sum_{m=1}^{h} (\alpha + \beta d_m^k). \qquad (4.8)$$

Different forms of this first-order path power consumption model have been used in the physical device field literature (see [52-54]). The values of α and β for several short-range wireless systems are shown in Table 4.1.

Now we consider the associated power models for a directional infrastructureless wireless network, where we include transmitter directivity and normalize the receive directivity gain to unity. Using the path-loss model, the received power at node j is increased by a factor corresponding to the transmitter directivity:

$$P_r^{ij} = \frac{\gamma D_{tx} P_t^{ij}}{d_{ij}^k}.$$ (4.9)

Therefore, the time-average total power consumed at node i, denoted P_i^{bf} [J/sec], can be modeled as:

$$P_i^{bf} = \sum_{j:\, j \neq i} (\alpha_r + \alpha_0) R_{ji} + \sum_{j:\, j \neq i} \left(\alpha_1 + \alpha_t + \frac{\eta N_0}{\gamma} \frac{d_{ij}^k}{D_{tx}} \right) R_{ij}.$$ (4.10)

We note that due to additional processing requirements for transmit and receive beamforming, the values for α_r and α_t (and consequently α) may increase in the directional network case. In the interest of a first-order comparative study, we let these values remain constant for the omnidirectional and directional network analyses. However, if the algorithmic implementation of beamforming were to create a significantly large increase in processing power, this "constant α" assumption may need to be modified to include the additional power requirements. Similarly, even though the exact value for β may change due to differences in the antenna construction and geometry, we keep this value constant over the two analyses in the interest of a first-order comparative study. Additional work is required to better characterize the values of these parameters in directional infrastructureless wireless networks, as they have been in omnidirectional infrastructureless wireless networks (see Table 4.1, for example).

Finally, as in the omnidirectional case, we define P_{path}^{bf} [J/sec] as the total end-to-end time-average path power consumption of a single transmission of rate λ which traverses h hops. From (4.10), we can show that:

$$P_{path}^{bf} = \lambda \sum_{m=1}^{h} \left(\alpha + \beta \frac{d_m^k}{D_{tx}} \right).$$ (4.11)

100

4.2 Uniform Capacity of Arbitrary Networks

In this section, we derive and present bounds on the uniform capacity of power-limited networks with n nodes located in a bounded region for an arbitrary uniform traffic pattern. We first consider omnidirectional and directional networks with fixed transmission rates, and then we consider these networks with variable transmission rates. The main results are summarized in Section 4.2.5, and they are used to study the scaling behavior of random networks in Section 4.3.

4.2.1 Uniform Capacity of Omnidirectional Networks with Fixed Transmission Rate

In this section, we derive bounds on the uniform capacity of an infrastructureless wireless network using omnidirectional transmit and receive antennas. In the fixed transmission rate scenario, a node is assumed to transmit at a fixed rate of R [bit/sec] whenever it transmits. This includes both new and pass-through traffic. Considering the per-node time-average power constraint P_{avg}, this fixed rate system places a maximum hop distance restriction on each transmission. If we let ρ [m] represent transmission hop distance, then ρ must satisfy the following in order for a transmission to be received correctly:

$$\rho \leq \left(\frac{1}{\beta} \left[\frac{P_{avg}}{R} - \alpha \right] \right)^{1/k} \triangleq \rho_{max}. \tag{4.12}$$

The expression in (4.12) comes from imagining that all P_{avg} is devoted to a single one-hop transmission in the path power model (4.8). As shown in (4.12), we define a maximum hop distance, ρ_{max}[m], and the constraint on transmission hop distance is $0 \leq \rho \leq \rho_{max}$.

101

We note that the per-node power constraint couples the routing decisions for all pass-through traffic of all n SD pairs exchanging data under uniform traffic, since each node's available power must be allocated to all outgoing links (not just a single link). This coupling makes the analysis difficult. In order to solve this problem and find an upper bound for uniform capacity, we relax the per-node power constraint to a total time-average network power constraint of nP_{avg}. The uniform capacity under the per-node power constraint is bounded from above by the uniform capacity under this relaxed total network power constraint. This bound is good when nodes are mobile, as in an infrastructureless wireless network, and their relative positions change ergodically over time. However, this bound is not good for relatively static situations where interior nodes expend more energy for pass-through traffic.

We now derive an upper bound on $\hat{\lambda}$ for a fixed rate omnidirectional network using hop counting arguments similar to the technique used for the derivation of the transport throughput upper bound in [11] and following the approach of [9]. In terms of notation, we let $\{L_i\}_{1 \leq i \leq n}$ [m] be the distance between the ith SD pair in the network. For an arbitrary network topology and arbitrary uniform traffic pattern, these are deterministic quantities. We denote the empirical average of distances between all n SD pairs as $\bar{L} = \frac{1}{n}\sum_{i=1}^{n} L_i$. For completeness, the proof is shown in Appendix C.1.

Lemma 1. *The uniform capacity of an arbitrary power-limited infrastructureless wireless network with fixed transmission rate R and using omnidirectional antennas is upper bounded by:*

$$\hat{\lambda} \leq \frac{R\rho_{max}}{\bar{L}}. \tag{4.13}$$

Equality in (4.13) is achieved if all n SD pairs are separated by exactly ρ_{max} and no node is selected more than once as a destination node. We then trivially get $\hat{\lambda} = R$ by direct transmission between all SD pairs. We consider two very important aspects of this bound. First, there is no explicit dependence on n, the number of network end-user devices. And second, as $\bar{L}$ is both topology-dependent and traffic-dependent, the uniform capacity bound becomes arbitrarily high as nodes are grouped closer and closer together in the operating environment. However, R is still the maximum uniform capacity that can be achieved by the constraint of the fixed transmission rate system.

To derive a lower bound on the uniform capacity, we consider a variant of the worst-case example as proposed by [9]. Pictorially, this example is shown in Fig. 4-1. In this example, we let n be odd. One node is located at the origin $(0,0)$, $\frac{n-1}{2}$ nodes called group A are located at $(-\rho_{max}, 0)$, and the other $\frac{n-1}{2}$ nodes called group B at located at $(\rho_{max}, 0)$. The uniform traffic is such that each node in group A chooses a destination node in group B, and each node in group B chooses a destination node in group A. The node at the origin chooses a destination node in either group A or group B. The traffic between group A and group B must all be routed through the bottleneck node located at the origin, since group A and group B are separated by more than the maximum transmission range. The bottleneck node here is subject to the maximum possible traffic load, $n\hat{\lambda}$. This is a worst-case example since uniform capacity is determined by the end-user subject to the most traffic (both new and pass-through). Since this bottleneck node is transmission rate constrained to R, we have $\hat{\lambda} = \frac{R}{n}$ in this scenario. Thus we have established the lower bound on uniform capacity, which is given in the following lemma.

Group A   Group B
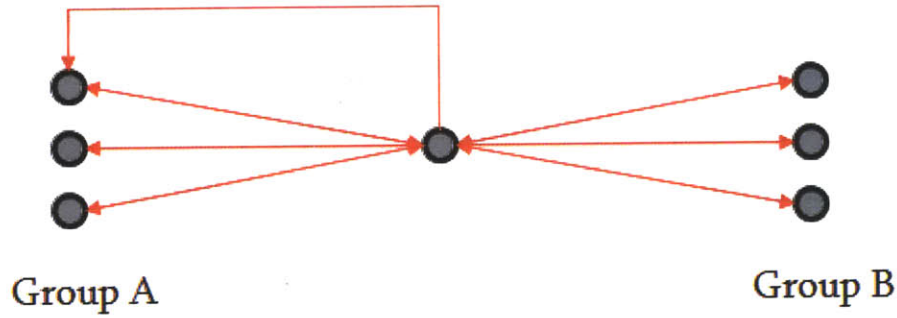
Figure 4-1: Example network that achieves the uniform capacity lower bound for networks with fixed rate transmissions.

Lemma 2. *The uniform capacity of an arbitrary power-limited infrastructureless wireless network with fixed transmission rate R and using omnidirectional antennas is lower bounded by:*

$$\hat{\lambda} \geq \frac{R}{n}. \tag{4.14}$$

This bound is not independent of the number of network end-user devices, and the uniform capacity can approach zero under the worst-case network topology and worst-case uniform traffic patterns as the number of nodes in the network increases.

4.2.2 Uniform Capacity of Directional Networks with Fixed Transmission Rate

We now proceed to derive bounds on the uniform capacity of an infrastructureless wireless network using directional transmit antennas (receive directivity is normalized to unity for notational simplicity). In the directional case, we use the notation $\hat{\lambda}^{bf}$ [bit/sec] for uniform

104

capacity to avoid confusion with the omnidirectional network results. The fixed rate transmission assumption again places a restriction on maximum transmission range, as in the omnidirectional case. Using the path power consumption model as before, we see that the modified constraint for the beamforming-enabled network is:

$$\rho \leq \left(\frac{D_{tx}}{\beta}\left[\frac{P_{avg}}{R} - \alpha\right]\right)^{1/k} \triangleq \rho_{max}^{bf}. \tag{4.15}$$

As can be seen in (4.15), the maximum hop distance, now denoted ρ_{max}^{bf} [m], has increased by a factor of $D_{tx}^{1/k}$ as expected. The constraint on hop distance is now summarized as $0 \leq \rho \leq \rho_{max}^{bf}$. This result depends on the "constant α" assumption as discussed in Section 4.1.3. If the value of α should be significantly larger in the beamforming network, then the maximum hop distance, ρ_{max}^{bf}, would be less than shown in (4.15).

We proceed as in the omnidirectional network analysis for fixed transmission rate. We first relax the per-node time-average power constraint to a total network time-average power constraint to avoid the problem of route computation coupling, and then derive the upper bound on uniform capacity in exactly the same way as presented in Appendix C.1. The result is presented in the following lemma.

Lemma 3. *The uniform capacity of an arbitrary power-limited infrastructureless wireless network with fixed transmission rate R and using directional transmit antennas with directivity D_{tx} is upper bounded by:*

$$\hat{\lambda}^{bf} \leq \frac{R\rho_{max}^{bf}}{\bar{L}}. \tag{4.16}$$

Equality in (4.16) is achieved if all n SD pairs are separated by exactly ρ_{max}^{bf} and no node is selected more than once as a destination node. Again, there is no explicit dependence on n, the number of network end-user devices. And as noted in the omnidirectional case, since $\bar{L}$

is both topology-dependent and traffic-dependent, the uniform capacity bound becomes arbitrarily high as nodes are grouped closer and closer together in the operating environment. Comparing (4.16) to the omnidirectional uniform capacity upper bound of an arbitrary network (4.13), we see an increase in the bound by a factor of $D_{tx}^{1/k}$ through the difference between ρ_{max}^{bf} and ρ_{max}. The maximum achievable uniform capacity is still constrained by R, the transmission rate constraint of the fixed rate transmission system. Uniform capacity improvement over the omnidirectional network case is realized for a topology in which an increased maximum hop distance of ρ_{max}^{bf} allows for a reduction in the number of hops per bit (when $\bar{L} \gg \rho_{max}$).

To derive the lower bound for uniform capacity in the directional network case, we again consider the worst-case topology and uniform traffic pattern of Fig. 4-1. This time we let group A be located at $(-\rho_{max}^{bf}, 0)$ and group B be located at $(\rho_{max}^{bf}, 0)$. With this worst-case topology and worst-case uniform traffic pattern, we again find that the bottleneck node dictates that $\hat{\lambda}^{bf} = \frac{R}{n}$. This establishes our lower bound on uniform capacity, and we present the result formally in the following lemma.

Lemma 4. *The uniform capacity of an arbitrary power-limited infrastructureless wireless network with fixed transmission rate R and using directional transmit antennas with directivity D_{tx} is lower bounded by:*

$$\hat{\lambda}^{bf} \geq \frac{R}{n}. \tag{4.17}$$

As in the omnidirectional network case, this bound is not independent of the number of network end-user devices, and thus the uniform capacity can approach zero under the worst-case network topology and worst-case uniform traffic patterns as the number of end-user devices in the network increases.

4.2.3 Uniform Capacity of Omnidirectional Networks with Variable Transmission Rate

We now establish bounds on the uniform capacity of omnidirectional infrastructureless wireless networks with variable rate transmission systems. This can be expressed as a multi-commodity flow problem and solved by standard multi-commodity flow algorithms [55]. If we allow node i to use link (l, m) to carry its traffic destined for node j at a rate of Λ_{lm}^{ij} [bit/sec], which includes new and pass-through traffic, we can express the multi-commodity flow problem as follows:

$$\hat{\lambda} = \max_{\Lambda_{lm}^{ij}, \forall (l,m), \forall (i,j)} \lambda$$

$$s.t.$$

$$\Lambda_{lm}^{ij} \geq 0, \forall (l, m), \forall (i, j) \tag{4.18}$$

$$\sum_{m:\, m \neq l} \sum_{(i,j)} \Lambda_{lm}^{ij} \left(\alpha + \beta d_{lm}^{k} \right) \leq P_{avg}, \forall l$$

$$\sum_{m:\, m \neq l} \Lambda_{lm}^{ij} - \sum_{m:\, m \neq l} \Lambda_{ml}^{ij} = \begin{cases} \lambda, & l = i \\ -\lambda, & l = j, \\ 0, & \text{otherwise} \end{cases} \forall (i, j), \forall l.$$

We do not solve this multi-commodity flow problem for specific networks, but instead derive bounds on the uniform capacity of arbitrary network topologies and arbitrary uniform traffic patterns as we did for fixed transmission rate systems. We first derive an upper bound on $\hat{\lambda}$. As in the fixed rate case, the routing decisions for all pass-through traffic for all n SD pairs are coupled by the per-node time-average power constraint, P_{avg}. As before, we relax this constraint to a total network time-average transmit power constraint of nP_{avg} and recognize that the uniform capacity under this relaxed constraint is an upper bound to $\hat{\lambda}$ under the more restrictive per-node constraint. As we are ultimately constrained by the

network power, uniform capacity maximization becomes equivalent to path power minimization (this is made clear through the proof procedure). We find the upper bound on $\hat{\lambda}$ for a variable rate omnidirectional network by minimizing path energy consumption, following the procedure presented in [51]. In order to perform this minimization, we can optimize the number of hops for the traffic of SD pair i, striking a balance between processing energy consumption and distance-dependent transmission energy consumption. If we let n_i^* denote the optimal number of hops for traffic of SD pair i and L_i be the distance between SD pair i, we can define an optimal, or characteristic, hopping distance, $d_{char} \triangleq \frac{L_i}{n_i^*}$ [m], as proposed in [54]. The proof shows that this characteristic hopping distance is independent of the index i. The characteristic hopping distance will be discussed in more detail once we have established all uniform capacity bounds for arbitrary networks. For completeness, the proof of the upper bound on uniform capacity is shown in Appendix C.2. The result is presented in the following lemma.

Lemma 5. *The uniform capacity of an arbitrary power-limited infrastructureless wireless network with variable transmission rate and using omnidirectional transmit antennas is upper bounded by:*

$$\hat{\lambda} \le \frac{P_{avg}}{c_1 \alpha \bar{L} \left(\frac{\beta}{\alpha}(k-1)\right)^{1/k} \left(1 + \frac{1}{c_2^k(k-1)}\right)} = \frac{P_{avg} d_{char}}{c_1 \alpha \bar{L} \left(1 + \frac{1}{c_2^k(k-1)}\right)} \quad (4.19)$$

where $d_{char} = \left(\frac{\alpha}{\beta(k-1)}\right)^{1/k}$ *and* c_1, c_2 *are positive constants.*

The positive constants c_1 and c_2 in (4.19) are a result of the integer constraint on the number of number of hops between the source and destination, since there is no guarantee that n_i^* will be integer-valued. This is also revealed in the proof procedure presented in Appendix C.2. Equality in (4.19) is achieved if all SD pairs are separated by d_{char}. As in the fixed rate

system, we see that the upper bound is not explicitly dependent on the number of end-user devices. Also, the uniform capacity can become arbitrarily high if nodes are grouped closer and closer in the operating environment, since $\bar{L}$ is both topology-dependent and traffic-dependent.

For a lower bound on the uniform capacity of arbitrary omnidirectional infrastructureless wireless networks with variable transmission rate, we recognize that there is no constraint on maximum transmission range. With the relaxed variable transmission rate consideration, all pairs of nodes in the network are capable of sustaining some rate of communication. Thus, the lower bound on uniform capacity is obtained by using direct transmission routing, where the source transmits to the destination node in one hop. We let $L_{max} = \max\{L_i\}$ for an arbitrary network topology and arbitrary uniform traffic pattern, then we have that the lower bound on the uniform capacity is determined by the longest separation between all n SD pairs. The following lemma summarizes this result.

Lemma 6. *The uniform capacity of an arbitrary power-limited infrastructureless wireless network with variable transmission rate and using omnidirectional transmit antennas is lower bounded by:*

$$\hat{\lambda} \geq \frac{P_{avg}}{\alpha + \beta L_{max}^k}. \tag{4.20}$$

We note that the lower bound on uniform capacity with variable rate transmissions is also independent of n, the number of end-user devices in the network.

4.2.4 Uniform Capacity of Directional Networks with Variable Transmission Rate

In this section, we derive bounds on the uniform capacity of directional networks with variable transmission rates. As in the omnidirectional case, this could be formulated as a multi-commodity flow problem (with slightly modified constraints). But rather than solve this problem for specific networks, we again focus on finding bounds on the uniform capacity using the same analytical framework as in Section 4.2.3. Since the proof techniques are the same, we will simply present the results here.

Lemma 7. *The uniform capacity of an arbitrary power-limited infrastructureless wireless network with variable transmission rate and using directional transmit antennas with directivity D_{tx} is upper bounded by:*

$$\hat{\lambda}^{bf} \leq \frac{P_{avg}}{b_1 \alpha \bar{L} \left(\frac{\beta}{\alpha D_{tx}} (k-1) \right)^{1/k} \left(1 + \frac{1}{b_2^k(k-1)} \right)}$$

$$= \frac{P_{avg} d_{char}^{bf}}{b_1 \alpha \bar{L} \left(1 + \frac{1}{b_2^k(k-1)} \right)}$$

(4.21)

where $d_{char}^{bf} = \left(\frac{\alpha D_{tx}}{\beta(k-1)} \right)^{1/k}$ and b_1, b_2 are positive constants.

Equality in (4.21) is achieved if all SD pairs are separated by d_{char}^{bf}. Again, we see that the upper bound is not explicitly dependent on the number of end-user devices. Also, the uniform capacity can become arbitrarily high as nodes are grouped closer and closer in the operating environment, since $\bar{L}$ is both topology-dependent and traffic-dependent. As we would expect, the characteristic hopping distance is increased by a factor of $D_{tx}^{1/k}$ over the

omnidirectional case, and the upper bound on the uniform capacity is also increased by this same factor as a result.

The lower bound on the uniform capacity for a directional network with variable transmission rate is derived using the direct transmission routing argument, as in the omnidirectional case.

Lemma 8. *The uniform capacity of an arbitrary power-limited infrastructureless wireless network with variable transmission rate and using directional transmit antennas with directivity D_{tx} is lower bounded by:*

$$\hat{\lambda}^{bf} \geq \frac{P_{avg}}{\alpha + \frac{\beta}{D_{tx}} L_{max}^k}. \tag{4.22}$$

This lower bound on uniform capacity for the variable rate transmission system is also independent of n, the number of end-user devices in the network, just as in the omnidirectional case.

4.2.5 Summary and Discussion of Uniform Capacity Results for Arbitrary Networks

Summarizing the results from Sections 4.2.1-4.2.4 and Lemmas 1-8, we establish the following theorem which contains all of the uniform capacity bounds for arbitrary infrastructureless wireless networks.

Theorem 1. *Uniform capacity of arbitrary, connected infrastructureless wireless networks in a bounded operating environment.*

(i) The uniform capacity of an arbitrary power-limited infrastructureless wireless network with fixed transmission rate R that uses either omnidirectional transmission antennas or directional transmission antennas with directivity gain D_{tx} is bounded by, respectively:

$$\frac{R}{n} \leq \hat{\lambda} \leq \frac{R\rho_{max}}{\bar{L}},$$

$$\frac{R}{n} \leq \hat{\lambda}^{bf} \leq \frac{R\rho_{max}^{bf}}{\bar{L}}$$

where n is the number of end-user nodes in the network, $\rho_{max} = \left(\frac{1}{\beta}\left[\frac{P_{avg}}{R} - \alpha\right]\right)^{1/k}$ and $\rho_{max}^{bf} = \left(\frac{D_{tx}}{\beta}\left[\frac{P_{avg}}{R} - \alpha\right]\right)^{1/k}$ are the maximum hop distances for nodes with omnidirectional transmission antennas and directional transmission antennas respectively, L_i is the distance between SD pair i, and $\bar{L} = \frac{1}{n}\sum_{i=1}^{n} L_i$ is the average distance between SD pairs.

(ii) The uniform capacity of an arbitrary power-limited infrastructureless wireless network with variable transmission rate and using either omnidirectional transmission antennas or directional transmission antennas with directivity gain D_{tx} is bounded by, respectively:

$$\frac{P_{avg}}{\alpha + \beta L_{max}^k} \leq \hat{\lambda} \leq \frac{P_{avg} d_{char}}{c_1 \alpha \bar{L}\left(1 + \frac{1}{c_2^k(k-1)}\right)},$$

$$\frac{P_{avg}}{\alpha + \frac{\beta}{D_{tx}} L_{max}^k} \leq \hat{\lambda}^{bf} \leq \frac{P_{avg} d_{char}^{bf}}{b_1 \alpha \bar{L}\left(1 + \frac{1}{b_2^k(k-1)}\right)}$$

where c_1, c_2, b_1, and b_2 are positive constants, L_{max} is the maximum distance between all SD pairs, and $d_{char} = \left(\frac{\alpha}{\beta(k-1)}\right)^{1/k}$ and $d_{char}^{bf} = \left(\frac{\alpha D_{tx}}{\beta(k-1)}\right)^{1/k}$ are the characteristic hop distances for omnidirectional networks and directional networks respectively.

Additionally, we provide corollaries that follow directly from the results presented in Theorem 1 and will be useful in discussing the implications of this analysis of uniform capacity in arbitrary networks.

Corollary 1. *The uniform capacity of arbitrary infrastructureless wireless networks with fixed transmission rate is $O(1)$ and $\Omega(\frac{1}{n})$ with respect to increasing n.*

Corollary 2. *The uniform capacity of arbitrary infrastructureless wireless networks with variable transmission rate is $\Theta(1)$ with respect to increasing n.*

First, we focus our discussion on fixed transmission rate systems. From these results, we see that taking long hops on the order of ρ_{max} achieves higher throughput in general. Using beamforming-enabled antennas with directivity gain increases the maximum hop distance and can decrease the number of hops needed to reach a destination. However, in terms of the scalability of these results, we see that the fixed rate systems are both $O(1)$ with increasing n in the best case (in other words, the uniform capacity does not scale with the number of user nodes), but can be as bad as $\Omega(\frac{1}{n})$ with increasing n for some worst-case topologies and worst-case uniform traffic patterns. The increased range of beamforming-enabled antennas does not save us from this worst-case scaling behavior, although it helps us to avoid these scenarios by making the occurrence of bottleneck topologies and traffic patterns less likely for a bounded operating region.

For variable rate transmission systems, however, we find that the uniform capacity is $\Theta(1)$ as the node density increases since both the upper and lower bounds have a scaling behavior independent of n. We can achieve this scaling behavior that is independent of n by taking $\Theta(1)$ hops under the direct transmission scheme as demonstrated by the lower bound, even though this routing scheme may not yield high throughput if SD pairs are separated by long distances within the bounded operating region. Yet, the uniform capacity under other routing schemes with $\Theta(1)$ hops can also achieve the $\Theta(1)$ scaling behavior as n increases as shown by the upper bound. This is a favorable result, since [56] has shown that routing schemes with $\Theta(1)$ hops (equivalently, the number of hops does not increase with increasing n) also attains the best per bit energy and end-to-end delay (in terms of number of hops) scaling behavior of $\Theta(1)$ as n increases for power-limited networks. These results are in contrast to previous power-limited network studies that invoked the zero processing energy assumption and claimed that taking a large number of short hops that increases with increasing node density is the optimal routing scheme. As mentioned in [9], it is for this reason that we should not assume WtNN as the de facto routing strategy for all infrastructureless wireless networks.

Theorem 1 further suggests that $\Theta(1)$ hop routing strategies should use d_{char} and d_{char}^{bf} as rough guidelines for hop distances in order to achieve the desirable throughput, energy per bit, and end-to-end delay (equivalently, total number of hops) scaling behavior. By taking hop lengths of this order (as long as the traffic load can be distributed evenly so as not to create a network bottleneck node), we minimize total network energy consumption and realize high network throughput. In effect, we are finding a balance between transmit energy consumption of each hop and processing energy consumption required at each hop. And even though omnidirectional and directional networks have the same scaling behavior for variable rate systems, we can increase the throughput-optimal hopping distance by a factor of $D_{tx}^{1/k}$ and correspondingly decrease the end-to-end delay (in number of hops) and

114

per bit energy consumption by using directional antennas. Fig. 4-2 shows how the characteristic distance d_{char}^{bf} grows as a function of transmitter directivity for the two different systems described in Table 4.1, noting that the far left of the plot is d_{char}, the omnidirectional network characteristic hopping distance as shown in the table. This visualization emphasizes the importance of transmitter directivity as a network design parameter for the network architect, as the optimal hopping distance (and consequently the number of hops, end-to-end delay, and path energy consumption) is directly related to this gain term.

As mentioned above, the characteristic distance is directly related to the end-to-end message delay through the number of hops between the source and destination. Given an arbitrary network topology, the maximum number of hops (our proxy for the end-to-end delay QoS metric) will be close to $\frac{L_{max}}{d_{char}}$ (or $\frac{L_{max}}{d_{char}^{bf}}$ in the directional network case) given high-enough end-user node density and a smart routing strategy. We can only say it will be close to this, because it would only be exactly $\frac{L_{max}}{d_{char}}$ (or $\frac{L_{max}}{d_{char}^{bf}}$) if each relay node along that route was on the straight line separating the SD pair at intervals of exactly d_{char} (or d_{char}^{bf}). As the characteristic hopping distance is related to the directivity through $D_{tx}^{1/k}$, we can decrease the maximum number of hops by approximately this factor as we leverage the directivity gain of beamforming-enabled nodes. Fig. 4-3 shows the maximum end-to-end delay behavior (using number of hops as a proxy metric) of the system as the transmitter directivity is increased, where the maximum end-to-end delay is normalized to unity for the arbitrary omnidirectional network (far left side of the plots). This is a guideline for beginning the discussion of providing QoS assurance for metrics related to the characteristic distance, such as end-to-end delay and path power consumption. It also highlights the importance of transmitter (and equivalently receiver) directivity as an important design parameter for the network architect. In our discussion of random networks to follow, we will describe what
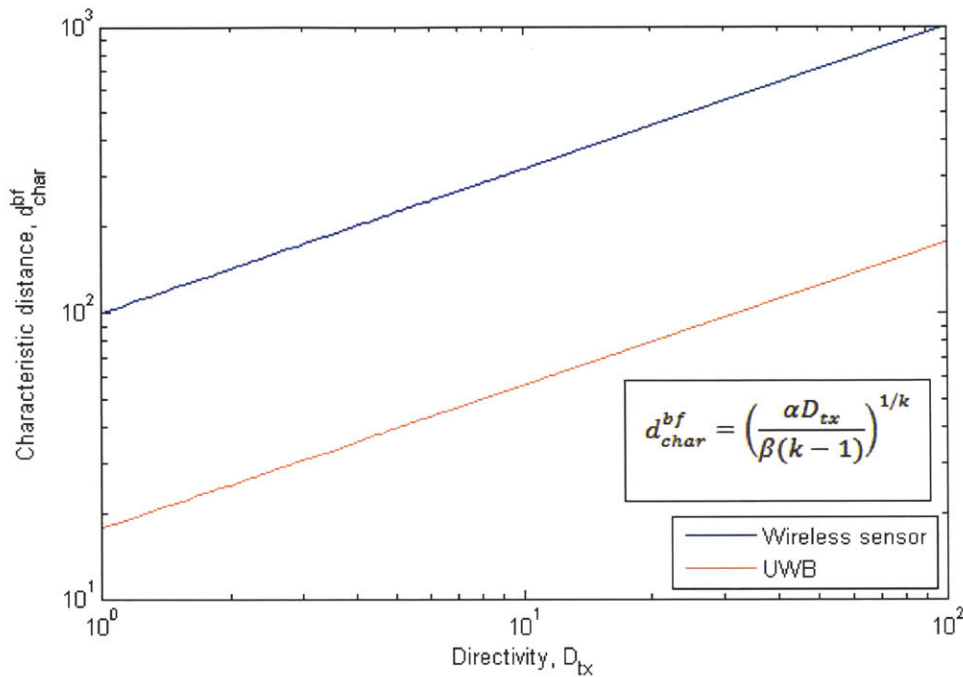
Figure 4-2: Characteristic hopping distance, d_{char}^{bf}, as a function of beamforming-enabled transmitter directivity, D_{tx}. The two systems shown here are those described in Table 4.1. For this figure, $k = 2$.

we mean by a smart routing strategy that leverages the characteristic distance to achieve this optimal scaling behavior.

We now turn to consider the uniform capacity of random networks of n nodes in a bounded operating region. In particular, we want to show that the undesirable behavior for fixed rate systems rarely occurs and that we are able to achieve the desirable scaling behavior with high probability by considering a uniform distribution of nodes and uniform traffic patterns. In doing so, we illustrate a specific routing scheme and show that its uniform throughput achieves the desirable uniform capacity scaling behavior with high probability for both fixed and variable rate systems.
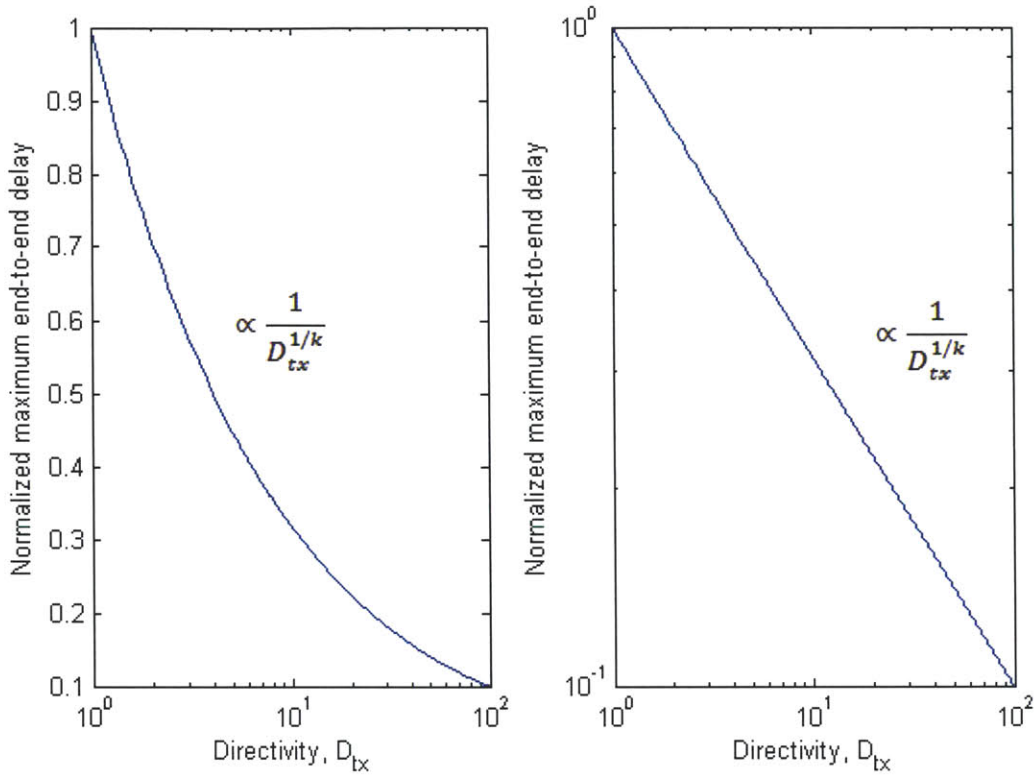
Figure 4-3: Maximum end-to-end delay behavior (normalized to omnidirectional case) as a function of the transmitter directivity factor. The left plot is in linear scale and the right plot is the same in logarithmic scale. For these plots, $k = 2$.

4.3 Uniform Capacity of Random Networks

Following the lead of [9], we now consider the uniform capacity of random infrastructureless wireless networks. In the previous section, we showed that arbitrary variable transmission rate networks demonstrate desirable scaling behaviors. We extend these results to random variable transmission rate networks using either omnidirectional transmit antennas or beamforming-enabled transmit antennas. However, we have seen that the uniform capacity of fixed transmission rate networks can have poor scaling behavior under certain worst-case

topologies and traffic patterns even with the availability of large enough system bandwidth and directional transmitter gain. An example topology and traffic pattern that exhibits this undesirable scaling behavior (see Fig. 4-1) involved a high level of end-user device clustering and a very specific uniform traffic pattern. In this section, we show that a uniform distribution of nodes and traffic patterns in a bounded operating region rarely results in these undesirable combinations of topology and uniform traffic pattern. Explicitly, the results show that both fixed and variable transmission rate random networks achieve the desirable scaling behavior independent of n (or increasing node density in the bounded operating area) with high probability (see Section 4.1.2 for an explanation of the phrase "with high probability").

Throughout this section, we consider a random network of n user nodes independently and randomly distributed in a bounded operating region (unit torus, for analytical simplicity) according to a uniform distribution over the area. We consider the uniform traffic pattern, where each node randomly selects another node and sends data to it at an average rate of λ. As n increases, we are interested in the scaling behavior of the uniform capacity achievable with high probability for fixed and variable rate networks (both omnidirectional and directional) and the scaling behavior of the uniform throughput for specific routing schemes (those which can achieve the desirable uniform capacity behavior and WtNN, which exhibits strictly suboptimal scaling behavior).

4.3.1 Fixed Rate Transmission Systems (Both Omnidirectional and Directional)

From Theorem 1, we see that both omnidirectional and directional fixed rate transmission systems demonstrate the same uniform capacity scaling behavior. In (4.13) and (4.16), we

118

have shown that $\hat{\lambda} \leq \frac{R\rho_{max}}{\bar{L}}$ and $\hat{\lambda}^{bf} \leq \frac{R\rho_{max}^{bf}}{\bar{L}}$ for omnidirectional networks and directional networks, respectively. In these upper bounds on the uniform capacity, the only random quantity for a randomly distributed network topology and traffic pattern is $\bar{L}$, since each $\{L_i\}_{1 \leq i \leq n}$ is a stochastic quantity determined by the random placement of nodes and randomly chosen SD pairs. However, as noted in [43], the law of large numbers dictates that $\bar{L} = \Theta(1)$ with high probability for a bounded operating region (in other words, the ensemble average distance between randomly chosen SD pairs in a bounded operating region converges to a constant value for large enough n). From (4.13) and (4.16) and this fact, we have that the uniform capacity $\hat{\lambda} = O(1)$ and $\hat{\lambda}^{bf} = O(1)$ with high probability for random networks.

However, we actually want to show that uniform capacity of fixed rate transmission systems is $\Theta(1)$ with high probability. To do this, we analyze the uniform throughput of a particular routing scheme introduced by [56] for interference-limited networks and extended to power-limited networks in [51] called cell routing. With this specific routing strategy, we show that we can achieve uniform throughput $\tilde{\lambda} = \Theta(1)$ and $\tilde{\lambda}^{bf} = \Theta(1)$ with high probability, thus establishing the desired uniform capacity result.

The cell routing scheme divides the unit torus operating region into equal-sized square cells of area $A = v \times v$, where we require that $\sqrt{\frac{2}{n}} \leq v \leq \frac{\rho_{max}}{2\sqrt{2}}$ in the omnidirectional antenna case and $\sqrt{\frac{2}{n}} \leq v \leq \frac{\rho_{max}^{bf}}{2\sqrt{2}}$ in the directional transmit antenna case. These requirements on cell area guarantee that there is at least one node in each cell with high probability and that nodes in adjacent cells are within one-hop communication distance of each other (unlike the balls and bins formulation of Chapter 3, this includes connectivity between diagonally-adjacent cells). Both of these constraints on v can be met with large enough n. A straight line can then be drawn between the source and destination node of a specific SD pair, and this line will cross

through a certain subset of cells. The cell routing strategy then dictates that data exchanged between this SD pair takes hops along this set of cells, while the pass-through traffic is evenly distributed over the set of nodes in any given cell. This routing scheme is illustrated in Fig. 4-4. We note that this is a routing scheme based on taking $\Theta(1)$ hops (the number of hops does not increase with increasing n) since the cell size does not change as n increases. Using this routing strategy, we can achieve $\tilde{\lambda} = \Theta(1)$ and $\tilde{\lambda}^{bf} = \Theta(1)$ with high probability for random networks. Thus, we have our desired results for uniform capacity using a fixed transmission system with either omnidirectional or directional transmit antennas: $\hat{\lambda} = \Theta(1)$ and $\hat{\lambda}^{bf} = \Theta(1)$ with high probability. For completeness, the full derivation of these results using cell routing is shown in Appendix C.3. We summarize these results in the following theorem.

Theorem 2. *The uniform capacity for a random power-limited infrastructureless wireless network in a bounded operating region with fixed transmission rate, either omnidirectional or directional transmission antennas, and large enough system bandwidth availability is $\Theta(1)$ as number of end-user devices increases whp.*

Theorem 2 agrees with the result from [51] for fixed rate systems, although we have shown that this result extends to random networks using beamforming-enabled antennas. Furthermore, the significance of this scaling result is demonstrated by the analysis in [9]. This work finds that the upper bound on uniform throughput using the WtNN routing scheme is strictly suboptimal. Explicitly, [9] shows that the uniform throughput of random infrastructureless wireless networks using WtNN routing is $O\left(\sqrt{\frac{\ln n}{n}}\right)$ with high probability. Since WtNN routing increases the number of hops with increasing end-user device density (in terms of cell routing, the cell area decreases with increasing n), the amount of pass-through traffic at each node also increases with high probability, leading to WtNN's
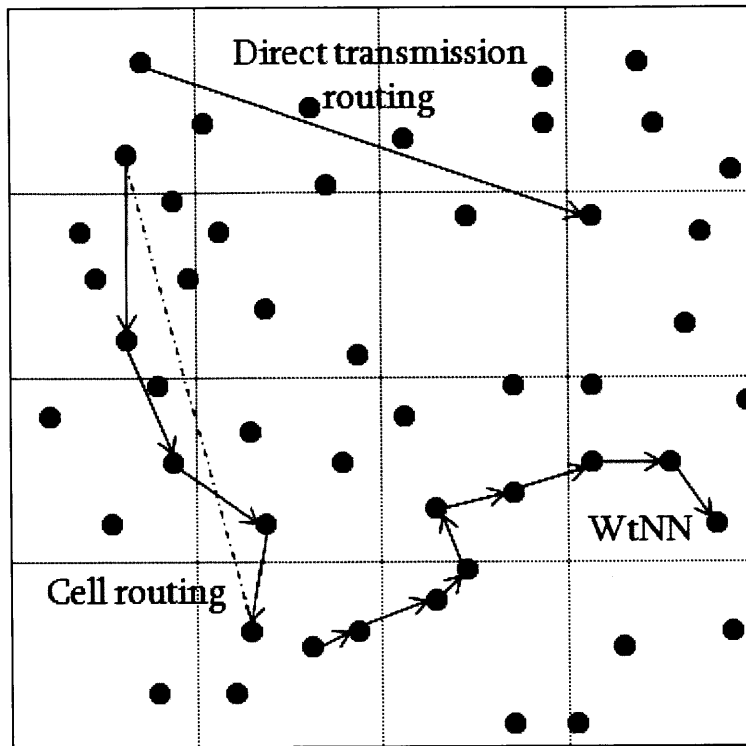
Figure 4-4: Visualization of different routing schemes discussed in this chapter.

undesirable throughput scaling behavior. The uniform throughput relationship between routing schemes with $\Theta(1)$ hops that achieve the desirable uniform capacity scaling behavior (such as cell routing) and WtNN can be seen in Fig. 4-5.

4.3.2 Variable Rate Transmission Systems (Both Omnidirectional and Directional)

We now consider variable rate transmission systems for infrastructureless wireless networks using omnidirectional and directional antennas. As presented in Theorem 1, both omnidirectional and directional variable rate transmission systems demonstrate the same

uniform capacity scaling behavior. In fact, Corollary 2 states this scaling behavior explicitly: the uniform capacity of arbitrary infrastructureless wireless networks with variable transmission rate is $\Theta(1)$ as n increases. Since $\bar{L} = \Theta(1)$ with high probability by the law of large numbers and L_{max} is bounded by a constant due to the fixed-sized operating region, we have the desired result, as stated in the following theorem.

Theorem 3. *The uniform capacity for a random power-limited infrastructureless wireless network in a bounded operating region with variable transmission rate, using either omnidirectional or directional antennas, and large enough system bandwidth availability is $\Theta(1)$ whp as the number of end-user devices increases.*

As in the fixed rate case, we can show that this scaling behavior can be achieved with high probability with the cell routing strategy. With variable rate transmissions, we do not have the maximum hop distance constraint used in the fixed rate case to constrain v. However, we can use the characteristic hop distance, either d_{char} or d_{char}^{bf}, to guide the constraint on the fixed-area cell size for this routing scheme, since we have already discussed that we want to take hops on the order of these characteristic distances when possible in our optimal scaling behavior routing schemes. Explicitly, we can require that $\sqrt{\frac{2}{n}} \leq v \leq \frac{d_{char}}{2\sqrt{2}}$ in the omnidirectional case and $\sqrt{\frac{2}{n}} \leq v \leq \frac{d_{char}^{bf}}{2\sqrt{2}}$ in the directional case. In this way, the cell area is fixed and does not change with increasing n. Furthermore, under the rules of the routing scheme, the hop distances are now upper bounded by a constant distance and we can proceed with the cell routing proof just as in the fixed rate transmission analysis. This establishes that cell routing can achieve uniform throughput that is $\Theta(1)$ with high probability as n increases in the bounded operating region by taking $\Theta(1)$ hops (the number of hops does not increase with increasing n).
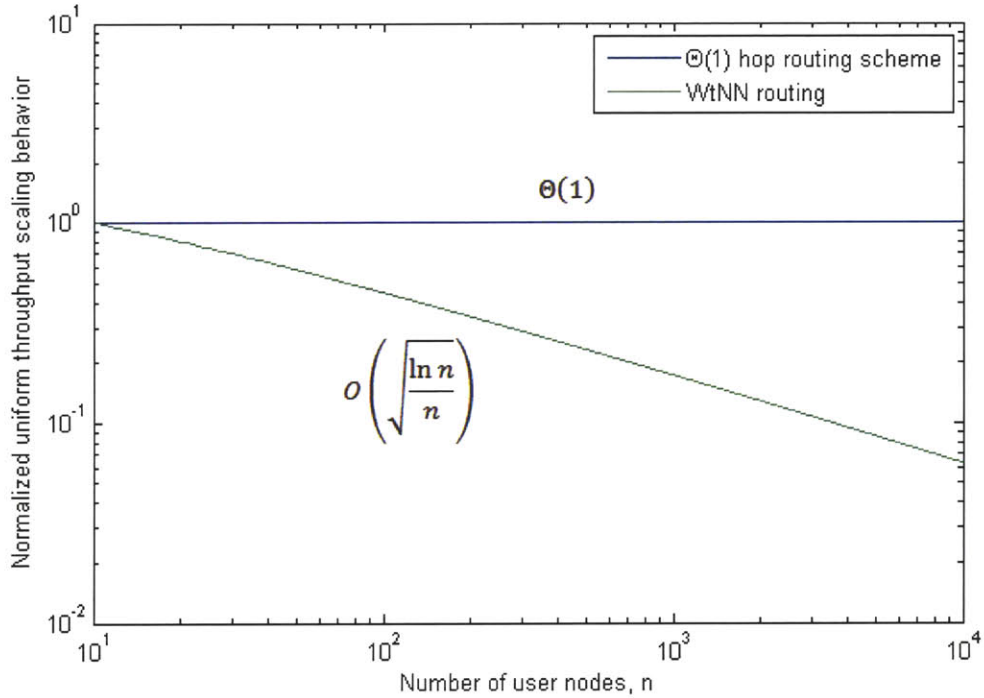
Figure 4-5: Comparison of throughput scaling behavior of $\Theta(1)$ hop routing strategies to WtNN routing.

We again emphasize the importance of this scaling result for random networks by comparing it to the WtNN uniform throughput behavior as shown in [51] for variable rate omnidirectional systems, which states that the uniform throughput is $O\left(\sqrt{\frac{\ln n}{n}}\right)$ with high probability even under the relaxed variable transmission rate scenario. For the same reasons as discussed in Section 4.3.1, WtNN is a strictly suboptimal routing strategy with high probability for power-limited infrastructureless wireless networks where processing energy is non-negligible.

4.3.3 Discussion of Throughput, End-to-end Delay, and Energy Optimal Schemes

Our analysis of uniform capacity scaling behavior for fixed and variable rate transmission systems for both omnidirectional and directional networks has led to some key insights that will help guide the design of routing strategies to achieve high network performance in terms of throughput, energy per bit consumption, and end-to-end delay. This scaling behavior is important to understand for QoS assurance. Without scalability, there is a point at which node density will bring network performance below the threshold required to maintain core services demanded by end-user applications. Luckily, we have shown that power-limited infrastructureless wireless networks operating in bounded regions are scalable (equivalently, their QoS behavior does not degrade with increasing n with high probability).

In [56], it was proven that routing schemes with $\Theta(1)$ hops attain the best energy per bit and end-to-end delay (in terms of number of hops) scaling behavior of $\Theta(1)$ as n increases for power-limited networks. We have proven that some routing strategies with $\Theta(1)$ hops attain the best uniform capacity scaling behavior of $\Theta(1)$ for power-limited networks using either omnidirectional or directional transmit antennas. Combining these results, we show that routing schemes with a number of hops that does not increase with increasing n is important for algorithmic routing design in power-limited networks in order to achieve optimal scaling performance in terms of all QoS metrics considered. The derivations in this chapter have revealed metrics that can be useful in guiding the hop distances used to achieve this optimal behavior.

In fixed rate, power-limited networks, routing schemes should attempt to take hops as close to ρ_{max} and ρ_{max}^{bf} as possible, unlike in interference-limited networks. This reduces the

124

network pass-through traffic, thus increasing the throughput and reducing both number of hops (our proxy metric for end-to-end delay) and energy consumption per bit. In addition to this, a throughput-optimal routing scheme should try to balance the pass-through traffic load at each node in order to avoid bottleneck situations that degrade network performance. Although both omnidirectional and directional networks attain the same scaling behavior, we see the benefit of the directional antennas in this discussion. For the directional network, the routing scheme should be designed to take longer hops, since $\rho_{max}^{bf} \geq \rho_{max}$. Thus, we can expect a reduction in the end-to-end delay and energy consumption, as well as a network throughput increase, due to reduced pass-through traffic load in the directional network.

For variable rate transmission systems, we have shown that throughput-optimal routing schemes should use hop distances on the order of either d_{char} or d_{char}^{bf}. Although direct transmission routing is possible in the variable rate system, this routing scheme may consume too much transmission energy and not achieve the best network throughput. By using the characteristic hopping distance to guide the routing scheme, we minimize the total path energy consumption and attain high network throughput. As in the fixed rate case, the routing scheme must make an effort to distribute pass-through traffic evenly over the nodes in the network while following this hop distance guideline, since otherwise this scheme could tax a specific node more heavily with pass-through traffic under certain topologies and traffic patterns. Also, if end-to-end delay is the primary QoS metric of concern, it could be argued that direct transmission routing is the preferred routing scheme despite the increased network energy consumption and lower sustainable throughput, since we have shown that even direct transmission routing attains the desirable scaling behavior.

4.4 Summary

In this chapter, we developed a network power model for infrastructureless wireless networks using either omnidirectional antennas or beamforming-enabled directional antennas. We used this power model to study the uniform capacity scaling of fixed and variable transmission rate arbitrary networks under uniform traffic, later extending these results to random networks. Our results showed that power-limited infrastructureless wireless networks operating in bounded regions with sufficient system bandwidth availability are scalable with high probability. We also showed that using either variable transmission rates or directional transmission antennas can improve network uniform capacity, but they do not change the order of the uniform capacity scaling results. These results led to a rough guideline for high uniform throughput routing schemes, which also achieve optimal end-to-end delay and energy consumption per bit scaling behavior. These routing strategies use hop distances on the order of a characteristic hopping distance that is related to the processing and transmission energy costs, the operating environment attenuation exponent, and the transmitter directivity of the beamforming-enabled devices. In the next chapter, we consider heuristic algorithmic approaches to routing based on these insights.

Before moving on, we quickly reiterate some shortcomings to the analysis presented in this chapter. First, all of the results presented here are subject to the power model that was used. If the algorithmic implementation of beamforming techniques in the end-user devices requires a significant amount of additional processing energy, the power model would need to be modified to abandon the "constant α" assumption as discussed in Section 4.1.3. The power-limited network analysis allowed us to develop performance upper bounds, which are applicable to interference-limited networks as well. Although we invoked the $W \to \infty$

approximation for the sake of tractable analysis, bandwidth cannot scale indefinitely with increasing n in practical systems. Thus we recognize that there is a point at which interference effects will begin to limit network performance. Future work should consider performance bounds of systems that are simultaneously power-limited and interference-limited. Also, we continued to use some other simplifications for analysis that restrict the applicability of our results, such as the path-loss channel model, RF environment homogeneity, uniform traffic patterns, and a homogeneous set of end-user devices. Changes in any of these models and assumptions may have an effect on the scaling behavior results presented in this chapter. So these results should all be interpreted as guidelines under the models and assumptions discussed, but not necessarily the final word for all future infrastructureless wireless network deployments.

Chapter 5

Routing Strategies for Quality of Service

In the last chapter, we looked at connected arbitrary networks and characterized bounds for the achievable capacity of these networks under a particular traffic pattern. We found that the addition of beamforming-enabled transmitters with directivity D_{tx} gave us gains proportional to $D_{tx}^{1/k}$ in the maximum achievable capacity for variable rate transmission systems. Then, using a smart routing strategy suitable for the proof, we showed that the optimal capacity scaling behavior (the uniform capacity does not decrease with increasing n) could be achieved with high probability in randomly deployed networks with random uniform traffic patterns using uniform distributions for node deployment and traffic source-destination pair selection. Furthermore, this result indicated that we should be able to achieve the $D_{tx}^{1/k}$ capacity gain with high probability for random networks with beamforming-enabled transmitters.

Throughout the last chapter, however, we emphasized the need for appropriately smart routing schemes without explicitly describing what these schemes are (except when required for the purpose of a proof). Furthermore, certain derivations of the achievable capacity for an arbitrary network required an optimally distributed topology and optimally chosen traffic pattern. These methods were important for understanding the scaling behavior of the system in terms of throughput, end-to-end delay, and energy consumption. Now, we consider the practical problem of route determination in infrastructureless wireless systems.

First, we consider routing schemes based on well-known routing solutions for the problem of optimizing one particular QoS metric at a time. Specifically, we consider end-to-end data rate, end-to-end delay (in terms of number of hops), and end-to-end path energy consumption. The chapter begins by providing background on the well-known routing solutions that can be used and then discusses the means of adapting them to choose best SD routes for the different QoS metrics. We next use the insights of Chapter 4 to design a heuristic routing strategy that simultaneously achieves the optimal scaling behavior of all QoS metrics considered for dense enough networks. Since achieving absolute optimal performance as characterized in Chapter 4 requires particular topology and traffic patterns, this routing solution does not guarantee the realization of these optimal bounds on throughput and consequently energy consumption and end-to-end delay. However, by using the characteristic distance as a guiding measure, the routing solution is designed to realize the desirable scaling behavior independent of increasing end-user device density in a bounded operating area and to strike a balance between reducing end-to-end hops and achieving high data throughput.

We continue to distinguish between fixed rate transmission systems and variable rate transmission systems when necessary, since the distinction between these systems leads to slightly different routing strategies. Furthermore, we make the distinction between

omnidirectional networks and directional networks when appropriate, discussing how the use of transmitter directivity may impact the performance of a particular routing algorithm.

5.1 Routing Tools

Throughout the discussion of routing schemes in this chapter, we assume the availability of particular information at each node. Since we discuss relatively simple routing schemes to optimize individual QoS metrics, we assume that each of the n end-user nodes in the network has global position knowledge available for computing routing decisions. In a real system, this information would need to be gathered by the individual nodes and then distributed through a protocol that allows each node to gather and aggregate this collected information. The network could use traditional omnidirectional transmission and reception to flood information to all of its neighbors. Or, in a directional system, nodes could employ more sophisticated scanning methods to distribute relevant information to their nearby and more distant neighbors. In this work it is simply assumed that each node in the network has the appropriate information available to it. Furthermore, as the network changes over time, this available routing information must be updated and refreshed. This is part of the process of distributing the appropriate routing information, and we assume for the purpose of this work that each node has up-to-date information on the current network state. The problem of position and link state sensing and information dissemination is left for another work.

The particular information required for computing routing decisions depends on the routing scheme we are using and the particular QoS metric under consideration. Thus, we develop a general routing information structure that can be adapted to the information required for the specific routing solution.

First, we define an $n \times n$ logical adjacency matrix A. Each individual element of this matrix, $a_{ij}, \forall i, j \in \{1, 2, \dots, n\}$, represents the existence or non-existence of a logical communication connection between a pair of nodes. Specifically, $a_{ij} = 1$ if nodes i and j are able to communicate directly, and $a_{ij} = 0$ otherwise. Furthermore, we define $a_{ii} \triangleq 0$, since we do not consider logical self-connections in our routing framework. The adjacency matrix A is symmetric about the main diagonal, since our assumption of end-user device and environment homogeneity means that node i connected to node j implies node j connected to node i. Given an adjacency matrix, A, we can interpret this visually as an undirected graph of n nodes and edges between nodes i and j when $a_{ij} = a_{ji} = 1$. Fig. 5-1 gives an example.

In the variable rate transmission system, we note that each $a_{ij}, i \neq j$ entry is set to 1, since each node is connected to and able to communicate with every other node in the network at some rate. This is true for both omnidirectional and directional antenna systems. So the adjacency matrix does not provide any useful routing information in the variable rate transmission system. However, in the fixed rate transmission system, the existence of a maximum hop distance means that the graph may not be fully-connected. Thus, the adjacency matrix will be populated with both 0 and 1 logical values. The end-user nodes in a fixed rate transmission system can populate the adjacency matrix using the known maximum hop distance and the location of all the other nodes in the network. Comparing omnidirectional and directional networks, we expect more 1s in the adjacency matrix of the directional network for a given end-user node topology as long as $D_{tx} > 1$ or $D_{rx} > 1$. For the remainder of this chapter, we focus only on the transmitter directivity and normalize the receive directivity to unity, recognizing that it is trivial to generalize the discussion to include receive beamforming gain.

$$A = \begin{bmatrix} 0 & 1 & 0 & 1 \\ 1 & 0 & 1 & 1 \\ 0 & 1 & 0 & 1 \\ 1 & 1 & 1 & 0 \end{bmatrix}$$
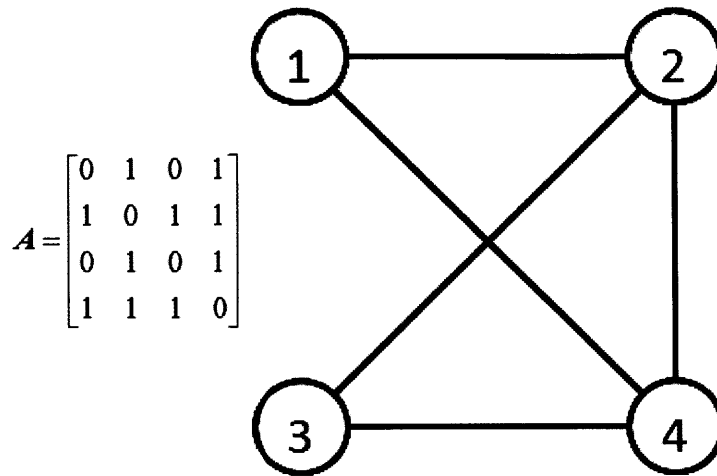
Figure 5-1: Adjacency matrix for $n = 4$ network and equivalent undirected graph representation.

Next, we define a $n \times 1$ localization vector $\underline{L}$. Although A gives us information about the logical communication connections in the network, it provides no information about the geographic location of each node (the physical network topology). Returning to Fig. 5-1, we recognize that the location of the nodes in the visualization are arbitrarily chosen. Each element of $\underline{L}$, denoted l_i, $i \in \{1, 2, \ldots, n\}$, provides the location of the associated end-user node in the network. For example, this information might be a GPS location readout as discussed in Section 2.4.1 or relative location information from the receive array processing technique discussed in Section 2.4.2. The information in $\underline{L}$ allows for a visualization of the physical topology of the network and is important for location-aware routing strategies. This information can be used for the calculation of other relevant routing information (such as the adjacency matrix in the fixed rate transmission system), or it can be used directly (for example, the cell routing scheme discussed in Chapter 4 assumes knowledge of the source and destination location to determine which cells to route a message through).

Finally, we define a general $n \times n$ cost matrix, C. This matrix is particularly general since its elements may not necessarily represent metrics that are typically referred to as "costs." The

general terminology and notation allows for analytical simplicity. Each element of this matrix $c_{ij}, \forall i, j \in \{1, 2, \ldots, n\}$ represents a "cost" (or "resource," when appropriate) assigned to the link between node i and node j, assuming that they are connected in A. By convention, we let $c_{ii} = 0$. If $a_{ij} = 0$, then we can either set $c_{ij} = 0$ or $c_{ij} = \infty$ depending on the particular routing solution. Since we assume a homogeneous RF environment and the use of a homogeneous node set, we recognize that $c_{ij} = c_{ji}$ for $i \neq j$. Thus we have a matrix that is symmetrical about the main diagonal. For generality, we can even let each element c_{ij} be a vector of cost information if we are interested in multiple cost metrics in our routing scheme.

We now discuss what information we may want to store in C. We may want to have information on the per bit energy consumption cost of using a link for communication. In this case, c_{ij} can be calculated using our power model from Chapter 4, the attenuation exponent for our RF operating environment (we assume that nodes have the capability of estimating the value of k), and the distance between the connected pair of nodes (from $\underline{L}$). For a fixed rate transmission system, we know the absolute energy cost of using a link, since nodes are assumed to transmit at a fixed rate when transmitting. In a variable rate transmission system, this link energy consumption cost may be parameterized by the communication rate and bounded from above by the time-averaged transmit power constraint of a node. Alternatively, we may want to have information about the maximum communication rate sustainable over a link in variable rate transmission system. The maximum communication rate sustainable over a link is not, strictly speaking, a "cost." It is better described as a "resource." However, for the purpose of uniform terminology, we use term "cost" for all possible entries of C, recognizing that the data may not represent an operational cost to the system. The maximum sustainable communication rate over a link can be calculated using the distance between a pair of nodes (determined from $\underline{L}$) and the maximum time-averaged node transmit power constraint. We discuss the determination of these cost matrix entries in more detail when we look at specific routing strategies.

Now given A and C, we can visualize an undirected graph, as in Fig. 5-1, with the elements of C assigned to the edges. The physical topology as described by $\underline{L}$ may not need to be included explicitly in the graph visualization if this information is already used in determining the costs assigned to the links in the graph. A general example of this graph theoretic visualization is given in Fig. 5-2.

5.2 Shortest and Widest Path Routing Overview

Many network routing schemes in practice are based on the framework of shortest path routing. Shortest path routing is a well-established topic, and a complete overview of the shortest path routing problem is provided in [57,58]. We provide a brief overview here. In shortest path routing, we consider an undirected graph with a length (or "cost" or "resource" in terms of C) assigned to each link (see Fig. 5-2). The length of a path, or a sequence of links, is the sum of the lengths of each individual link in the path. The shortest path problem, then, is to find the path between a SD pair of nodes with the minimal path length. Two well-known algorithms to solve this problem when global knowledge is available to the node computing the route are the Bellman-Ford Algorithm and Dijkstra's Algorithm.

The Bellman-Ford Algorithm is generally used for distance vector protocols, where each node periodically informs its neighbors about its shortest route to all other network nodes. Each node periodically distributes its routing table to its neighbors either due to changes in the table (triggered updates) or scheduled refreshes (periodic updates), and the neighbors update their routing tables by using the Bellman-Ford algorithm, which is described in full in [57].

135

$$A = \begin{bmatrix} 0 & 0 & 1 \\ 0 & 0 & 1 \\ 1 & 1 & 0 \end{bmatrix}$$

$$C = \begin{bmatrix} 0 & \infty & a \\ \infty & 0 & b \\ a & b & 0 \end{bmatrix}$$
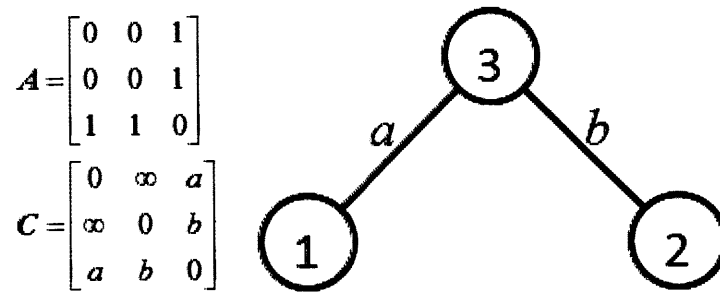
Figure 5-2: Adjacency and cost matrices for $n = 3$ network and equivalent weighted undirected graph representation.

The Bellman-Ford Algorithm produces the optimal shortest paths between the source node and all possible $n - 1$ destination nodes in the network, as long as all cycles not containing the source node have nonnegative lengths. We consider only positive-valued link "costs" (lengths) in this chapter, so this condition is satisfied. The Bellman-Ford Algorithm terminates in at most n iterations. The worst-case running time of the algorithm grows as $O(n^3)$, since each iteration requires a minimization for each of the $n - 1$ nodes over $n - 1$ possibilities.

Alternatively, Dijkstra's Algorithm is generally used for link state protocols, where each node learns about the entire network graph through reliable flooding of update packets (called link state packets). As does the Bellman-Ford Algorithm, this algorithm computes the shortest paths from the source node to all other $n - 1$ destinations in the network. This algorithm requires that all link lengths are strictly nonnegative, which is satisfied by our assumptions on link "costs" used in this chapter. However, its worst case running-time grows as $O(n^2)$, which is better than the worst-cast running time of the Bellman-Ford Algorithm. Thus, throughout the remainder of the chapter, we consider Dijkstra's Algorithm when using a shortest path algorithm.

Dijkstra's Algorithm operates by labeling each node with an estimate of the shortest path length to the source node. On each iteration, an additional node is added to a set of permanently-labeled nodes once it is clear that its label truly represents the shortest path length to the source node. After adding a node to the permanent set (denoted P), all the nodes not in the permanent set update their label estimates of the shortest path length, since their shortest path must pass exclusively through the nodes in the permanent set P. This idea is illustrated in Fig. 5-3. Dijkstra's Algorithm is described in full in [57].

When Dijkstra's Algorithm terminates after $n - 1$ iterations, the final labels represent the shortest path length from the source node to all possible $n - 1$ destination nodes. The worst-case running time is $O(n^2)$ since there are $n - 1$ iterations of this algorithm and each requires a number of operations proportional to n.

Both of these algorithms require the link lengths to be additive in nature. This matches our understanding of some link costs, such as delay or power consumption. However, certain metrics such as end-to-end sustainable data rate (an important "resource" metric to consider for QoS assurance routing) are not additive in nature. Therefore, we discuss a variant to the shortest path problem, commonly known as the widest path problem [58]. The widest path problem is that of discovering the SD path with the optimal performance in terms of a non-additive concave "cost" or "resource" metric, such as sustainable link capacity. When considering a path with this type of metric, it is the minimum "cost" or "resource" link that determines the overall path "cost" (this is easy to understand in terms of end-to-end capacity). Therefore, our goal in finding the optimal route between a source and destination is to maximize the minimum link "cost" in the chosen path. It is this maximization of the minimum "cost" link in a path that gives the name "widest path" to the problem. Luckily, Dijkstra's Algorithm can be adapted to solve the widest path problem [59]. Since this algorithm is less-common in the literature, we describe it in full.

Shortest path for m+1 closest node must
pass only through nodes in P

Source node

$m+1$ closest node to node 1

P P^c

The m closest nodes to node 1
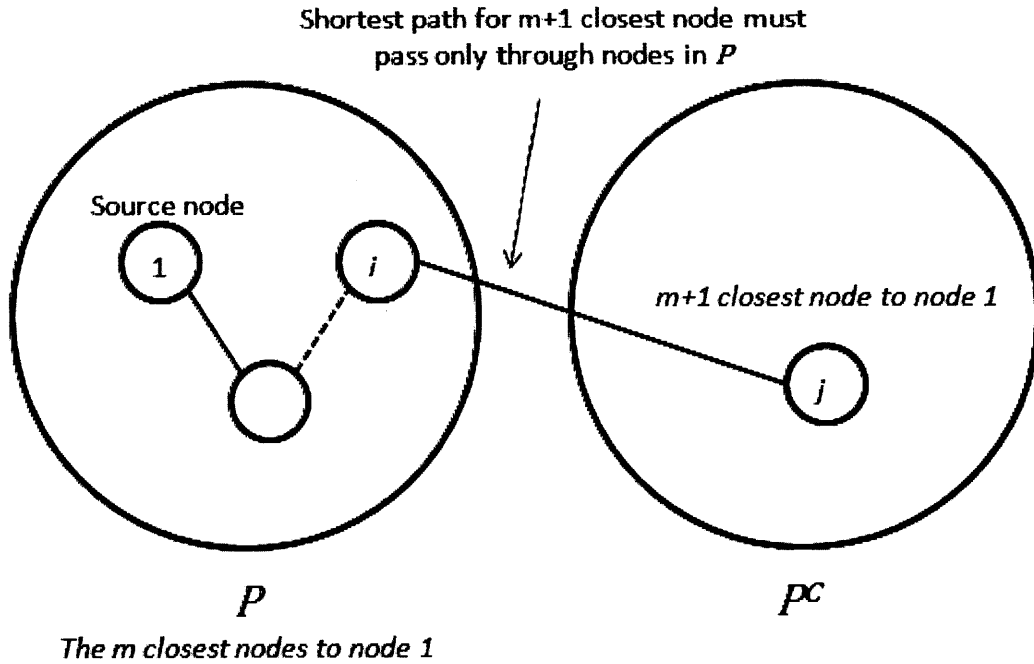
Figure 5-3: Illustration of the main idea behind the operation of Dijkstra's Shortest Path Algorithm for routing [57].

Algorithm 1. Dijkstra-based Widest Path Algorithm

For notation, we let node 1 be the source node that is determining the widest path to all other destinations in the n node network. We assume a connected network, such that there is at least one path between every source and destination pair. We let P represent the set of permanently-labeled nodes in the network. We let the current estimate of the widest path "width" (the minimum cost/resource/length on the path) from node 1 to node i on the tth iteration be denoted by D_i^t. By convention, $D_1^t = \infty, \forall t$.

Initiate:

- $P = \{1\}$.

- $D_j^1 = \begin{cases} c_{1j}, & \text{if node } j \text{ connected to node 1} \\ 0, & \text{otherwise} \end{cases}, \forall j \neq 1.$

Iterate (t^{th} iteration):

- *Add node with current widest path estimate to the permanent set*

138

- o *Find $i \notin P$ such that $D_i^t = \max_{j \notin P} D_j^t$.*
- o *Set $P := P \cup \{i\}$.*
- o *If $P^C = \emptyset$, terminate algorithm. Else, continue.*
- **Update labels**
  - o *$\forall j \in P$, set $D_j^{t+1} := D_j^t$.*
  - o *$\forall j \notin P$, set $D_j^{t+1} := \max[D_j^t, \min\{D_i^t, c_{ij}\}]$, where $c_{ij} = 0$ if node i and j are not connected.*

Algorithm 1 runs in a very similar manner to Dijkstra's Algorithm, with slight modifications to the adding of a node to the permanent set P on each iteration and the label update rules. Fig. 5-4 illustrates the operation of Algorithm 1 for a simple six end-user node network with the logical connections and link lengths as shown at the top of the figure. As in our description of the algorithm, node 1 is assumed to be the source node computing the widest paths to all other nodes in the network.

Before moving forward, we recognize that more optimal routing schemes exist based on multi-commodity flow routing [55]. The drawback to the shortest path and widest path framework is that the source chooses only one route to the destination, when multiple routes may be available. The flow routing framework allows a flow to be spread over multiple paths. Single path routing may leave some links in the network completely unused, whereas flow based routing optimally divides the flow over all SD paths. Flow routing also helps cope with failures that may arise in a single path. For our work, however, we do not consider multi-commodity flow routing due to the computational complexity involved in solving the routing problem and the fact that many practical routing solutions are currently based on shortest and widest path techniques.
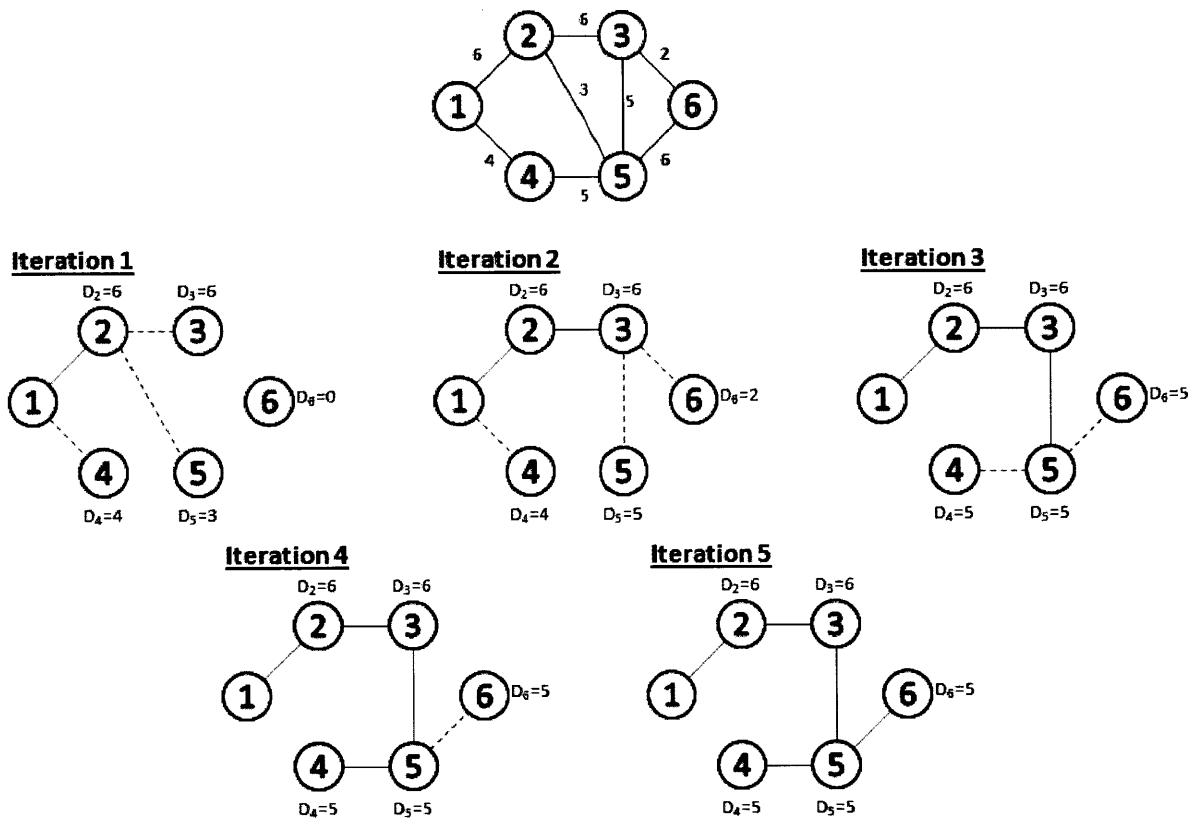
Figure 5-4: Example of the operation of the Dijkstra-based Widest Path Algorithm. The graph at the top of the figure shows all of the possible logical connections and associated non-additive concave link lengths. At each iteration, the blue links are those added to the widest path spanning tree of the network rooted at node 1, the source node. The red dotted lines at each iteration show the link associated with the current length estimate at each node not in the permanently-labeled set P. The algorithm terminates in exactly $n - 1$ iterations.

5.3 Routing Solutions for Individual QoS Metrics

Using the algorithmic tools discussed in Section 5.2, specifically Dijkstra's Algorithm and the Dijkstra-based Widest Path Algorithm, we proceed to formulate algorithmic routing solutions to optimize SD paths for individual QoS metrics. We consider three different QoS

metrics in this section: end-to-end data rate, end-to-end delay (in terms of number of hops), and end-to-end path energy consumption.

5.3.1 End-to-end Data Rate

We first consider an algorithmic solution to determine the optimal path with the maximum end-to-end data rate between a source and destination pair in our infrastructureless wireless network.

The fixed rate transmission system is not an interesting case. Given the adjacency matrix for a fixed rate transmission system, either omnidirectional or directional, each link would have the same length in terms of the rate that it can support due to the fixed transmission rate constraint. The end-to-end rate between a source-destination pair would be the fixed rate R [bit/sec] regardless of which path is chosen. The difference between the omnidirectional and directional networks is that the directional network would either have more links in the adjacency matrix A for a specific rate R, or the directional network would have approximately the same adjacency matrix as the omnidirectional network with a higher fixed rate transmission constraint than R.

We turn our focus to the more interesting case, the variable rate transmission system (both omnidirectional and directional). In the variable rate transmission system, each node is connected to every other node in the network. However, the physical separation between each pair of nodes, the RF environment attenuation exponent, and the maximum time-averaged transmitter power constraint at each end-user node determines the communication rate that each node pair can support. Specifically, for node i and node j constrained by a

maximum time-averaged transmission power constraint of P_{avg} [J/sec] and separated by a distance of d_{ij} [m], the communication link between the two nodes can support a data rate of R_{ij} [bit/sec] upper-bounded by the Shannon Capacity of the link, as given by (4.2) in the limit of large bandwidth for our power-limited scenario:

$$R_{ij} \leq C_{ij} \xrightarrow[W \to \infty]{} \frac{\gamma_{ij} P_{avg}}{N_0 d_{ij}^k} \tag{5.1}$$

where C_{ij}[bit/sec] is the capacity of link (i,j), γ_{ij} is the RF gain factor (including antenna gains and RF processing losses), k is the attenuation exponent of the path-loss model, and N_0 is the noise spectral density. For simplicity, we assume that appropriate channel coding is employed such that we can achieve the Shannon Limit of the channel. As in Chapter 4, we assume device homogeneity and let $\gamma_{ij} = \gamma$, $\forall i,j$. And as mentioned before, each device is assumed to be able accurately estimate channel conditions such that it knows both k and N_0. Then, the source node can use the location information in $\underline{L}$ to calculate d_{ij}, $\forall i,j$, and use this information to calculate R_{ij}, $\forall i,j$. For the routing problem of determining the path with maximum end-to-end data rate, we let each element of the cost matrix (or, more descriptively, resource matrix) $c_{ij} = R_{ij}$. Thus, the source node can use the information it has to fill in all the values of C. Explicitly, for the infrastructureless wireless network using omnidirectional antennas, we have for each (i,j) pair:

$$c_{ij} = \frac{\gamma P_{avg}}{N_0 d_{ij}^k}. \tag{5.2}$$

And for the infrastructureless wireless network using directional antenna arrays or apertures with directivity D_{tx}, we have for each (i,j) pair:

$$c_{ij} = \frac{\gamma D_{tx} P_{avg}}{N_0 d_{ij}^k}. \tag{5.3}$$

As we can see, the assigned "costs" or "resources" to each link for a given network topology will be higher for the directional network due to the transmitting antenna directivity gain factor.

Now, each link in the complete network graph has an assigned length that represents the sustainable communication rate over that link, as computed by the source node. Since rate is a non-additive concave metric over an end-to-end path (in other words, the sustainable data rate on a path is determined by the minimum rate link on that path), the source node can use the populated C to compute the optimal end-to-end rate paths between itself and all possible destinations in the network by running Algorithm 1, the Dijkstra-based Widest Path Algorithm.

5.3.2 End-to-end Delay (Number of Hops)

We next consider an algorithmic solution to determine the optimal path with the minimal end-to-end delay between a source and destination pair in our infrastructureless wireless network in terms of number of hops in the path.

The less interesting case when routing specifically for this QoS metric is the variable rate transmission system. In this system, we can imagine a fully-connected network graph between all n nodes in the network. Thus, the minimal-hop path between the source and destination is always the one-hop direct path between the SD pair in both omnidirectional and directional networks. The only issue to consider here is that while this routing scheme minimizes the hop count, it may be possible that the data rate sustainable over the direct SD link is so low due to large physical separation between the two end-users that the

transmission delay exceeds the total end-to-end delay of a multi-hop path between the source and destination. Specifically, if the message to be transmitted between node i and node j is of length L [bits], then the transmission delay is $\frac{L}{R_{ij}}$. Since the directional network is able to achieve a higher data rate for a node pair separated by a given distance, this would be less of an issue in the directional network compared to the omnidirectional network. Still, the network designer should be aware of this possibility. If the direct transmission data rate becomes so low and delay is measured in units of time, it may be beneficial to use a multi-hop path. For the purpose of this thesis, we focus our analysis on hop-induced delay.

For fixed rate transmission systems, we recognize that the fixed rate constraint imposes a maximum hop distance. Thus, a fixed rate transmission system (both omnidirectional and directional) may not have a fully-connected network graph. The optimal end-to-end delay path (in terms of number of hops) can then be discovered algorithmically through a simple scheme. Given the adjacency matrix A, the source node can assign a cost of unity to each link described by the adjacency matrix. Equivalently, if $a_{ij} = 1$, then we assign $c_{ij} = 1$. Otherwise, $c_{ij} = \infty$. We note that in the fixed rate transmission system, the source node can calculate the adjacency matrix A from the data in $\underline{L}$, since it is the distance between a pair of nodes and the maximum hop distance that determines if a pair of nodes are connected. As shown in Chapter 4, the maximum hop distance for an omnidirectional system using our power model is given as:

$$\rho_{max} = \left(\frac{1}{\beta} \left[\frac{P_{avg}}{R} - \alpha \right] \right)^{1/k}. \tag{5.4}$$

where R is the fixed transmission rate, P_{avg} is again the maximum time-averaged transmission power constraint, k is the attenuation exponent of the path-loss model, α is a per bit processing energy consumption cost as described in Chapter 4, and β is a per bit transmission energy consumption cost as also described in Chapter 4. The parameters α and β are device-dependent, and we assume they are known to the end-user nodes. Similarly,

the maximum hop distance for a directional system with transmit antenna directivity D_{tx} is given as:

$$\rho_{max} = \left(\frac{D_{tx}}{\beta} \left[\frac{P_{avg}}{R} - \alpha \right] \right)^{1/k}.$$ (5.5)

With the populated cost matrix C, the source node has a complete picture of the network graph. Since hop count is an additive metric, the source node can compute the optimal end-to-end delay paths (in terms of number of hops) between itself and all possible destinations in the network by running Dijkstra's Algorithm. Comparing the omnidirectional network to the directional network, we would expect the shortest paths of the directional network to have fewer hops for a given topology, since the maximum hopping distance of the directional network is increased by a factor of $D_{tx}^{1/k}$.

5.3.3 End-to-end Path Power

Finally, we consider an algorithmic solution to determine the optimal path with the minimal end-to-end energy consumption between a source and destination pair in our infrastructureless wireless network. In determining the best path for this QoS metric, we continue to use the path power model developed in Chapter 4. In Section 4.1.3, we showed that the end-to-end power for a particular path in the omnidirectional network can be expressed as:

$$P_{path} = \lambda \sum_{m=1}^{h} (\alpha + \beta d_m^k)$$ (5.6)

where λ [bit/sec] is the end-to-end transmission rate, α is a per bit processing energy consumption cost, β is a per bit transmission energy consumption cost, d_m is the distance of

145

the mth hop in an end-to-end path of h hops, and k is the attenuation exponent of the path-loss model. Similarly, we showed that for a directional network with transmitter directivity D_{tx}, the end-to-end power consumption for a particular path is given by:

$$P_{path} = \lambda \sum_{m=1}^{h} \left(\alpha + \beta \frac{d_m^k}{D_{tx}} \right). \tag{5.7}$$

In a fixed rate transmission system, $\lambda = R$. Thus, we can assign an absolute measure for the path power consumption over all candidate paths. For the variable rate transmission system, since λ is not constrained to a fixed rate, it is easier to parameterize the path power consumption by the end-to-end data rate. We assume that, given a set of candidate paths between a source and destination in a particular variable rate network, the source and destination wish to communicate at a data rate that is end-to-end sustainable over all of the paths in this set (since we are not optimizing the end-to-end data rate QoS metric here). Thus, for the variable rate system, we can assign a relative measure for the path power consumption over each candidate path parameterized by a common data rate λ.

Next, we recognize that the end-to-end path power is additive, a summation of the per hop power, which is evident from (5.6) and (5.7). Therefore, we can break the path power expression into individual hop power requirements. Using information available to the source node in our routing scenario, including $\underline{L}$ and A (which may be computed from $\underline{L}$ and the known maximum hop distance in the fixed rate transmission system or is trivially populated in the complete graph variable transmission rate system), the cost matrix C can be filled in according to the following rules, where each entry c_{ij} represents the power cost of using that link at the specified or parameterized data rate.

For the fixed rate transmission system, if $a_{ij} = 1$, then:

$$c_{ij} = R\left(\alpha + \beta\frac{d_{ij}^k}{D_{tx}}\right) \tag{5.8}$$

where d_{ij} is the distance between node i and node j as given by the information in $\underline{L}$. Note that we can use this expression for both the omnidirectional and directional network case; we simply set $D_{tx} = 1$ for an omnidirectional transmitting antenna. Furthermore, if $a_{ij} = 0$, then we let $c_{ij} = \infty$. In the fixed rate transmission system, the cost c_{ij} corresponds to an absolute measure of power in [J/sec] for using a particular link (i,j). Comparing the omnidirectional and directional networks, we expect to see two major differences. First, we expect more links in the directional network for a given topology due to an increased maximum hop distance. Second, the costs assigned to comparable links in the two network scenarios for a given topology will be lower in the directional network due to the antenna directivity gain factor.

For the variable rate transmission system where all $a_{ij} = 1, i \neq j$, we use:

$$c_{ij} = \alpha + \beta\frac{d_{ij}^k}{D_{tx}}. \tag{5.9}$$

Again, this expression works for both the omnidirectional and directional network case; we just set $D_{tx} = 1$ for omnidirectional transmission antennas. The cost c_{ij} in the variable rate transmission system corresponds to a relative measure of power consumption, since we do not explicitly include the multiplicative data rate in the determination of the cost metric. Equivalently, we can see c_{ij} as the cost of using link (i,j) measured in [J/bit]. Comparing omnidirectional and directional networks, the costs assigned to links in the directional network will be lower than those in the omnidirectional network for a given topology due to the antenna directivity gain factor.

With the populated cost matrix C, the source node now has a complete picture of the weighted network graph. Since per hop power is an additive metric, the source node can compute the optimal end-to-end paths to all possible destinations in terms of path power by running Dijkstra's Algorithm. Comparing the omnidirectional network to the directional network for a given topology, we would expect the shortest paths of the directional network to achieve better end-to-end path power performance, since the directional network can leverage antenna directivity to get a $\frac{1}{D_{tx}}$ savings in distance-dependent transmission power at a particular data rate.

5.4 A Heuristic Approach to Best QoS Performance Routing

As shown in Section 5.3, we can compute optimal routes for QoS metrics individually. While the routing schemes we have discussed so far based on computing weights for standard shortest path and widest path routing achieve desirable behavior with respect to the intended QoS metric, these schemes may not achieve the desired scaling behavior for the other QoS metrics. The major insight regarding best routing strategies that we gained from the scaling behavior study of Chapter 4 is that our routing scheme should be based on a characteristic hopping distance (or maximum hop distance in the fixed rate transmission system case). We proved that routing schemes based around this premise not only achieve the optimal throughput scaling behavior with high probability, but simultaneously achieve the optimal end-to-end delay (in terms of number of hops) and path energy consumption scaling behavior with high probability. Specifically, a routing strategy of this form achieves behavior in the infrastructureless wireless network scenario that does not scale with n. Thus, as the end-user node density increases, the achievable network capacity does not decrease (although more system bandwidth is needed as the density of end-user devices

increases). Additionally, as the end-user density increases, the end-to-end delay and communication energy consumption do not increase. Since we wish to formalize a strategy for traffic routing that recognizes this best scaling behavior from all considered QoS metrics (even though it may not optimize the performance of each QoS metric individually), we motivate and develop a new algorithmic routing scheme in this section.

One possibility for an algorithmic routing scheme based on a characteristic hopping distance (or maximum hopping distance) would be the direct translation of the cell routing scheme used as a proof technique in Chapter 4. However, cell routing requires splitting up the operating region into cells a priori and thus becomes a relatively static strategy. We develop a more adaptive routing scheme based on these hop distance metrics that does not require a pre-routing tessellation of the operating area. As a result, it can achieve better QoS metric performance under some physical network topologies than cell routing can.

The algorithmic computation of routes based on a characteristic hopping distance does not lend itself easily to the standard shortest path optimal route calculation framework. Instead, we formulate a sub-optimal heuristic routing algorithm that directly leverages our knowledge of node locations and characteristic hopping distance (or maximum hopping distance). Since the variable rate transmission system is fundamentally different from the fixed rate transmission system in the framework of geographical routing (the fixed rate transmission system has a limited hopping range, whereas the variable rate system can theoretically take arbitrarily long hops), we develop separate algorithms for these systems. While the routing solutions presented here are clearly sub-optimal heuristic methods that are best fined-tuned to a particular network under consideration, our simulation results show that these presented algorithms can consistently achieve uniform throughput (see Chapter 4 for definition and discussion of this metric) within ten percent of the maximum achievable

uniform capacity. With some optimization and tuning, it may be possible to realize even better performance from heuristic algorithms of this type.

Before describing the algorithms for the variable rate and fixed rate transmission systems, we briefly define notation that will be used throughout the remainder of this section. We adopt a polar coordinate system (r, ϕ) in the plane of operation as shown in Fig. 5-5. The pole (origin) for the coordinate system is always considered to be the node currently finding the next hop towards the destination (this will not necessarily be the source node, even though the source node is doing the route computation). The $\phi = 0°$ direction is then the straight line between the node currently finding the next hop towards the destination and the destination node. The radial r represents the distance of transmission, and it extends from the pole.

The following algorithmic parameters are illustrated in Fig. 5-6. We let ϕ_o be the initial angle of consideration, and we define $\tilde{\phi}$ as the angular increment. Similarly, we define d_o as the initial radial range, and we define $\tilde{d}$ as the radial range increment. These are tunable parameters that determine the performance of the presented heuristic routing algorithms. We provide some insight into how these parameters should generally be set by the network architect, but the best parameter values will be highly dependent on the network end-user density, RF operating environment, underlying network graph sparsity, and other factors. We also continue to use d_{char} to denote the characteristic hopping distance of a variable rate transmission system (exactly as computed in Chapter 4) and ρ_{max} to denote the maximum hopping distance of a fixed rate transmission system. We do not distinguish between d_{char} and d_{char}^{bf} (or ρ_{max} and ρ_{max}^{bf}) since the algorithms are the same for both omnidirectional and directional networks. Also, as these hopping distance parameters are dependent on node energy consumption parameters and the attenuation exponent of the path-loss model, we continue to assume a homogeneous end-user node set and a homogeneous RF operating
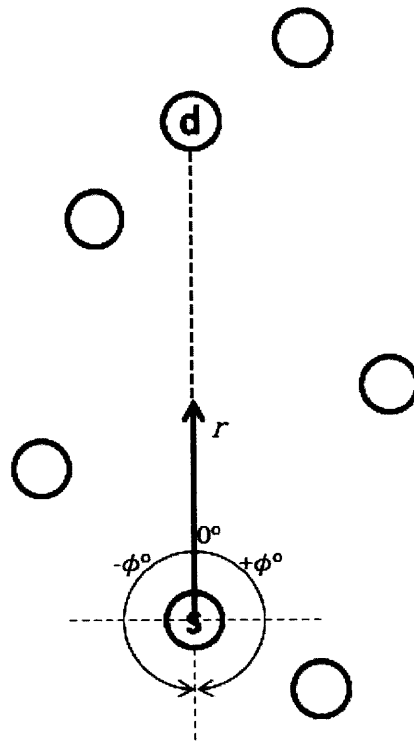
Figure 5-5: Polar coordinate system used in the description of our heuristic routing algorithms.

environment, such that these hopping distance parameters are the same for all nodes in the network under consideration.

5.4.1 Variable Rate Transmission System Routing Algorithm

As suggested by our analytical results in Chapter 4, the source node attempts to compute a route to the destination node composed of hops of length d_{char}. As shown in the previous chapter, a route is uniform capacity optimal if it is composed only of hops exactly of length d_{char} between the source and destination, although this is not necessarily possible to achieve
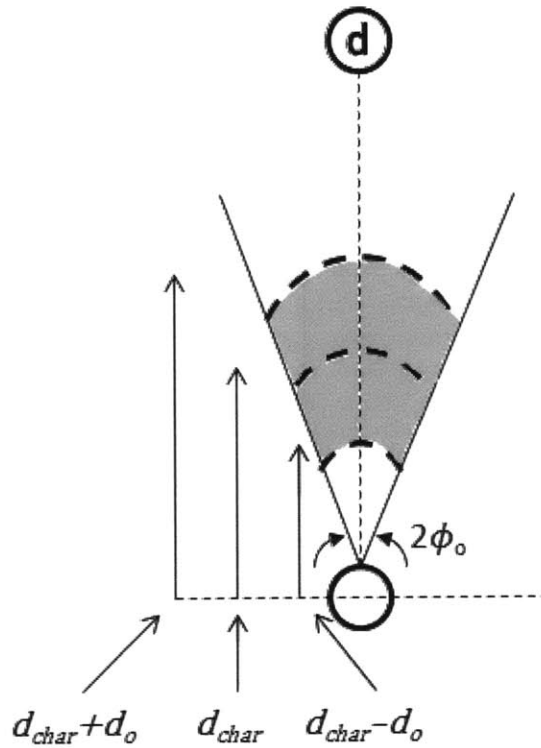
Figure 5-6: Illustration of additional parameters used in our heuristic routing algorithms.

given an arbitrary network topology and arbitrary SD pair. Thus, d_{char} serves as a hopping distance guideline.

After each hop in the route is determined, the next node takes the place of the "source," and again looks for a near-d_{char} hop close to the straight line path between it and the destination node. At each hop, since we cannot expect a node to lie exactly at distance d_{char} along the straight line path to the destination, we initially consider a fixed width area defined by d_{char}, ϕ_o, and d_o. Instead of considering only the straight line path between the current node and the destination, we consider an angle of ϕ_o to each side of the straight line path, defining a cone that extends from the current node. Furthermore, instead of considering a hopping distance of exactly d_{char}, we consider a hopping range of $[d_{char} - d_o, d_{char} + d_o]$ within the cone that extends from the current node. Together, these sweep out an area of next hop

consideration as shown in grey in Fig. 5-6. Nodes within this area are considered as the set of candidates for the next hop from source to destination. We allow the next hop to be randomly chosen among this set of next hop consideration according to a uniform distribution over the set to attempt to distribute traffic load evenly across the network. The only exception to this area of next hop consideration description is when the destination node falls anywhere within the hopping range $(0, d_{char} + d_o]$. In this case, the next hop is always the destination node.

With appropriate initial parameters for a given network density, this might be enough to define our heuristic algorithm. However, we have to consider the scenario where there are no next hop candidates in our initial area of next hop consideration. In this case, we allow the hopping range of consideration to be extended by $\tilde{d}$ on each end, and we allow the cone of consideration extending from our current node to be increased by $\tilde{\phi}$ on each side. This effectively sweeps out a larger area for next hop node consideration. The nodes that fall in this area are then considered the set of next hop candidates, and again we allow the next hop to be chosen randomly among the set of next hop consideration according to a uniform distribution over the set. Also, as before, if the destination node falls anywhere within $(0, d_{char} + d_o + \tilde{d}]$, it automatically becomes the next hop. It is possible to imagine that the set of next hop candidates is still empty after the area of consideration is extended the first time. Thus, we allow this process to be repeated as necessary until the set of next hop candidates is non-empty. Finally, in the variable rate transmission system, it is never necessary to take a hop "backwards," since every node is technically connected to every other node in the network. Thus, we dictate that the cone of consideration can never exceed $(-90°, +90°)$. If the cone of consideration has reached this point and the set of next hop candidates is still empty, then only the hopping range of consideration can be extended on successive algorithm iterations to increase the area of next hop consideration. In the worst

case, the destination node will eventually be included in the area of next hop consideration, and this node will automatically become the next hop in the route.

We proceed to describe the algorithmic process of a source node, node i, computing the route to the destination node, node j, in a variable rate transmission system. The source node uses only information known about the homogeneous node set and channel estimation of the RF environment attenuation exponent (these are used to compute d_{char}), the information in $\underline{L}$, and the parameters of the heuristic algorithm.

Algorithm 2. A d_{char}-based Routing Algorithm for Variable Rate Transmission Systems
We assume that the source node, node i, knows the following information: d_{char}, $\underline{L}$ (vector with location information for all n nodes in the network), and the parameters of the routing algorithm $(\phi_o, d_o, \tilde{\phi}, \tilde{d})$. We let the destination node be denoted node j. The area swept out by Lower Hop Bound, Upper Hop Bound, Left Cone Width, Right Cone Width is as shown in grey in Fig. 5-6.
Initiate:

- Current Node := *node i*
- Destination Node := *node j*

New Current Node:

- Lower Hop Bound := $d_{char} - d_o$
- Upper Hop Bound := $d_{char} + d_o$
- Left Cone Width := $-\phi_o$
- Right Cone Width := $+\phi_o$

Candidate Next Hop:

- *If* Destination Node *is in* (0, Upper Hop Bound] *from* Current Node
    - o Next Hop := Destination Node
    - o ***Terminate algorithm***

154

- *Else*
  - *Assign nodes in area swept out by* Lower Hop Bound, Upper Hop Bound, Left Cone Width, Right Cone Width *to next hop candidate node set K*
  - *If K ≠ ∅*
    - *Randomly assign* Next Hop *from nodes in K*
    - Current Node := Next Hop
    - *Go to New Current Node procedure*
  - *Else*
    - Lower Hop Bound := Lower Hop Bound $- \tilde{d}$
    - Upper Hop Bound := Upper Hop Bound $+ \tilde{d}$
    - Left Cone Width := max(Left Cone Width $- \tilde{\phi}$, $-90°$)
    - Right Cone Width := min(Right Cone Width $+ \tilde{\phi}$, $+90°$)
    - *Go to Candidate Next Hop procedure*

This heuristic algorithm is sub-optimal due to the restrictive nature of the area of next hop consideration determined by the algorithmic parameters. It is possible to imagine a scenario where a slightly larger initial area of next hop consideration could yield an overall more optimal path to the destination when you consider the distance of the subsequent hops in the path. In this scenario, if a next hop candidate node is found in the smaller initial area of next hop consideration, the more optimal end-to-end path using the node outside this initial area of consideration would never be chosen. This scenario indicates why the choice of algorithmic parameters is crucially important the performance of the algorithm. In general, a more densely-packed network can use a smaller initial area of next hop consideration and smaller parameter increments, since it is more likely to find potential next hop candidates clustered around the straight line path between the source and destination. However, in a sparsely populated network operating region, the initial area of next hop consideration should be larger, and larger parameter increments can be used to speed up the algorithm

running time. In our simulation environment, for both dense and sparse network considerations, we were able to attain within ten percent of the maximum uniform capacity as presented in Theorem 1 of Section 4.2.5. However, the algorithmic parameters were manually optimized for these simulations. The procedure for choosing the best parameters may be of interest for further study, but for now we simply state that this algorithm can achieve high uniform throughput and the optimal end-to-end delay and path power consumption scaling behavior that is independent of increasing n. In our simulation environment, we ran a series of one-hundred simulations where the area of next hop consideration was increased once more after the first set of next hop candidates was found to see if a better SD route would be discovered. In all one-hundred trials, a higher uniform throughput was not realized through this algorithm variant. Thus, we have reason to believe that this heuristic algorithm can achieve desirable network performance in many operating scenarios.

5.4.2 Fixed Rate Transmission System Routing Algorithm

For the fixed rate transmission system, we can use a heuristic routing algorithm similar to that described in Algorithm 2. However, there are a few key changes that must be made to ensure that the algorithm is able to successfully compute an end-to-end path for any arbitrary network topology and any arbitrary SD pair within the network. This is due to the fundamental attribute of the fixed rate transmission system, which is the existence of a maximum hopping distance ρ_{max}. For the sake of space, we do not write a formal algorithm for the fixed rate transmission system, but we instead discuss the necessary changes to Algorithm 2 and provide a fundamental example of why the most significant change is required. We assume that the underlying network graph is connected when discussing this

routing algorithm. If the underlying network graph were to be disconnected, then at least one SD pair would not be able to sustain any end-to-end traffic. We refer the reader back to Chapter 3, where we identify regimes of high probability of network connectivity given n end-user nodes in a bounded operating region for the fixed rate transmission case.

First, we must change the incremental procedure of sweeping out larger and larger areas of next hop consideration. In the fixed rate transmission system, we would like to take hops of distance ρ_{max} along the straight line path from the source to the destination. Again, we consider an angular range from this straight line path parameterized by ϕ_o. However, we now consider only an initial hopping range of $[\rho_{max} - d_o, \rho_{max}]$. If no next hop candidates are found in this initial area of consideration, we can incrementally increase the angular range by $\tilde{\phi}$ as before, but we must modify how we increase the hopping distance range. Since we cannot take a hop longer than ρ_{max}, only the lower bound on the range can be further decreased by increments of $\tilde{d}$.

The other adjustment that we need to make to Algorithm 2 is to add a memory of the set K at each step of the algorithm in computing the end-to-end path. In the fixed rate transmission scenario, it is possible to reach a dead-end, where the current node is separated from the destination node by a distance of more than ρ_{max} and with no candidate next hop neighbors. In this case, the algorithm has to be designed to take a step back, delete that dead-end node from the last next hop candidate set K, and proceed by choosing another node from K. If K were to become empty at this point, it would need to revert to increasing the area of next hop consideration and find new next hop candidates. Along with this change in Algorithm 2, we need to remove the restriction on "backwards" hops, since this may be the only way to reach a destination node given a specific network topology in the fixed rate transmission system. Fig. 5-7 shows an example network topology that illustrates both of these issues. In this example, the first next hop candidate would indeed become a dead-end path. The source
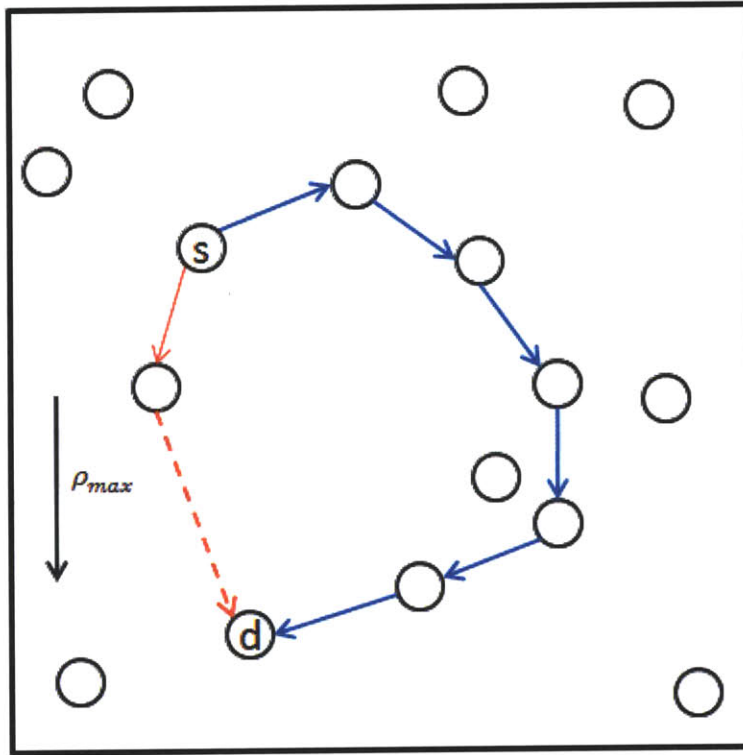
157

Figure 5-7: Example fixed transmission rate network that illustrates the changes required in Algorithm 2 to adapt the strategy to a fixed rate transmission system. The red path shows the first path that the source would try to compute based on the modified algorithm, but the dotted hop of the path fails since the hop distance exceeds the shown ρ_{max}. The successful end-to-end path between the source and destination node requires first taking a "backwards" hop to discover the connected route, as shown in blue.

node would then need to continue expanding its area of next hop consideration until it takes a backwards hop and discovers the connected path to the destination node. In a practical operating scenario, given a high enough network density (such as we discussed when analyzing cell routing in Chapter 4), these network topologies may rarely, if ever, occur.

While these changes add to the computational complexity of Algorithm 2 and impose additional memory requirements on the source node that is doing the route computation, these changes allow for a heuristic fixed transmission rate system routing algorithm that uses near-ρ_{max} length hops when possible to achieve high network throughput and low end-to-end delay and path energy consumption.

5.5 Summary

We considered algorithmic route determination in both omnidirectional and directional infrastructureless wireless networks in this chapter. After discussing general, but optimal, graph theoretic routing techniques and tools, we showed how to adapt these tools to find optimal routes for our individual QoS metrics of consideration. Specifically, we applied Dijkstra's Algorithm and the Dijkstra-based Widest Path Algorithm to the problem of determining the optimal end-to-end paths in terms of sustainable data rate, total delay (end-to-end number of hops), and end-to-end path power for both fixed rate transmission systems and variable rate transmission systems. In order to apply these algorithmic routing solutions to our specific problems, we derived methods to assign link lengths to the underlying network graph. We then developed a new geographic routing algorithm that leverages localization information and the results from Chapter 4 indicating that we could realize optimal throughput, end-to-end delay, and path energy consumption scaling behavior simultaneously in our infrastructureless wireless network scenario by taking hops on the order of a characteristic hopping distance (or maximum hopping distance in the fixed rate transmission system). This routing scheme was based on a heuristic approach to finding a route between the source and destination with the known characteristic hopping distance as a general guideline. Initial simulation results showed that even this sub-optimal heuristic approach can attain the desired performance when the algorithmic parameters are tuned and optimized to the specific network scenario.

We now briefly discuss some of the shortcomings of the routing solutions presented in this chapter and some areas for future investigation. Throughout this chapter, we continued to look at a homogeneous end-user node set and homogeneous RF operating environment. Additional work is needed to adapt these algorithms to a heterogeneous RF operating

environment or to end-user device heterogeneity. More importantly, we assumed in this chapter that every node had global, up-to-date network information. The dissemination of this information throughout the network is a popular subject of academic study, but the question remains if the network is capable of disseminating this information on an appropriate time scale. It is possible that by the time that every node receives global knowledge of every other node's location and channel estimations, the network state has changed. This issue becomes more critical when considering more dynamic channel models and end-user node mobility. Thus, future work is needed to develop efficient distributed routing algorithms. Although distributed versions of Dijkstra's Algorithm and the Bellman-Ford Algorithm exist, they need to be adapted to our specific QoS-based routing problem. Our proposed d_{char}-based routing algorithm also requires additional development for a distributed implementation. Finally, as briefly mentioned before, another area for future work is to find techniques to automatically optimize the parameters of our proposed geographical routing algorithm based on the specific network under consideration (using information such as the end-user node density, the availability of transmitter and receiver beamforming, the RF environment of operation, and so forth).

Chapter 6

Conclusion

As identified in [9], current approaches to infrastructureless wireless network architecture, including MANETs and DTNs, are unable to satisfy the QoS requirements of mission-critical communications. These designs are intended to provide best-effort services only, which is not enough when facing the crisis of a natural disaster that has left human life in peril or the foreign battle theater where late message delivery could result in casualties or the failure of a campaign. It is for these time-critical scenarios that we must design an infrastructureless wireless network architecture capable of meeting mission-critical network demands. We need an infrastructureless wireless network architecture that not only provides guarantees on achievable end-to-end throughput, but is also designed to offer guarantees on end-to-end delay and network longevity through efficient management of energy consumption.

The approach of adding strategically-placed data relays to combat network disconnection was used in [9]. These relays also reduce the pass-through traffic burden on end-user nodes and help meet mission-critical QoS demands. And while the results presented in that work were promising, the addition of these data relays incur a high capital cost and greatly increase network management overhead. Instead of pursuing this direction further, we explored the option of using more sophisticated antenna geometries capable of electronic beamforming to bolster network performance and tackle the requirements of an infrastructureless wireless networks designed to provide time-critical core services. The main academic interest in this thesis was to consider the impact of antenna directionality on the performance of the network with respect to several important QoS metrics.

We first studied the impact of directionality on the probability of connectivity of a randomly deployed network with a finite number of end-user devices. Network connectivity was identified as a factor of primary importance, since the ability of a network to provide QoS guarantees is first dependent on that network being connected. Our analysis found that even a modest level of antenna directivity could provide significant benefits in the probability of connectivity. These results provide general guidelines for a network architect regarding required end-user node density to attain a high instantaneous probability of connectivity. While the analysis presented made a strong argument for the inclusion of end-user beamforming capabilities, there is still room for future development and research. Particularly, it would be of interest to quantify the probability of network connectivity under more realistic and time-varying channel scenarios and in a non-homogeneous RF operating environment. Additionally, the assumption of a homogeneous end-user device set may not be applicable to some of the driving applications considered here. War and natural disaster, for example, brings together individuals from varied armed and public service branches. Thus, extending all of the analysis presented in this thesis to device heterogeneity may be a rewarding endeavor. Also, future work should try and quantify network

connectedness when end-users are moving in the bounded operating region. Although considering random networks is a first-step feasibility analysis, the question remains if these identified deployment regimes with high instantaneous probability of connectivity hold under the addition of a mobility model.

The next chapter analyzed the scalability of the infrastructureless wireless network using beamforming-enabled end-user devices in the power-limited regime. We first quantified the achievable capacity of arbitrary networks. A comparison of omnidirectional and directional networks here showed that directionality allows for increased achievable capacity in a variable rate transmission system, again making a strong case for the inclusion of beamformers in an infrastructureless wireless network architecture. We proved that the desired throughput performance of the network could be achieved with high probability under specific routing schemes given a random network. This was an important step because it showed that these directional (and omnidirectional) infrastructureless wireless networks are capable of scaling in density without performance degradation with respect to achievable throughput, end-to-end delay, and energy consumption, and it also provided a routing strategy guideline that we developed more concretely in the following chapter. This analysis again left room for future research. We used bandwidth scaling to suppress interference effects and consider a power-limited network regime to find an upper bound on system performance. Future work could consider a network that is limited both by power constraints and by interference effects. This would be of particular interest for directional networks, since two of the primary benefits of beamforming that were missing in our analysis are interference reduction and spectral reuse. This type of analysis could also introduce the benefit of electronic nulling for additional interference suppression. Also, the analysis presented in these scaling results continued to use some simplifying assumptions, such as a homogeneous RF operating environment and homogeneous end-user device set, that could be removed by future research on the topic.

Finally, we considered some algorithmic approaches to routing that focus on QoS optimization. In addition to developing routing schemes to optimize these QoS metrics individually, we developed a heuristic routing algorithm designed to achieve the scaling-optimal behavior of all of these QoS metrics simultaneously. These algorithms made it clear that the beamforming-enabled network is capable of providing better QoS performance for core service, despite achieving the same overall scaling behavior as the omnidirectional baseline network. Specifically, the increase in the characteristic hopping distance of the directional network allows for routing decisions under our proposed heuristic algorithm with fewer end-to-end hops and a reduction in path energy consumption (although this would ultimately depend on the additional per bit processing energy cost of electronic beam steering and is worthy of further investigation). In addition to future work suggestions already mentioned, this chapter focused on routing algorithms with global device location knowledge. Future study could consider the collection and dissemination of location and channel state information, the development of distributed network algorithms for characteristic hop distance routing, and the effect of node mobility on the stability of the routes computed by the proposed solutions.

Ultimately, the work of this thesis is a first step to the thorough analysis of a directional infrastructureless wireless network. Our primary focus was to motivate the inclusion of directional transmitters and receivers at the end-user nodes by showing the directional network performance benefits over the omnidirectional case. We believe that our results indeed justify further work on the topic. However, there is still a long way to go before the deployment of a directional infrastructureless wireless network capable of providing core service is possible. Although we have shown that these networks are capable of better performance than omnidirectional networks, the absolute performance capabilities still need to be quantified. For example, we need to know if it is capable of providing a one second guarantee for end-to-end message delivery with 99.9% confidence. We need to know that it

is robust against adversarial attacks. These questions and others will require a more detailed analysis of the directional infrastructureless wireless network and the application requirements. And they may even require the synthesis of different infrastructureless wireless network solutions, such as the combination of proactive mobile helper node deployment, network disconnection prediction techniques, and beamforming-enabled end-user devices.

Appendix A

Derivation of (2.8) in Chapter 2

We let the omnidirectional transmission range be r, which is determined by the maximum time-averaged radiated power constraint at the transmitting node (which we denote P_t here), the attenuation exponent of the particular homogenous RF operating environment, and the minimum power-threshold for signal reception at the receiving node.

From the path-loss channel model (2.1), we have:

$$10 \log_{10} P_r = 10 \log_{10} P_t \gamma - 10 k \log_{10} d.$$

We define the minimum power-threshold for signal reception at the receiver as P_r^{min} and then let $\Gamma_{dB} \triangleq 10 \log_{10} P_r^{min}$. When the receiver power is exactly the threshold Γ_{dB}, then the receiver is at a distance $d = r$ from the transmitter. Thus:

$$\Gamma_{dB} = 10 \log_{10} P_t \gamma - 10k \log_{10} r.$$

Re-arranging, we have:

$$r = 10^{\frac{1}{k} \log_{10} P_t \gamma - \frac{1}{10k}\Gamma_{dB}}$$

$$= 10^{\log_{10}(P_t\gamma)^{1/k}} 10^{-\frac{1}{10k}\Gamma_{dB}}$$

$$= (P_t\gamma)^{\frac{1}{k}} 10^{-\frac{1}{10k}\Gamma_{dB}}.$$

Similarly, for the directional transmitting antenna with directivity D_{tx}, we can write:

$$10 \log_{10} P_r = 10 \log_{10} P_t D_{tx} \gamma - 10k \log_{10} d.$$

Maintaining the same notation as above, when the receiver power is exactly the threshold Γ_{dB}, then the receiver is at a distance $d = r_{bf}$ from the transmitter. Thus:

$$\Gamma_{dB} = 10 \log_{10} P_t D_{tx} \gamma - 10k \log_{10} r_{bf}.$$

Re-arranging as before, we have:

$$r_{bf} = 10^{\frac{1}{k} \log_{10} P_t D_{tx} \gamma - \frac{1}{10k}\Gamma_{dB}}$$

$$= 10^{\log_{10}(P_t D_{tx}\gamma)^{1/k}} 10^{-\frac{1}{10k}\Gamma_{dB}}$$

$$= (P_t D_{tx}\gamma)^{\frac{1}{k}} 10^{-\frac{1}{10k}\Gamma_{dB}}$$

$$= D_{tx}^{\frac{1}{k}} \left[(P_t\gamma)^{\frac{1}{k}} 10^{-\frac{1}{10k}\Gamma_{dB}} \right].$$

Recognizing the bracketed portion of this last equality as r, we have the result shown in (2.8):

$$r_{bf} = r D_{tx}^{1/k}. \qquad \blacksquare$$

Appendix B

Derivation of (3.16) in Chapter 3

We let the m equal-sized cells of the tessellated operating area be indexed from 0 to $m - 1$. We define event A_i, $i \in \{0,1,2,\dots,m-1\}$, as the event that the ith cell is empty (none of the n end-user nodes is in this cell). We also define a complementary event for each of these events, $\overline{A_i}$, as the event that the ith cell is not empty (there is at least one end-user node in this cell). Since we want to determine $P_C^{bb}(n,m)$, the probability that there is at least one end-user node in each cell (alternatively, no cells are empty), we are interested in the event $\bigcap_{i=0}^{m-1} \overline{A_i}$. Using De Morgan's law of logic, we have:

$$\bigcap_{i=0}^{m-1} \overline{A_i} = \overline{\bigcup_{i=0}^{m-1} A_i}.$$

Therefore, we can write:

$$P_C^{bb}(n,m) = \Pr\left\{\bigcap_{i=0}^{m-1} \overline{A_i}\right\}$$

$$= \Pr\left\{\overline{\bigcup_{i=0}^{m-1} A_i}\right\}$$

$$= 1 - \Pr\left\{\bigcup_{i=0}^{m-1} A_i\right\}.$$

By the construction of the problem, the cell that includes the origin of the operating area is always deterministically filled. We call this cell 0, and we have $\Pr\{A_0\} = 0$, or equivalently $\Pr\{\overline{A_0}\} = 1$. Thus, we can rewrite $P_C^{bb}(n,m)$ as:

$$P_C^{bb}(n,m) = 1 - \Pr\left\{\bigcup_{i=1}^{m-1} A_i\right\}.$$

Using the fact that an end-user node is equally likely to land in any cell due to the uniform distribution and equal-sized cells, we can apply the inclusion-exclusion principle to determine $\Pr\{\bigcup_{i=1}^{m-1} A_i\}$ exactly. The inclusion-exclusion principle gives us the following:

$$\Pr\left\{\bigcup_{i=1}^{m-1} A_i\right\} = \sum_{i=1}^{m-1} \Pr\{A_i\}$$

$$- \sum_{i,j:1\le i<j\le m-1} \Pr\{A_i \cap A_j\}$$

$$+ \sum_{i,j,l:1\le i<j<l\le m-1} \Pr\{A_i \cap A_j \cap A_l\} - \cdots$$

$$+ (-1)^{m-2} \Pr\{A_1 \cap A_2 \cap \ldots \cap A_{m-1}\}$$

170

$$= (m-1)\left(1-\frac{1}{m}\right)^n - \binom{m-1}{2}\left(1-\frac{2}{m}\right)^n + \cdots$$

$$= \sum_{i=1}^{m-1}(-1)^{i-1}\binom{m-1}{i}\left(1-\frac{i}{m}\right)^n.$$

We substitute this result back into the expression for $P_C^{bb}(n,m)$ and we get:

$$P_C^{bb}(n,m) = 1 - \sum_{i=1}^{m-1}(-1)^{i-1}\binom{m-1}{i}\left(1-\frac{i}{m}\right)^n$$

$$= \sum_{i=0}^{m-1}(-1)^{i}\binom{m-1}{i}\left(1-\frac{i}{m}\right)^n. \quad \blacksquare$$

Appendix C

Derivation of Results in Chapter 4

C.1 Derivation of Lemma 1

We consider an infrastructureless wireless network of n end-user nodes in a bounded region. These nodes are equipped with omnidirectional transmit and receive antennas (it is trivial to extend this proof to the directional transmit and receive antenna case) and are capable only of fixed rate transmission. Thus, when a node transmits, it does so at a rate of R [bit/sec]. The maximum transmission range of each node based on this rate constraint is ρ_{max} [m]. We consider a uniform traffic pattern, where each of the n nodes randomly chooses a destination node and sends data to it at an average rate of λ [bit/sec]. We are interested in finding the

upper bound on the uniform capacity $\hat{\lambda}$, the maximum achievable rate that all SD pairs can sustain subject to our power constraint. As discussed in Section 4.2.1, we consider a relaxed total network time-average power constraint of nP_{avg} [J/sec].

We assume a fixed time period T [sec]. Under uniform traffic, $n\hat{\lambda}T$ total bits of traffic are generated in T. We can enumerate each of these bits, b_i, $i \in \{1,2,\dots,n\hat{\lambda}T\}$. We focus on bit b_i, which we allow to traverse $h(b_i)$ hops from source to destination. We can further enumerate each of these hops of bit b_i, denoted h_j^i, $j \in \{1,2,\dots,h(b_i)\}$. We denote the length of hop h_j^i as r_j^i. As discussed in Section 4.2.1, we let $\bar{L}$ be the average distance between all n SD pairs. Thus, $\bar{L} = \frac{1}{n}\sum_{i=1}^{n} L_i$, where L_i is the distance between SD pair i. From this, we can write that the total distance traveled by all bits satisfies the following, since hops aren't necessarily along the straight line path between source and destination:

$$\sum_{i=1}^{n\hat{\lambda}T} \sum_{j=1}^{h(b_i)} r_j^i \geq n\hat{\lambda}T\bar{L}.$$

We can bound each hop distance from below (trivially) and from above as follows:

$$0 \leq r_j^i \leq \rho_{max}.$$

Using these upper bounds on the hop distances, we can now write:

$$\sum_{i=1}^{n\hat{\lambda}T} \sum_{j=1}^{h(b_i)} r_j^i \leq \sum_{i=1}^{n\hat{\lambda}T} \sum_{j=1}^{h(b_i)} \rho_{max}$$

$$= \rho_{max} \sum_{i=1}^{n\hat{\lambda}T} h(b_i).$$

We denote the total number of hops of all bits as $H \triangleq \sum_{i=1}^{n\hat{\lambda}T} h(b_i)$, and we observe that H is equivalent to the effective number of bits transported by the network in T. Since each node

174

is subject to our transmission rate constraint of R, H cannot exceed nTR. Combining this statement with the bounds developed above, we have:

$$n\hat{\lambda}T\bar{L} \leq \rho_{max}H \leq \rho_{max}nTR.$$

Manipulating this, we get the result as presented in Lemma 1:

$$\hat{\lambda} \leq \frac{R\rho_{max}}{\bar{L}}. \quad \blacksquare$$

C.2 Derivation of Lemma 5

We consider the same scenario as in the fixed rate case as discussed in Appendix C.1, except we relax the fixed transmission rate constraint and allow the nodes to transmit at variable rates. Again, we look at a infrastructureless wireless network of n end-user nodes operating in a bounded region and equipped with omnidirectional transmit antennas (extending this proof to the directional network case is trivial) under uniform traffic. As in the fixed rate analysis, we are interested in an upper bound on the uniform capacity $\hat{\lambda}$ under the relaxed total network time-average power constraint of nP_{avg}. As mentioned in Section 4.2.3, the decoupling of routing decisions allowed by this relaxed power constraint makes it such that uniform capacity maximization is equivalent to path power minimization.

Given a fixed period of time T [sec], $n\hat{\lambda}T$ bits of traffic will be generated by our network under uniform traffic. Using our power model and from Chapter 4 and the notation introduced in Appendix C.1, we denote the total energy consumed by the network in T as E_{tot}, and we have:

$$E_{tot} = \sum_{i=1}^{n\hat{\lambda}T} \sum_{j=1}^{h(b_i)} \left(\alpha + \beta\left(r_j^i\right)^k \right).$$

Our total power constraint dictates that $E_{tot} \leq nTP_{avg}$. We now want to find a lower bound on E_{tot}. To do this, we consider an individual SD pair i, $i \in \{1, 2, \ldots, n\}$, which generates $\hat{\lambda}T$ bits of traffic in the fixed time period. We denote the path energy consumed by SD pair i in T as E_i, and, as in [50], we minimize E_i by breaking the path down into some number of equal lengths hops along the straight line between source and destination. We denote the number of hops in the SD pair i path as n_i, and then each equal-length hop is $\frac{L_i}{n_i}$. Thus, we can write the following expression for E_i:

$$E_i = \hat{\lambda}Tn_i\left(\alpha + \beta\left(\frac{L_i}{n_i}\right)^k \right).$$

If we take the derivative with respect to n_i and set this derivative to 0, we can minimize this total path energy consumption for SD pair i while ignoring the integer constraint on n_i. This yields the optimal value for n_i that minimizes E_i, denoted n_i^*:

$$n_i^* = L_i\left(\frac{\beta}{\alpha}(k-1)\right)^{1/k}.$$

We now want to reintroduce the integer constraint on n_i, since the optimal value is not necessarily an integer. For analytical tractability, we do not use ceiling and floor functions on n_i^*. Instead, we recognize that $\exists c_1^i > 0$ such that $\left[c_1^i L_i\left(\frac{\beta}{\alpha}(k-1)\right)^{1/k}\right] = \lfloor n_i^* \rfloor \in \mathbb{N}$ and $\exists c_2^i > 0$ such that $\left[c_2^i L_i\left(\frac{\beta}{\alpha}(k-1)\right)^{1/k}\right] = \lceil n_i^* \rceil \in \mathbb{N}$. Substituting n_i^* into the expression for E_i gives us a minimum that we denote E_i^{min}. Thus, using our integer values, we can write:

$$E_i^{min} \geq \hat{\lambda}Tc_1^i L_i\left(\frac{\beta}{\alpha}(k-1)\right)^{1/k}\left(\alpha + \beta\left(\frac{L_i}{c_2^i L_i\left(\frac{\beta}{\alpha}(k-1)\right)^{1/k}}\right)^k \right)$$

$$= \hat{\lambda} T c_1^i L_i \alpha \left(\frac{\beta}{\alpha} (k-1) \right)^{1/k} \left(1 + \frac{1}{c_2^{i^k}(k-1)} \right).$$

Summing E_i^{min} over all SD pairs and letting $c_1 = \min_i \{c_1^i\}$ and $c_2 = \max_i \{c_2^i\}$, we have:

$$E_{tot} \geq \hat{\lambda} T c_1 \alpha \left(\frac{\beta}{\alpha} (k-1) \right)^{1/k} \left(1 + \frac{1}{c_2^k(k-1)} \right) \sum_{i=1}^{n} L_i.$$

Now we employ the upper bound on E_{tot} to get:

$$n T P_{avg} \geq \hat{\lambda} T c_1 \alpha \left(\frac{\beta}{\alpha} (k-1) \right)^{1/k} \left(1 + \frac{1}{c_2^k(k-1)} \right) \sum_{i=1}^{n} L_i.$$

Rearranging, and recognizing that $\bar{L} = \frac{1}{n} \sum_{i=1}^{n} L_i$, we get the result as presented in Lemma 5:

$$\hat{\lambda} \leq \frac{P_{avg}}{c_1 \alpha \bar{L} \left(\frac{\beta}{\alpha} (k-1) \right)^{1/k} \left(1 + \frac{1}{c_2^k(k-1)} \right)}$$

$$= \frac{P_{avg} d_{char}}{c_1 \alpha \bar{L} \left(1 + \frac{1}{c_2^k(k-1)} \right)}.$$

The final equality here comes from identifying the characteristic hopping distance, d_{char}, as the optimal hop distance from the minimization of the path energy consumption: $d_{char} \triangleq \frac{L_i}{n_i^*} = \left(\frac{\alpha}{\beta(k-1)} \right)^{1/k}.$ ∎

C.3 Derivation of Theorem 2

We want to prove that uniform capacity is $\Theta(1)$ with high probability with increasing n for a random infrastructureless wireless network of n nodes using omnidirectional or directional transmit antennas and fixed-rate transmissions in a fixed-sized (unit torus) operating region.

To do so, we show that the cell routing strategy achieves this uniform throughput scaling with high probability for a randomly distributed network. The cell routing scheme is described in detail in Section 4.3.1. The proof using this routing scheme requires the following lemma (which is proven elsewhere, as indicated by the references).

Lemma 9. *Consider a random network under uniform traffic with n nodes independently and randomly distributed on a unit torus operating region according to a uniform distribution. The torus is divided into square cells of equal area $a(n)$.*

(i) If $a(n) = A$, then each cell has at least $\frac{nA}{2}$ nodes with high probability [9].

(ii) The number of SD lines passing through any cell under uniform traffic is $O\left(n\sqrt{a(n)}\right)$ with high probability [37].

Under the cell routing scheme, we know that each cell is assigned a fixed size $A = v \times v$ that does not change with increasing n. From the first part of Lemma 9, we see that each cell will have at least one node in it with high probability as long as $v \geq \sqrt{\frac{2}{n}}$. Given large enough n, it is possible to satisfy the absolute cell-sizing conditions for cell routing: $\sqrt{\frac{2}{n}} \leq v \leq \frac{\rho_{max}}{2\sqrt{2}}$ in the omnidirectional antenna case and $\sqrt{\frac{2}{n}} \leq v \leq \frac{\rho_{max}^{bf}}{2\sqrt{2}}$ in the directional transmit antenna case. Now, combining the first part of Lemma 9 with the second part, we have that any given node must transmit $O\left(\frac{n\sqrt{A}}{nA/2}\right) = O\left(\frac{2\sqrt{A}}{A}\right) = O(1)$ traffic at most with high probability as long as we distribute the pass-through traffic evenly over all nodes in the cell. Given a fixed transmission rate R, the fact that uniform capacity is $\hat{\lambda} = O(1)$ (or $\hat{\lambda}^{bf} = O(1)$ for the directional network case) with high probability, and the maximum pass-through traffic a node must relay is $O(1)$ with high probability, we establish that the achievable uniform throughput $\tilde{\lambda}$ (or $\tilde{\lambda}^{bf}$ for the directional network case) under cell routing is $\Theta(1)$ with high probability for both omnidirectional and directional random networks with fixed

178

transmission rate. Since cell routing can achieve this scaling with high probability for random networks, we have proven Theorem 2, that the uniform capacity for random power-limited infrastructureless wireless networks with fixed transmission rate is $\Theta(1)$ with high probability as n increases. ∎

As discussed in Section 4.3.2, the cell routing strategy results extend trivially to the variable rate transmission case for both omnidirectional and directional networks.

Bibliography

[1] O. Tonguz and G. Ferrari, *Ad Hoc Wireless Networks*. John Wiley and Sons Ltd., 2006.

[2] C. Murthy and B. Manoj, *Ad Hoc Wireless Networks: Architectures and Protocols*, ser. Prentice Hall Communications Engineering and Emerging Technologies Series. Pearson Education, Inc., 2004.

[3] F. Zhao and L. Guibas, *Wireless Sensor Networks: An Information Processing Approach*. Elsevier Inc., 2004.

[4] E. Callaway, *Wireless Sensor Networks: Architectures and Protocols*. CRC Press LLC, 2004.

[5] M. Conti and S. Giordano, "Multihop ad hoc networking: the reality," *IEEE Communications Magazine*, vol. 45, no. 4, pp. 88-95, 2007.

[6] *Delay Tolerant Networking*. Internet Research Task Force (IRTF), 2010, URL: http://www.dtnrg.org/wiki/.

[7] S. Farrell and V. Cahill, *Delay- and Disruption-Tolerant Networking*. Artech House Publishers, 2006.

[8] R. Krishnan, C. Small, R. Ramanathan, J. Mikkelson, and P. Basu, "DTN reference system architecture," BBN Technologies, Tech. Rep., 2007.

[9] L. Dai, "Proactive Mobile Wireless Networks," Ph.D. dissertation, Massachusetts Institute of Technology, 2008.

[10] V. Chan, 6.972 "Heterogeneous Networks: Architecture, Transport, Protocols, and Management" Course Notes, Massachusetts Institute of Technology Electrical Engineering and Computer Science, 2009.

[11] P. Gupta and P. Kumar, "The capacity of wireless networks," *IEEE Transactions on Information Theory*, vol. 46, no. 2, pp. 388-404, 2000.

[12] S. Yi, Y. Pei, and S. Kalyanaraman, "On the capacity improvement of ad hoc wireless networks using directional antennas," *Mobile Ad Hoc Networking and Computing*, pp. 108-116, 2003.

[13] H. Van Trees, *Optimum Array Processing*, part IV. John Wiley and Sons, Inc., 2002.

[14] E. Godoy, "Antenna Beamforming for Infrastructureless Wireless Networks," M.Eng. thesis, Massachusetts Institute of Technology, 2007.

[15] A. Goldsmith, *Wireless Communications*. Cambridge University Press, 2005.

[16] D. Tse and P. Viswanath, *Fundamentals of Wireless Communication.* Cambridge University Press, 2005.

[17] R. Gallager, *Principles of Digital Communication.* Cambridge University Press, 2008.

[18] J. Liberti and T. Rappaport, "Statistics of shadowing in indoor radio channels at 900 and 1900 MHz," *Military Communications Conference (MILCOM),* vol. 3, pp. 1066-1070, 1992.

[19] C. Oestges, D. Vanhoenacker-Janvier, and B. Clerckx, "Channel characterization of indoor wireless personal area networks," *IEEE Transactions on Antennas and Propagation,* vol. 54, no. 11, pp. 3143-3150, 2006.

[20] D. Laselva, X. Zhao, J. Meinila, T. Jamsa, J. Nuutinen, P. Kyosti, and L. Hentila, "Empirical models and parameters for rural and indoor wideband radio channels at 2.45 and 5.25 GHz," *IEEE International Symposium on Personal, Indoor and Mobile Radio Communications,* pp. 654-658, 2005.

[21] D. Cassioli and A. Durantini, "A time-domain propagation model of the UWB indoor channel in the FCC-compliant band 3.6-6 GHz based on PN-sequence channel measurements," *IEEE Vehicular Technology Conference,* pp. 213-217, 2004.

[22] S. Ghassemzadeh, R. Jana, C. Rice, W. Turin, and V. Tarokh, "A statistical path loss model for in-home UWB channels," *IEEE Conference on Ultra Wideband Systems and Technologies,* pp. 59-64, 2002.

[23] S. Geng, J. Kivinen, and P. Vainikainen, "Propagation characterization of wideband indoor radio channels at 60 GHz," *IEEE International Symposium on Microwave, Antenna, Propagation and EMC Technologies for Wireless Communications*, pp. 314-317, 2005.

[24] H. Yang, P. Smulders, and M. Herben, "Indoor channel measurements and analysis in the frequency bands 2 GHz and 60 GHz," *IEEE International Symposium on Personal, Indoor and Mobile Radio Communications*, pp. 579-583, 2005.

[25] M. Marsan, G. Hess, and S. Gilbert, "Shadowing variability in an urban land mobile environment at 900 MHz," *Electronic Letters*, vol. 26, no. 10, pp. 646-648, 1990.

[26] A. Algans, K. Pedersen, and P. Mogensen, "Experimental analysis of the joint statistical properties of azimuth spread, delay spread, and shadow fading," *IEEE Journal on Selected Areas in Communications*, vol. 20, no. 3, pp. 523-531, 2002.

[27] J. Weitzen and T. Lowe, "Measurement of angular and distance correlation properties of log-normal shadowing at 1900 MHz and its application to design of PCS systems," *IEEE Transactions on Vehicular Technology*, vol. 51, no. 2, pp. 265-273, 2002.

[28] E. Perahia, D. Cox, and S. Ho, "Shadow fading cross correlation between basestations," *IEEE Vehicular Technology Conference*, pp. 313-317, 2001.

[29] L. Brouwer, "On continuous vector distributions on surfaces," Proc. Royal Acad. (Amsterdam) 11, pp. 850, 1909.

[30] C. Balanis, *Antenna Theory: Analysis and Design*. John Wiley and Sons, Inc., 2005.

[31] V. Chan, *private communication*, 2011.

[32] H. Van Trees, *Detection, Estimation, and Modulation Theory*, part I, III. John Wiley and Sons, Inc., 2001.

[33] M. Desai and D. Manjunath, "On the connectivity in finite ad hoc networks," *IEEE Communication Letters*, vol. 6, no. 10, pp. 437-439, 2002.

[34] M. Grewal, *Global Positioning Systems, Inertial Navigation, and Integration*, 2nd ed. John Wiley and Sons, Inc., 2007.

[35] B. Hiebert-Treuer, "An introduction to robot SLAM (simultaneous localization and mapping)," Ph.D. dissertation, Middlebury College, 2007.

[36] H. David, *Order Statistics*. John Wiley and Sons, Inc., 2003.

[37] A. Gamal, J. Mammen, B. Prabhakar, and D. Shah, "Throughput-delay trade-off in wireless networks," *IEEE Infocom*, pp. 464-475, 2004.

[38] A. Gore, "Comments on 'on the connectivity in finite ad hoc networks'," *IEEE Communications Letters*, vol. 10, no. 2, pp. 88-90, 2006.

[39] M. Penrose, *Random Geometric Graphs*. Oxford University Press, 2003.

[40] P. Gupta and P. Kumar, "Critical power for asymptotic connectivity," *IEEE Conference on Decision and Control*, pp. 1106-1110, 1998.

[41] R. Motwani and P. Raghavan, *Randomized Algorithms.* Cambridge University Press, 1995.

[42] G. Grimmett and D. Stirzaker, *Probability and Random Processes.* Oxford University Press, 2001.

[43] A. Gamal, J. Mammen, B. Prabhakar, and D. Shah, "Optimal throughput-delay scaling in wireless networks - part I: the fluid model," *IEEE Transactions on Information Theory*, vol. 52, no. 6, pp. 2568-2592, 2006.

[44] T. Cormen, C. Leiserson, R. Rivest, and C. Stein, *Introduction to Algorithms*, 2nd ed. Cambridge: The MIT Press, 2002.

[45] R. Min and A. Chandrakasan, "Top five myths about the energy consumption of wireless communication," *ACM Sigmobile Mobile Communication and Communications Review*, vol. 7, no. 1, pp. 65-67, 2003.

[46] B. Calhoun, D. Daly, N. Verma, D. Finchelstein, D. Wentzloff, A. Wang, S. Cho, and A. Chandrakasan, "Design considerations for ultra-low energy wireless microsensor nodes," *IEEE Transactions on Computers*, vol. 54, no. 6, pp. 727-740, 2005.

[47] F. Lee and A. Chandrakasan, "A 2.5nJ/b 0.65v 3-5GHz subbanded UWB receiver in 90nm CMOS," *IEEE International Solid-State Circuits Conference*, pp. 116-117, 2007.

[48] D. Wentzloff, "Pulse-based ultra-wideband transmitters for digital communication," Ph.D. dissertation, Massachusetts Institute of Technology, 2007.

[49] R. Negi and A. Rajeswaran, "Capacity of power constrained ad-hoc networks," *IEEE Infocom*, pp. 443-453, 2004.

[50] H. Zhang and J. Hou, "Capacity of wireless ad-hoc networks under ultra wide band with power constraint," *IEEE Infocom*, pp. 455-465, 2005.

[51] L. Dai and V. Chan, "Throughput of power-limited wireless networks with processing energy considerations," *IEEE Global Telecommunications Conference (GLOBECOM)*, pp. 1-6, 2006.

[52] W. Heinzelman, A. Chandrakasan, and H. Balakrishnan, "Energy-efficient communication protocol for wireless microsensor networks," *Hawaii International Conference on System Sciences*, vol. 2, pp. 1-10, 2000.

[53] P. Chen, B. O'Dea, and E. Callaway, "Energy efficient system design with optimum transmission range for wireless ad hoc networks," *IEEE International Conference on Communications (ICC)*, vol. 2, pp. 945-952, 2002.

[54] M. Bhardwaj, T. Garnett, and A. Chandrakasan, "Upper bounds on the lifetime of sensor networks," *IEEE International Conference on Communications (ICC)*, pp. 785-790, 2001.

[55] R. Ahuja, T. Magnanti, and J. Orlin, *Network Flows.* Prentice-Hall, Inc., 1993.

[56] A. Gamal and J. Mammen, "Optimal hopping in ad hoc wireless networks," *IEEE Infocom*, pp. 1-10, 2006.

[57] D. Bertsekas and R. Gallager, *Data Networks*, 2nd ed. Prentice-Hall, Inc., 1992.

[58] D. Medhi and K. Ramasamy, *Network Routing: Algorithms, Protocols, and Architectures.* Elsevier, Inc., 2007.

[59] Z. Wang and J. Crowcroft, "Quality-of-service routing for supporting multimedia applications," *IEEE Journal on Selected Areas in Communications*, vol. 14, no. 7, pp. 1228-1234, 1996.